

**MANUFACTURE AND CHARACTERISTICS OF PASTILLES
AND
THEIR COATING BY CRYSTALLIZATION PROCESS**

DISSERTATION

zur Erlangung des akademischen Grades

Doktor-Ingenieur (Dr.-Ing.)

genehmigt durch die

Mathematisch-Naturwissenschaftlich-Technische Fakultät
(Ingenieurwissenschaftlicher Bereich)
der Martin-Luther-Universität Halle-Wittenberg

von Herrn M.Sc. Jung-Woo Kim
geb. am 20.08.1972 in KyoungNam / Süd Korea

Dekan der Fakultät: Prof. Dr. Ludwig Staiger

Gutachter:

1. Prof. Dr. -Ing. habil. Joachim Ulrich
2. Prof. Dr. habil. Karsten Mäder
3. Dr. -Ing. Ulrich Teipel

Halle (Saale), den 15. 12. 2003

urn:nbn:de:gbv:3-000006229

[<http://nbn-resolving.de/urn/resolver.pl?urn=nbn%3Ade%3A3Agbv%3A3-000006229>]

CONTENTS

1. INTRODUCTION	1
2. TECHNICAL BACKGROUND AND THEORY	3
2.1. Melt solidification	3
2.1.1. Technical background of melt solidification processes	3
2.1.2. Approximation of crystallization rate	5
2.1.3. Degree of deformation	5
2.2. Porosity	7
2.3. Nucleation and crystal growth in solution	11
2.3.1. Nucleation	11
2.3.1.1. Types of nucleation	11
2.3.1.2. Kinetic of nucleation	12
2.3.1.3. Surface nucleation	14
2.3.2. Growth rate	16
2.3.2.1. Theory of crystal growth	16
2.3.2.2. Kinetic of crystal growth	17
2.4. Agglomeration mechanism	19
2.5. Interfacial tension	21
2.6. Seeding technology	23
3. STATE OF ART AND OBJECTIVES OF THESIS	24
3.1. State of art	24
3.1.1. Crystallization time of drops	24
3.1.2. Coating mechanism in a crystallization process	25
3.1.2.1. Zone of surface nucleation	25
3.1.2.2. Growth mechanism in a crystallization process	26
3.2. Objectives of thesis	28

4. CONTACT ANGLE AND CRYSTALLIZATION TIME	30
4.1. Introduction	30
4.2. Experimental setup and procedure	31
4.3. Measurement of contact angle	34
4.3.1. Shape and size of pastilles	34
4.3.2. Surface and internal structure of pastilles	35
4.3.3. Spreading and rebounding phenomena	35
4.3.4. Measurement of contact angle	36
4.3.4.1. Influence of viscosity	36
4.3.4.2. Influence of Reynolds number	37
4.3.4.3. Influence of surface properties	39
4.3.4.4. Influence of degree of subcooling	41
4.4. Determination of normalized deformation and crystallization time	43
4.4.1. Degree of deformation	43
4.4.2. Crystallization time	45
5. INVESTIGATION OF POROSITY IN THE PASTILLES	48
5.1. Introduction	48
5.2. Preparation of solid drugs and mercury incursion porosimeter	49
5.2.1. Preparation of pastille and tablet	49
5.2.2. Technique of mercury porosimetry	50
5.3. Structure and size distribution of pores in pastilles and tablets	51
5.3.1. Pores structure of pastilles and tablets	51
5.3.2. Pore size distribution of pastilles and tablets	52
5.4. Total porosity	54
5.4.1. Total porosity in tablets	54
5.4.2. Total porosity in the pastille	55
5.4.2.1. Effect of degree of subcooling	56
5.4.2.2. Effect of surface properties	57
5.4.2.3. Effect of Reynolds number	59
5.5. Correlation between total porosity and overall growth rate	61

6. COATING OF PASTILLES BY A CRYSTALLIZATION PROCESS	64
6.1. Introduction	64
6.2. Material and experiment setup	66
6.2.1. Metastable zone width of coating materials	66
6.2.2. Core materials and procedure of the crystallization coating process	67
6.3. Measurement of metastable zone width	68
6.4. Surface nucleation and formation of a coating	71
6.4.1. Surface nucleation	71
6.4.2. Formation of a coating	71
6.4.3. Structure of coating	75
6.5. Surface morphology and thickness of coating	75
6.5.1. Interfacial tension	76
6.5.1.1. Effect of surface properties	76
6.5.1.2. Effect of concentration of solution	79
6.5.2. Effect of degree of subcooling	81
6.5.2.1. Degree of subcooling	81
6.5.2.2. Growth rate versus supersaturation in a coating process	84
6.5.3. Effect of agitation speed.	85
7. SUMMARY	88
8. ZUSAMMENFASSUNG	91
9. NOTATIONS	94
10. REFERENCES	98

1. INTRODUCTION

The development of the chemical process industry has accounted for increasing requirements concerning both quality and physical properties of the final products. Crystallization is one of the fundamental process steps in the final treatment of chemical, pharmaceutical and food products. During the last several decades crystallization technologies have widely been applied in fields of purification and separation of substances. The field of application for crystallization processes is enlarging. Interest is coming from areas such as the crystalline-formed medicines and the drug delivery system.

Complex tablet technologies and coating by spray drying technologies have been widely employed in the pharmaceutical industry to control the drug dissolution rate. Tableting techniques are commonly used in the production of a solid complex of pharmaceutical materials. The solid complex is, however, still not optimal since there are problems such as fast dissolution, side effects (excipient and binder) and instabilities. To help to solve these problems here a solidification technology is introduced. E.g., the pastillation process is used to obtain the crystalline dosage form (pastilles). This technology brings melts into dispersed crystalline dosage form in high-speed, mono-size distribution and dust free. Crystalline-formed medicines should improve the stability and control the drug delivery system. The contact angle of drops in the field of metal alloys, paintings and coating of materials are widely investigated as tool to control the size and shape of drops. However, only in a few papers a pastillation technology is examined in the field of pharmaceutical industry. Moreover, no one has considered the crystallization time as an important parameter. The crystallization time is the important parameter for the selection of the optimum production rate and the design of the solidification technology. During the pastillation process the pores and the cracks should be formed in the bodies or on the surface of pastilles. The main reason therefore is the temperature difference between the cooled surface of substrate and the warm molten drops. Both porosity and micro-cracks are critical surface features of pastilles, especially, in drug delivery systems concerning stability. However, investigations of porosity (micro-pores and cracks) in pastilles have not been studied until today. A mercury porosimeter and SEM

technologies are employed to characterize the porosity in the pastilles. *The first and second part of this work* therefore describes the rule of the contact angle, the crystallization time of drops, the phenomenon of formation of pores in pastillation processes and the correlation between the porosity and the crystallization kinetics.

Another common method to control dissolution rates of drugs in pharmaceutical industry is a coating. Often the coating results from a spray drying coating process with an atomizer. It is one of the oldest pharmaceutical coating processes that still is used today. These processes are, however, not suitable for an application to all areas of pharmaceutical materials because of non-uniformities and non-crystallinities of the coatings. A cracking phenomenon takes place in the coatings and the coatings are sticking on each other. One of the technologies to solve these problems is a production of a crystalline-formed coating. Here comes the option of an application of crystallization processes into the game. The merits of a coating process by crystallization are compact equipment, no necessity to use binders and/or additives and the ability to control the coating thickness. The main idea of a crystallization coating process is that core materials (drugs/foods) act as heterogeneous seeds in supersaturated solutions. One prior study [DOR97] has reported results of crystal growth on a surface of heterogeneous seeds and the formation of coatings in the supersaturated solution. Dorozhkin elucidated that the mechanism of coating formation is only an agglomeration. Here, however, it will be clarified that the formation of coatings in the supersaturated solutions is a combination of agglomeration and crystal growth mechanisms. *The last part of this work* demonstrates consequentially a coating process consisting of the surface nucleation on heterogeneous seed particles and the following coating mechanism in the solution crystallization equipment. Finally optimum operating conditions are determined by means of an investigation of the effect of operating conditions to the surface morphology and the crystal growth rate.

2. TECHNICAL BACKGROUND AND THEORY

2.1. Melt solidification

2.1.1. Technical background of melt solidification process

Product-specific requirements are the most important criteria to be considered when selecting equipment for melt solidification processes. Such product-specific conditions are: (1) the required shape of the product, (2) the proportion of fines and small crystals in the product, (3) the capital costs, and (4) the energy requirements. A variety of equipment is available to meet the various requirements of industrial implementation of melt conditioning processes: drum crystallizer, conveyor belt crystallizers, conveyor belt crystallizers with pelleting systems, pilling towers, sprayed fluidized beds and screw crystallizers. Each process has been explained in literature ([KAI70], [MAS91], [PRE70]) and it is summarized in *Table 2.1*.

The following questions must be resolved when considering the introduction of an industrial solidification process: (1) Can the crystallization kinetics determine the product rate? (2) What temperature of cooling surface at a particular crystallization time is to be expected? Is there a minimum crystallization time? (3) Has seeding any effect on the crystallization time? And if so, what kind of an effect? These questions may be answered by carrying out basic experiments. It will give some useful indications for the selection of the right equipment.

Table 2.1: Melt solidification equipment

	Drum crystallizer	Conveyor belt crystallizer	Pelleting unit on conveyor belt	Screw crystallizer	Prilling tower	Sprayed fluidized bed
Device	Cooling drum, dove tail like grooves	Revolving steel belt, scraper	Pelleting system (nozzle and needle, barrel and plunger)	Screw heat exchanger, extruder	Tower, separator, dryer	Sprayer, fluidized bed, separator (sieve)
Product form	Flakes, crumbs	Strips, flakes, crumbs	Pellets	Extruded forms	Spherical particles	Spherical/irregular particles
Proportion of dust and fines in the product	High	Medium to high	Low	Low	Low	Low to medium
Solidification time, or residence time of melt	< 2min	2-10 min	< 10 min	< 10 min	< 15 s	< 1 h
Capital costs	Low	Low	Medium to high	High	High	Medium, ^a high ^b
Energy requirement	Low	Low	Medium	Medium	Low, ^a medium	Medium, ^a high ^b
Reference	[PRE70]	[MAT79]	[KAI70]	[WHI91]	[MAS91]	[UHL90]

^aLow specification for waste air cleaning.

^bHigh specification for waste air cleaning.

2.1.2. Approximation of crystallization rate

The rate at which melt solidification occurs is determined primarily by heat transfer and is, therefore, simple to control. The rate of nucleation and crystal growth increases as the degree of subcooling is increased (see *Figure 2-1* [TAM22]). As shown qualitatively, both nucleation and crystal growth rates pass through different maximum concerning the under cooling. Thereafter, both phenomena again fall back to zero. Here the deformation of a drop (phenomenon of spreading and rebounding) hardly influences the crystallization kinetics. The molten drop nucleates slightly below the melting temperature, T_{mp} . The driving force is the temperature difference between temperature of the melting point and temperature of the cooled substrate, T_{sub} . The approximation of the crystallization time, t_c is proportional to the square of the drop thickness, x_s^2 :

$$t_c \approx \frac{x_s^2}{T_{mp} - T_{sub}} \quad (2-1)$$

Equation 2-1 indicates that the crystallization time can be shortened by reducing the mean wall temperature, which can be achieved either by using a lower coolant temperature or by improving the heat transfer at the internal cooling surface. However, the *equation 2-1* shows only the crystallization time correlation between temperature deviation and thickness of the drop. The equation cannot be used to estimate the degree of deformation of the drop and the crystallization time. Physical properties of molten materials (i.e., densities of liquid and solid phase of drop, viscous energy, latent heat) have to be considered in order to predict the degree of deformation and the crystallization time.

2.1.3. Degree of deformation

To estimate the drop deformation, a variety of models such as the models of Jones [JON71], Collings et al. [COL90], Chandra and Avedisian [CHA91], Berg and Ulrich [BER97], and Madejski [MAD76] are discussed. They presented the drop deformation as an explanation of the degree of solidification.

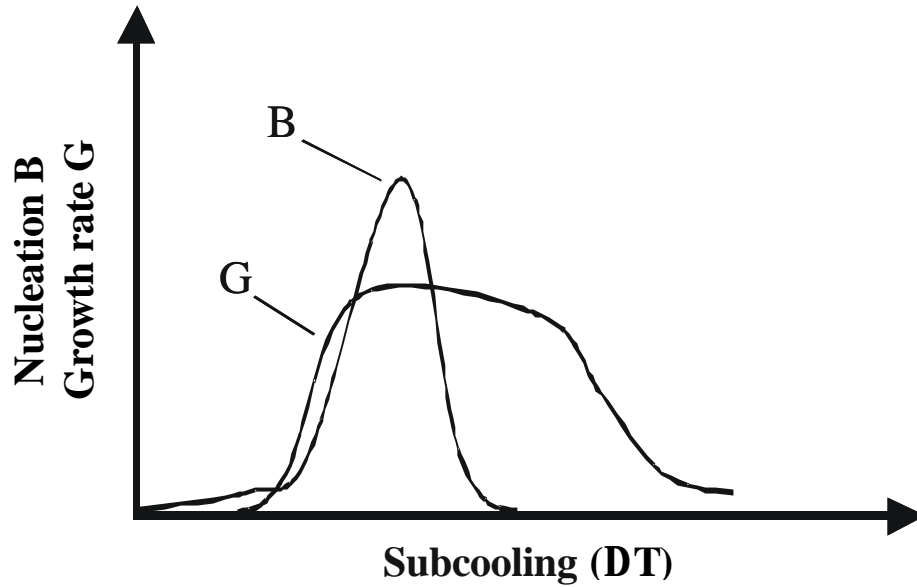


Figure 2-1: Nucleation and growth rates as a function of the temperature of the cooling surface [TAM22].

The most advanced treatment of the drop deformation problems was presented by Madejski [MAD76] for the case of splat quenching. Madejski has developed a simple model for the motion and solidification of a drop on a surface based on an energy balance. Madejski's equations are solved for one-dimensional half-space heat conduction and superheated liquid solidification conditions. The physics of impact are related to the velocity and shape of the impacting drop. Madejski was able to produce analytical expressions for some special cases. Namely, with the assumption that the drop remains as one mass of liquid that translates its momentum radially without any initial kinetic losses to the surroundings. It is also assumed that the drop forms a cylinder at the moment of impact and the liquid spreads uniformly with the solidification front growing from the substrate-liquid interface to the exposed surface of the drop. These geometrical considerations are made to limit the complexity in generating the necessary equations to describe the deformation and solidification of the drop.

Madejski model accounts for viscous energy dissipation, surface tension effects and simultaneous solidifying of the drop. He modelled the drop kinetics as a spreading cylindrical cake, assuming that the flow is laminar and the advancement rate of the freezing in the splat is a heat transfer limited Stefan solidification problem [CAR59]. Madejski's treatment of the surface tension was analogous to that of Collings et al.

[COL90] except that he considered only the surface tension between the liquid interfaces and vapour interface, excluding the introduction of the contact angle. Madejski expressed the viscous energy dissipation in terms of the shear stress invoked by the velocity gradient within the spreading drop. Madejski's numerical analysis yielded the degree of deformation as a function of four parameters.

The parameters are Reynolds number, Re , Weber number, We , Péclet number, Pe and a dimensionless parameter of Madejski's treatment, \mathbf{k} , respectively. The \mathbf{k} introduced in Madejski's derivation reflects the degree at which the solidification arrests the flattening of the drop. For the case in which \mathbf{k} is zero, the drop flattens without solidification. Moreover, the effect of the Weber number and Péclet number on the degree of deformation is trivial, because the inner force of the drop is much more important than the surface tension force in the case of formation of the drop. Here the degree of deformation, D_t/D_o is defined as the ratio of the final diameter of a drop, D_t , to the initial diameter of a drop, D_o . Madejski produced analytical expressions based on his analysis of some special cases. In the case in which the flattening of the drop arrests independently by viscous dissipation of energy the splat, $\mathbf{k} = 0 = We^{-1}$, Madejski found the degree of deformation is only a function of the Reynolds number. Some other researchers (Hamarani et al. [HAM89], Watanabe et al. [WAT92]) also obtained a similar equation as Madejski's equation.

$$\frac{D_t}{D_o} = \dot{a} Re^{0.2} \quad (2-2)$$

Here \dot{a} is the coefficient of the Reynolds number. In all experimentally found equations, the degree of deformation is proportional to the 0.2 power of the Reynolds number. However, the equations for the estimation of the degree of deformation have never considered crystallization time.

2.2. Porosity

In manufacturing processes involving the consolidation of numerous solidifying drops, micro- and macro-porosity is an inherent problem. Porosity typically reduces useful

properties such as bone strength, hardness and corrosion resistance. It is further degrading the deposited coatings on the solidified drops.

Both porosity and micro-cracks are critical surface features of pastilles since they strongly influence the hardness and the dissolution rate of materials. Porosities are often desired and of importance in medicines, catalysts and sorbents. Many researchers ([BRO97], [DON02a], [DON02b], [FUK99], [FUK01a], [FUK01b]) have already studied the entrapment of porosity for example in the area of ceramics, food and pharmaceutical industries. Especially, on the entrapment of porosity in the tablets a lot of research has been done, because it is an important parameter to control the drug release rate. However, investigations of porosity entrapped in pastilles have not been studied until today. Therefore, an investigation of the internal and external structure of the pastille should be conducted to determine the entrapment of porosity in pastilles. The data of the found porosity should be provided for the design of a solidification technology.

During drop solidification, the entrapment of porosity in the pastilles is influenced essentially by the manufacturing conditions of pastilles such as the composition of the materials, the temperature difference between cooled substrate and the melting point of the materials (so called degree of subcooling), the surface property of used cooled substrate and the physical properties of the materials. The most important influencing factors are the composition of the materials and the degree of subcooling.

As described in literature ([DUL92], [HIL95]), there are two different types of porosities that must be considered. These are open pores (surface pores, column pores, Hollow pores) and isolated pores (inclusion pores). The entrapment of porosity (effective porosity) is defined as the ratio of the pore volume of a solid sample, V_p to the bulk volume of the solid sample, V_b as described by *equation 2-3*.

$$F = \frac{V_p}{V_b} \quad (2-3)$$

According to this definition, inclusion pores are not considered. If all interconnected elements of the pore volume are taken into account, the effective porosity is obtained

from the *equation 2-3*. The sum of effective, F_{eff} and inclusion, F_i porosities gives the total porosity, F_t :

$$F_{eff} = F_t - F_i \tag{2-4}$$

As mentioned in literature ([BUE97], [ALD92], [NEU94]) *Figure 2-2* shows the pore size distribution and the crystal growth rate while the pastilles are solidifying.

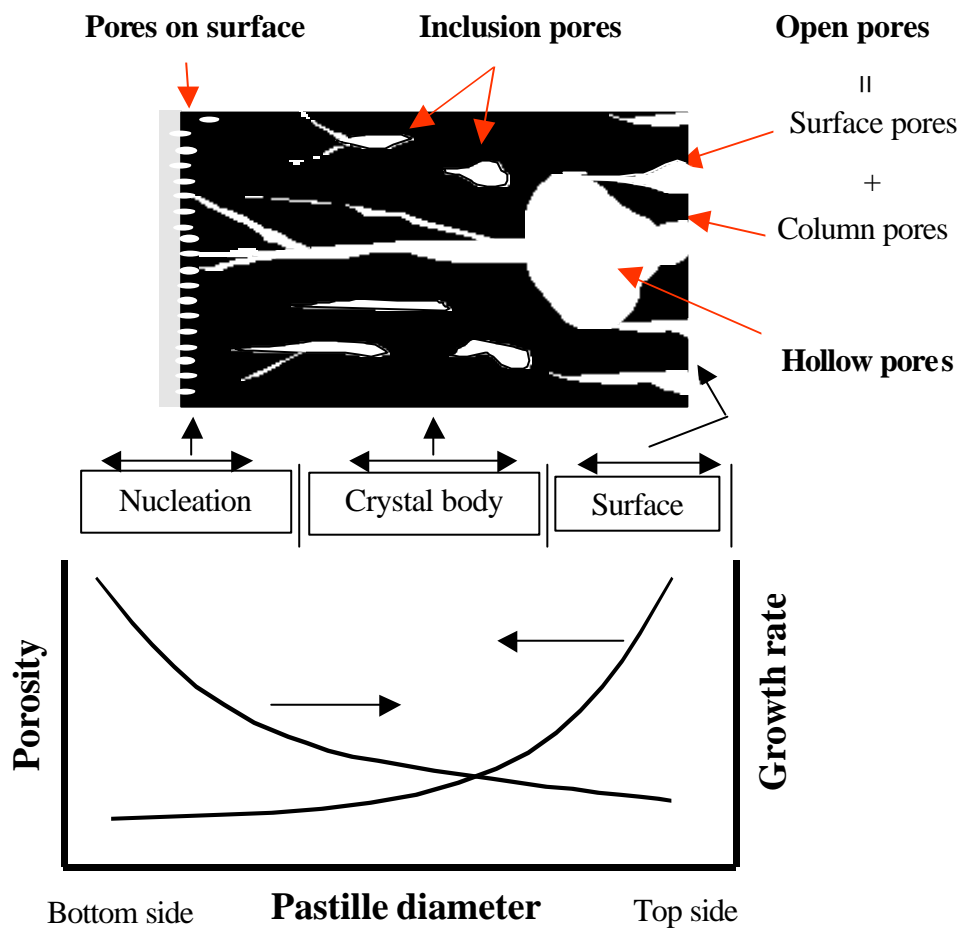


Figure 2-2: Types of porosity, pore size distribution and growth rate of pastilles.

A relatively high amount of porosity is incorporated in the top part of pastilles compare to bottom. There are four main sources of porosity. The first is occurrence of porosity due to rapid nucleation on the bottom side of the pastille. Nucleation usually takes place concentrically around the starting point of the cooled surface. As a consequence of high heat transfer, fast crystal growth takes place. Here porosity and growth rate are related

to the temperature gradient as well as the surface properties of the used substrate. The second source of porosity is the growth rate being too fast. Especially, the growth rate during the solidification process is extremely fast due to high temperature gradient. A high growth rate evokes constructional pores in the layer. The third sources of porosity are cracks and splits on the surface in top part of pastille. Cracks and splits are generated due to the temperature gradient, the composition of materials and the property of materials. The fourth source for pores are a hollow space due to density difference resulting from the phase change in solidification. When the drops impact on the cooled surface they start to solidify from bottom to top and also from outside to inside of pastilles. However, the appearance of those pores depends on the manufacturing conditions.

One prior study [LIUH94] has reported results of a performed numerical simulation to investigate formation of a micro-porosity, since the deformation and solidification behaviour of single drop takes place on a cooled substrate. In order to investigate quantitatively the effect of processing parameters on the formation of micro-pores, micro-porosity is calculated using the data of the VOF (volume of fluid) function. The micro-porosity is defined as the volume fraction of the micro-voids that are entrapped in the splat during deformation and eventually contained within the solidified layer due to rapid solidification. The full Navier-Stokes equations coupled with VOF functions were solved to determine the exact movement and interaction of droplets. The two-phase flow continuum model and the two-domain method were used for the flow problem with a growing solid layer and for the thermal field and solidification problem. On the basis of the numerical results, the possible mechanisms governing the formation of micro-pores during the flattening and interaction in the drop were discussed. However, in the study only a numerical simulation was undertaken. Therefore, the experimental investigation of the relationship between the porosity and the crystallization kinetic (nucleation, growth rate) are necessary, since the drop deforms and solidifies. The effects of important processing parameters, such as Reynolds number (related to drop impacting velocity, viscosity, density of molten drop and diameter of initial drop), degree of subcooling (temperature gradient between melting point of material and cooled substrate temperature) and surface properties of the used cooled substrate are addressed here. Ultimately, the relationship (*equation 2-5*) will be used to determine the processing conditions that are required in order to minimize the porosity. Here an

overall growth rate, G_f is introduced. It is defined as the ratio of the vertical height of pastille (crystalline layer thickness), x_s to the crystallization time (overall solidification time), t_c .

$$G_f = \frac{x_s}{t_c} \quad (2-5)$$

As mentioned previously the crystalline layer thickness, x_s is an input of the measured experimental data and the crystallization time, t_c can be expressed numerically as a function of Reynolds number and degree of subcooling. Therefore, the porosity, F can experimentally be obtained from the relationship and be expressed by a function of the crystal growth rate:

$$F \approx F(G_f) \quad (2-6)$$

2.3. Nucleation and crystal growth in solution

2.3.1. Nucleation

2.3.1.1. Types of nucleation

Crystals are created when nuclei are formed and grow. The kinetic processes of nucleation and crystal growth requires a supersaturation, which can generally be obtained by a change in temperature, by removing the solvent (usually by evaporation), by adding a drowning-out agent, or by adding reaction partners. The system then attempts to achieve thermodynamic equilibrium again through nucleation and the following growth of the nuclei.

If a solution contains neither solid foreign particles, roughness of the walls of its container nor crystals of its own type, nuclei can be formed only by homogeneous nucleation. If foreign particles are present, nucleation is facilitated and the process is known as heterogeneous. Both homogeneous and heterogeneous nucleation visually takes place in the absence of solution-own crystals and is collectively known as primary

nucleation. This occurs when a specific supersaturation, known as the metastable supersaturation $DC_{met, S}$ is exceeded. However, in semicommercial and industrial crystallizes, it has often been observed that nuclei occur even at a very low supersaturations $DC < DC_{met}$ when crystals of the solute are already present or deliberately added (e.g., in the form of attrition fragments or added homogeneous/heterogeneous seeds). Such nuclei are known as secondary nuclei. However, it should be noted that a distinction is made between nucleation resulting from contact, shearing action, breakage, abrasion, and needle fractionation (see *Figure 2-3*). Details of the above can be found by e.g. ([MER01], [MUL93], [MYE01], [ULR02]).

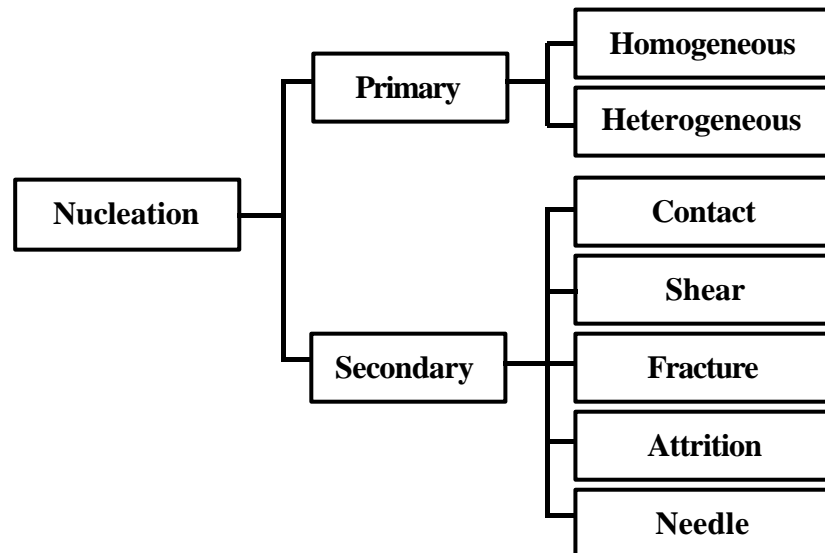


Figure 2-3: Nucleation mechanisms, according to [MER01].

Additionally *Figure 2-4* illustrates the dependence of supersaturation of several types of nucleation processes plotted against temperature. Here metastable zone width is shown decreasing gradually in width according to the nucleation processes homogeneous, heterogeneous and secondary. The knowledge of the width of the metastable zone is important in crystallization because it helps in understanding the nucleation behaviour.

2.3.1.2. Kinetic of nucleation

Secondary nucleation is a complex phenomenon and is not well understood. A general theory for the prediction of secondary nucleation rates does not exist. Several

correlations based on a power law model can, however, be found to explain most of the experimental data satisfactory. Such a power law [BEC35] is given, e.g., here:

$$B = k_N DC^n \tag{2-7}$$

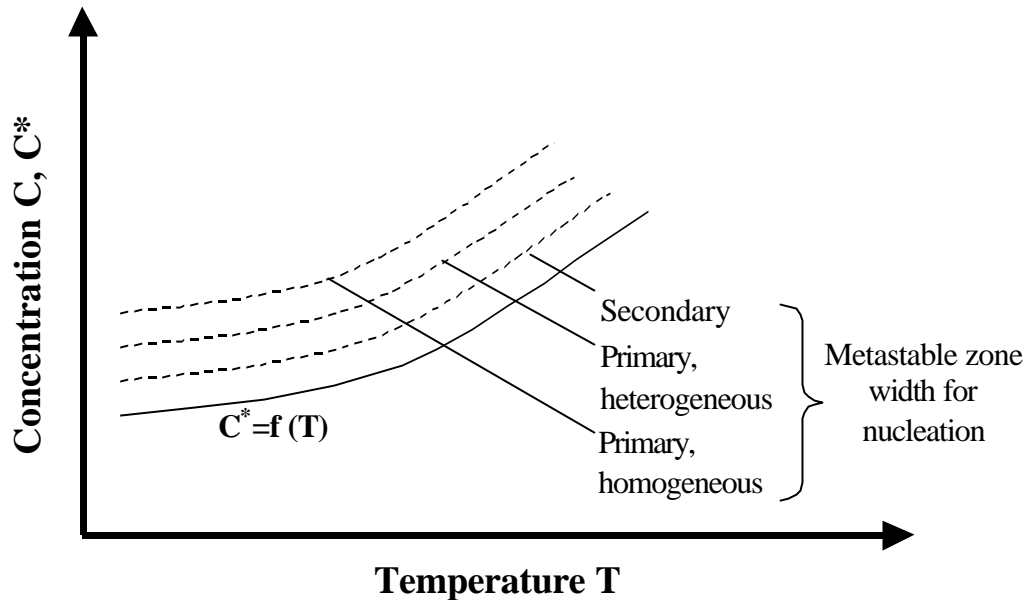


Figure 2-4: Concentration against temperature for several types of nucleation process [MER01].

Here B is the nucleation rate. The nucleation rate in this case is independent of the suspension concentration. In industrial crystallizers, most of the nuclei are generated by contact with the crystallizer walls and the stirrer or the pump. The nucleation rate in this case is a function of the degree of agitation, the suspension density and the supersaturation.

$$B = k'_N W^i M_T^j (DC^n) \tag{2-8}$$

Where W is the agitation rate and M_T is the suspension density. It is important to remember that the constants k_N and k'_N have different units. When equation 2-7 is used in a situation in which secondary nucleation is important, the constant k_N will actually vary with the conditions in the crystallizer (suspension density and agitation rate). In some situations an equation is used which does not include the effect of agitation:

$$B = k_N'' M_T^j \mathbf{DC}^n \quad (2-9)$$

In this case, k_N'' may vary with agitation rate.

2.3.1.3. Surface nucleation

With increasing supersaturation the probability of surface nucleation rises. Therefore, the supersaturation is an essential parameter for surface nucleation. Some other parameters such as the surface properties and the specific power input also effect the formation of surface nucleation [STR68].

Surface nuclei are formed when the relative supersaturation, $S_{met,S}$ is exceeded. According to Nielsen ([NIE81], [NIE84a], [NIE84b]), this supersaturation depends on the edge energy, γ_e and the maximum difference on the free energy, $\mathbf{DG}_{max,S}$:

$$\mathbf{n} \ln S_{met,S} = \mathbf{P} \frac{\mathbf{g}_e^2 a^2}{\mathbf{kT} \mathbf{DG}_{max,S}} \quad (2-10)$$

With the approximation $a \approx d_m \approx (C_C N_A)^{-1/3}$ and the interfacial energy $\mathbf{g}_{CL} \approx \mathbf{g}/d_m$, the following equation is obtained:

$$\frac{\mathbf{DG}_{max,S}}{\mathbf{kT}} = \mathbf{P} \frac{\mathbf{g}_{CL}^2 d_m^4}{(\mathbf{kT})^2 \mathbf{n} \ln S_{met,S}} \quad (2-11)$$

Again, the expression

$$\frac{\mathbf{g}_{CL} d_m^2}{\mathbf{kT}} = K \ln \left(\frac{C_C}{C^*} \right) \quad (2-12)$$

is introduced for interfacial tension \mathbf{g}_{CL} . Combining the last two equations gives:

$$\frac{\mathbf{DG}_{max,S}}{\mathbf{kT}} \approx \mathbf{P} \frac{[K \ln(C_C / C^*)]^2}{\mathbf{n} \ln S_{met,S}} \quad (2-13)$$

The rate of surface nucleation, B_S , in nuclei per square meter surface of crystal and per second, depends on the diffusivity, D_{AB} and the nucleation energy, $\mathbf{DG}_{max,S}$ according to literature ([NIE81], [DIR91]).

$$B_S = \frac{D_{AB}}{d_m^4} \exp\left(-\frac{\mathbf{DG}_{max,S}}{\mathbf{kT}}\right) \quad (2-14)$$

or

$$B_S \approx \frac{D_{AB}}{d_m^4} \exp\left(-\mathbf{P} \frac{[K \ln(C_C / C^*)]^2}{\mathbf{n} \ln S_{met,S}}\right) \quad (2-15)$$

In general, the following relationship is obtained:

$$\frac{B_S d_m^4}{D_{AB}} = f\left(\frac{C^*}{C_C}, \mathbf{s}_{met,S}, \mathbf{n}\right) \quad (2-16)$$

$$\text{with } \mathbf{s}_{met,S} = \frac{\mathbf{DC}_{met,S}}{C^*} = S_{met,S} - 1$$

With increasing supersaturation, S the number of surface nucleation events rises rapidly with the consequence that the surface gets rougher and rougher. This roughening is accompanied by another effect that supports this process – the decrease in the critical radius, r_s^* leads to a locally different equilibrium concentration.

$$\frac{r_s^*}{d_m} = \frac{\mathbf{g}_{CL} d_m^2}{\mathbf{kT} \mathbf{n} \ln S} = K \left(\frac{\ln(C_C / C^*)}{\mathbf{n} \ln S} \right) \quad (2-17)$$

Surface nuclei are formed when the relative supersaturation, $S_{met,S}$ is exceeded. According to Nielsen [NIE81] (see also [DIR91]), the rate of polynuclear growth, \mathbf{u}_{PN} is given by:

$$\begin{aligned}
 \mathbf{u}_{PN} &= \frac{D_{AB}}{3d_m} \left(\frac{\mathbf{DC}}{C_C} \right)^{2/3} \exp \left(- \frac{\mathbf{DG}_{max,S}}{\mathbf{kT}} \right) \\
 &= \frac{D_{AB}}{3d_m} \left(\frac{\mathbf{DC}}{C_C} \right)^{2/3} \exp \left(- \mathbf{p} \frac{[K \ln(C_C / C^*)]^2}{\mathbf{n} \ln S} \right)
 \end{aligned} \tag{2-18}$$

It is important to mention that the rate of \mathbf{u}_{PN} is increased rapidly with increasing supersaturation because this crystal growth is an activated process.

2.3.2. Growth rate

2.3.2.1. Theory of crystal growth

Crystals and their growth and habit have been in the interested of scientists for long. Much early work on crystal growth centered on explaining the differences in observed crystal habits from the thermodynamic point of view. Of more interest in industrial crystallization are theories that deal with kinetics (rates) of crystal growth. There are a variety of mechanisms of crystal growth, which take place in competition and lead to different growth regimes. Reviews on crystal growth theories can be found e.g. in the works of Ohara and Reid [OHA73], Strickland-Constable [STR68] and Nyvlt et al. [NYV85]. Many of the theories are mathematically rather complex, however, there are certain features of these theories that are worth reviewing and are quite helpful in understanding the nature of the crystal growth process. *Table 2.2* provides a summary of these growth models.

Table 2.2: Growth rate models (according to [OHA73])

<i>Two-dimensional growth models</i>	
PN model	$ \mathbf{u}_{PN} = \frac{D_{AB}}{3d_m} \left(\frac{\mathbf{DC}}{C_C} \right)^{2/3} \exp \left(- \mathbf{p} \frac{[K \ln(C_C / C^*)]^2}{\mathbf{n} \ln S} \right) $
	$ \text{With } \mathbf{n} = \frac{\dot{n}\tilde{M}}{\mathbf{r}_C} $
B+S model	$ \mathbf{u}_{B+S} = K_{B+S} \left(\frac{\Delta C}{C^*} \right)^{5/6} \exp \left(\frac{K'_{B+S}}{T} \frac{C^*}{\Delta C} \right) $

<i>BCF surface diffusion model</i>	
BCF Model	$\mathbf{u}_{BCF} = K_{BCF} T \left(\frac{\mathbf{DC}}{C^*} \right)^2 \tan h \left(\frac{K'_{BCF} C^*}{T \mathbf{DC}} \right)$
<i>Diffusion layer model</i>	
Only convection and diffusion	$\dot{n} = k_d (C - C_i)$
Only surface integration	$\dot{n} = k_r (C_i - C^*)$ with $k_r = k_{r0} \exp(-\mathbf{DE}_r/RT)$,
	Elimination of $C_i \dot{n} = k_r \left(\mathbf{DC} - \frac{\dot{n}}{k_d} \right)^r$
Special case r = 1	$\dot{n} = \frac{\mathbf{DC}}{1/k_d + 1/K_r}$
Special case r = 2	$\dot{n} = k_d \mathbf{DC} + \frac{k_d^2}{2k_r} - \sqrt{\frac{k_d^4}{4k_r^2} + \frac{k_d^3 \mathbf{DC}}{k_r}}$

2.3.2.2. Kinetic of crystal growth

Supersaturation is the most important parameter controlling the kinetics of crystal growth. Usually the following forms express supersaturation, \mathbf{DC} :

$$\mathbf{DC} = c - c^* \quad (2-19)$$

Here c and c^* are concentration of solution and concentration solution at equilibrium, respectively.

The development and operation of industrial crystallization processes is significantly easier if the kinetics of crystal growth is available. This information can be incorporated in process models and can be used in process and crystallizer design. In the previous *section 2.3.2.1*, a number of different crystal growth theories are reviewed. These provide a theoretical basis for the correlation of experimental crystal growth data and the determination of kinetic parameters from the data to be used in models of industrial

crystallization processes. In general, two basic expressions are used to express the relationship between supersaturation and crystal growth.

$$G = k_g \mathbf{DC}^g \quad (2-20)$$

and

$$R_G = K_g \mathbf{DC}^g \quad (2-21)$$

Here \mathbf{DC} and g are supersaturation and coefficient of crystal growth rate, respectively. *Equation 2-20* employs a linear crystal growth rate (m/s). However, *equation 2-21* employs a mass increase as crystal growth rate (kg/m²). The constants in *equations 2-20* and *2-21* can be related to each other through the expression:

$$K_g = 3 \frac{\mathbf{a}}{\mathbf{b}} \mathbf{rk}_g \quad (2-22)$$

The constants K_g and k_g are temperature-dependent and usually fit to the Arrhenius equation to obtain a general expression of the growth rate as function of the temperature. The Arrhenius equation can be written as:

$$k_g = A \exp(-E_G / RT) \quad (2-23)$$

Where A is a constant and E_G is activation energy. The activation energy can be used to obtain information whether the rate-controlling step is the diffusion or the surface integration one ([MER89], [NYV85], [WIL71]). A complete crystal growth expression that includes both the effect of temperature and supersaturation on the growth rate would, therefore, be written as:

$$G = A \exp(-E_G / RT) \mathbf{DC}^g \quad (2-24)$$

There are a number of experimental methods that can be used to obtain the date of crystal growth rate, which are needed to obtain the kinetics (see e. g. [MER95], [MUL93], [ULR97], [NYV85]).

2.4. Agglomeration mechanism

Agglomeration depends on the crystallizing system in terms of physical chemistry, technology and on crystallization conditions. Under certain condition crystals stick together and generate by this way new (larger) particles. According to Hartel et al. ([HAR86], [SCH81]) agglomeration is the unification of primary particles that are cemented by chemical forces (e.g., by a crystalline bridge between two or more crystals). The formation of such a bridge requires crystal growth. Here the supersaturation is an essential prerequisite. There are different types of agglomeration processes that may be distinguished: (a) flocculation or coagulation, (b) agglomeration and (c) aggregation. However, it is sometime difficult to distinguish among these processes. Aggregation and flocculation can occur in saturated or undersaturated solutions. However, robust agglomeration is generated only in supersaturated solutions.

To obtain the agglomerates, three successive steps have to take place: (a) collision of two particles, (b) a sufficient time interval and (c) bridging of the two particles (by crystal growth). Here fluiddynamic conditions, nature of the solvent, size and habit of the crystals, population density of the crystals, supersaturation and the cohesion forces are the key parameters of the agglomeration process.

In general the agglomeration phenomenon takes places in supersaturated solutions after small particles (nuclei) are formed [OOS90]. Thereafter, the particles gradually stop to agglomerate when the size of agglomerates approximately reach 10 to 30 μm . Here the critical particle size depends on the fluiddynamics, the suspension density and the growth rate. This phenomenon was investigated by Steemson et al. [STE84]. They found that the small particles (nuclei) start to agglomerate when the particle is within a certain, the critical size range. Hostomsky [HOS91] also observed that the agglomeration does not take place in supersaturated solution, when the particles are larger than a certain size.

The modelling of agglomeration is based on materials and population balances, interparticle forces and crystallization kinetics. Smoluchowski [SMO17] has derived the agglomeration equations in two groups consisting of (a) *perikinetik* and (b) *orthokinetic*

agglomeration. Perikinetic agglomeration is caused by Brownian motion of monodisperse and submicron particles in solution. Orthokinetic agglomeration is induced by fluid-mechanical forces. *Table 2.3* shows the equations of perikinetic and orthokinetic agglomeration.

Table 2.3: Perikinetic and orthokinetic agglomeration

<i>Perikinetic agglomeration</i>
$\frac{dN(t)}{dt} = -4\mathbf{p}D_{AB}L(t)N^2$
$Z \equiv \frac{N_0}{N(t)} = 1 + 4\mathbf{p}D_{AB}L(t)N^2t$
$N(t) = \frac{N_0}{1 + 4\mathbf{p}D_{AB}L(t)N^2t}$
<i>Orthokinetic agglomeration</i>
$\frac{dN(t)}{dt} = -\frac{2}{3\mathbf{a}} A_{agg}\mathbf{g}\mathbf{j}_T N(t) ; \mathbf{j}_T = \mathbf{a}L^3(t)N(t)$
$Z \equiv \frac{N_0}{N(t)} = \exp\left(\frac{2A_{agg}\mathbf{g}\mathbf{j}_T t}{3\mathbf{a}}\right)$
$N(t) = \frac{N_0}{\exp\left(\frac{2A_{agg}\mathbf{g}\mathbf{j}_T t}{3\mathbf{a}}\right)} = \frac{\mathbf{j}_T}{\mathbf{a}L^3(t)}$

Here N_0 is the starting number of crystals per unit volume after nucleation, A_{agg} is an attachment factor and \mathbf{g} represents the shear rate which is proportional to the stirrer speed, s in a stirred vessel or to the expression, w_L/D in pipes with diameter, D . According to these equations a plot of $N_0/N(t)$ against time, t yields a straight line in case of perikinetic agglomeration and the logarithm of $N_0/N(t)$ is proportional to time in case of the orthokinetic agglomeration. When dealing with orthokinetic agglomeration, the logarithm of $N_0/N(t)$ is proportional to time. For orthokinetic agglomeration in a plot of $\ln L^3(t)$ against time, t , a straight line is obtained. The slope of this line should increase with increasing agitation (stirrer speed) and concentration:

$$\ln\left[\frac{\mathbf{a}}{\mathbf{j}_T} N_0 L^3(t)\right] = \frac{2A_{agg}\mathbf{g}\mathbf{j}_T}{3\mathbf{a}} t \quad (2-25)$$

Many researchers have experimentally confirmed the equation of Smoluchowski. According to these relationships the collision rate depends on the motion of the primary particles, that is (a) the Brownian or diffusion flows in case of very small particles in a motionless liquid, (b) the shear rate, \dot{g} for larger particles and (c) the differential setting.

2.5. Interfacial tension

The essential driving forces for formation of a coating by crystallization processes are the degree of subcooling respectively the degree of concentration which is the state of supersaturation of the solution (i.e. the position in the MZW) as well as the interfacial tension, g_L . The interfacial tension between the seed particle and the surrounding liquid. The interfacial tension results from the surface properties of seed particles (i.e. surface roughness) and the concentration of the coating materials. The interfacial tension has an effect on the nucleation and the crystal growth rate. It is, therefore, an important parameter which determines whether or not there is a surface nucleation on the surface of the seed particles.

It is generally agreed on that the measurement of the contact angles on a given solid surface is the most practical method to obtain surface energies (e.g. [WU98], [WU99]). It is well established that contact angle measurements can be used to calculate surface tensions of solids. In the past decades numerous techniques (e.g. [FOW87], [KWO99], [NEU74], [SPE96]) have been tested to measure contact angles, which were inspired by the idea of using the equation derived by Young [YOU05].

$$g_L \cos \theta = g_s - g_{SL} \quad (2-26)$$

Where g is the experimentally determined surface energy (surface tension) of the liquid, θ is the contact angle, g_s is the surface energy of the solid and g_{SL} is the solid/liquid interfacial energy. There are many approaches to determine g and g_{SL} .

An acid-based approach (one of the most important advances) is introduced by Fowkes et al. [FOW87] and van Oss [OSS94]. The surface free energy is seen as the sum of a Lifshitz-van der Waals component, \mathbf{g}^{LW} (corresponding to \mathbf{g}^d) and a polar, or Lewis acid-base component, \mathbf{g}^{AB} (corresponding to \mathbf{g}^p). The acid-base component \mathbf{g}^{AB} can be further subdivided according to following equation:

$$\mathbf{g}_i^{AB} = 2\sqrt{\mathbf{g}_i^+ + \mathbf{g}_i^-} \quad (2-27)$$

Where \mathbf{g}_i^+ is the electron-acceptor parameter of the acid-base surface free energy component or Lewis acid parameter of surface free energy and \mathbf{g}_i^- is the electron-donor parameter of the acid-base surface free energy component or Lewis base parameter of surface free energy. The mathematical approach for the solid/liquid interfacial tension is given by:

$$\mathbf{g}_{SL} = \mathbf{g}_S + \mathbf{g}_L - 2\left(\sqrt{\mathbf{g}_S^{LW} \mathbf{g}_L^{LW}} + \sqrt{\mathbf{g}_S^+ \mathbf{g}_L^-} + \sqrt{\mathbf{g}_S^- \mathbf{g}_L^+}\right) \quad (2-28)$$

In order to determine the surface free energy component (\mathbf{g}_S^{LW}) and parameters \mathbf{g}_S^+ and \mathbf{g}_S^- of a solid, the contact angle of at least three liquids with known surface tension component \mathbf{g}_L^{LW} , \mathbf{g}_L^+ and \mathbf{g}_L^- , two of which must be polar, has to be determined ([WU99], [FOW87], [VAN88]).

According to the transformation of Young the following equation is found ($y = mx + b$):

$$x = \sqrt{\frac{\mathbf{g}_L - \mathbf{g}_L^-}{\mathbf{g}_L^+}} = \sqrt{\frac{\mathbf{g}_L^+}{\mathbf{g}_L^-}} \quad y = \frac{1 + \cos \mathbf{q}}{2} = \frac{\mathbf{g}_L}{\sqrt{\mathbf{g}_L^-}} \quad (2-29)$$

This results into:

$$\mathbf{g}_S^- = m^2 \quad \text{and} \quad \mathbf{g}_S^+ = b^2 \quad (2-30)$$

2.6. Seeding technology

In industrial crystallization seeding has been known for a long time as an effective technique to produce good crystals in a process of batch crystallization. Seeding technology is an appropriate way: (a) starting the crystallization process under reproducible operating conditions, (b) avoiding primary nucleation, (c) preventing spontaneous nucleation and (d) achieving improved CSD. Some researchers (e. g. [Heffels et al. [HEF99], Kubota [KUB01], Funio [FUN01]) recommended a seeding policy for industrial crystallization processes which include the following points:

- It is recommended that the size of seeds is bigger than 10 μm , because a size less than 10 μm of the seed crystal is difficult to create with a narrow crystal size distribution.
- Usually the temperature of the seeds should be equal to the crystallizer temperature.
- Seed crystals should be added generally to a supersaturated solution.
- The seed crystals should be washed or slightly dissolved to remove adherent crystalline dust.
- The location for the induction of the seeds should be considered carefully (i.e., near the stirrer, in a by-pass or loop of the crystallizer).

In crystallization coating processes heterogeneous seeds (core materials: i.e., solid dosage form pastilles and tablets, foods and fertilizers) are used to function as core for the coating. The heterogeneous seeds are generally added to supersaturated solutions of the coating material. Nucleation on the surface of the seed particles occurs under the same conditions of the solution as nucleation would occur in a supersaturated seed free solution. The core materials should not be soluble in or harmful to the coating material. The other seeding policy is the same as with homogeneous seeds as mentioned above.

3. STATE OF ART AND OBJECTIVES OF THESIS

3.1. State of art

3.1.1. Crystallization time of drops

From the simple model for droplet solidification [WAT92], the normalized crystallization time can be calculated by the degree of the deformation. A cylindrical droplet is still molten impacting on the cooled substrate as illustrated in *Figure 3-1*. The latent heat of crystallization at differential layers is conducted to the substrate through the solid layer with the height, x_s :

$$dE = r_l \left(\frac{1}{4} \rho D^2 \right) L dx = k_s \left(\frac{1}{4} \rho D^2 \right) \frac{(T_{mp} - T_{sub})}{x_s} dt \quad (3-1)$$

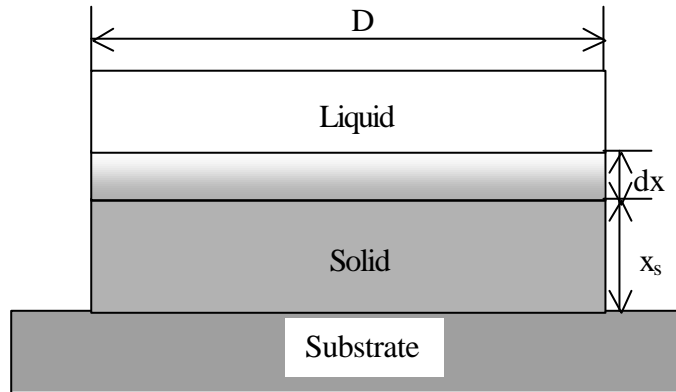


Figure 3-1: Simple solidification model of droplet impacting.

The latent heat is transferred from the droplet to the cooled substrate. The crystallization time, t_c is derived from the *equations 2-2 and 3-1* and expressed as a function of Reynolds number:

$$t_c = \frac{\dot{a}^2 \mathbf{r}_l L D_o^2}{k_s (T_{mp} - T_{sub})} Re^{0.4} \quad (3-2)$$

The dimensionless normalized deformation time, \mathbf{t}_d and crystallization time, \mathbf{t}_c are expressed by the deformation time, t_d as an input from experimental data and crystallization time, t_c as a numerical value which is derived from the *equations 3-1* and *3-2*.

$$\mathbf{t}_d = \frac{t_d \mathbf{u}_o}{D_o} \quad (3-3)$$

$$\mathbf{t}_c = \frac{t_c \mathbf{u}_o}{D_o} \quad (3-4)$$

From *equations 3-3* and *3-4*, the normalized deformation and crystallization times are numerically calculated. It means that the required crystallization time should be estimated on the basis of that relation because the deformation time can easily be measured experimentally.

As mentioned before, the required crystallization time is the important parameter for the design of the solidification technology since the crystallization rate (crystallization growth rate) as kinetic value determines the size of equipments (i.e., the size of crystallizer, speed of cooling belt). Furthermore, it will give some useful indications for the selection of the right solidification equipment.

3.1.2. Coating mechanism in a crystallization process

3.1.2.1. Zone of surface nucleation

Figure 3-2 shows the general phenomenon of nucleation in the bulk and on the surface of seed crystals in batch crystallization processes. In the supersaturated solutions, there are three periods in relation to elapsed time: (1) seeding period, (2) surface nucleation period and (3) growth period (agglomeration and crystal growth). Homogeneous/heterogeneous nuclei occur in the time period (1) within the metastable zone width (MZW). Secondary nucleation in the bulk can take place in time period (2)

due to presence of the seeds. This means that the width of metastable zone becomes more narrow. At the same time also surface nucleation take place on the surface of the seed crystals. However, the number of surface nuclei will be lower than those in the supersaturated bulk. After secondary nucleation and surface nucleation happened these nuclei start to agglomerate and grow in the time period (3) on the surface of seed particles simultaneously. The crystal growth and agglomeration mechanisms influence the growth of crystals in the bulk and on the surface of seed crystals.

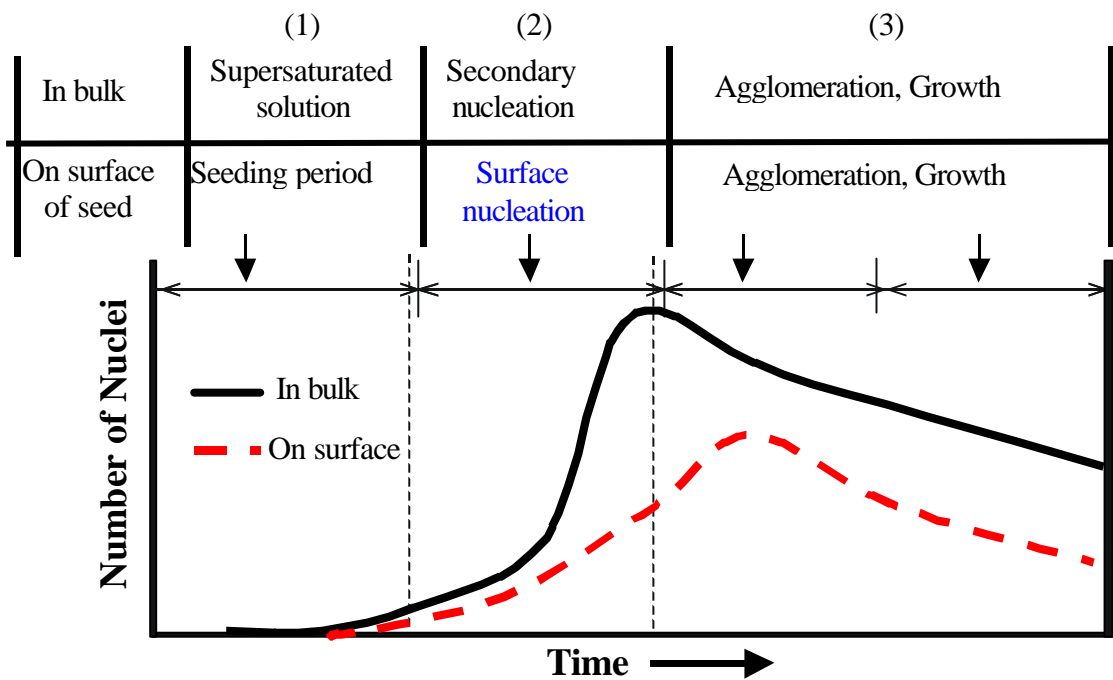


Figure 3-2: Typical phenomenon of nucleation in bulk and surface of seeds.

Additionally the rate of surface nucleation increases rapidly with increasing supersaturation. It is also known that the possibility of surface nucleation is increased with increasing number of spontaneous nuclei.

3.1.2.2. Growth mechanism in a crystallization process

The surface nucleation as mentioned in the *section 2.3.1.3*, has been explained by considering that the crystal seeds employed the same material as the bulk solution. Toyokura et al. ([TOY94], [TOY99]) introduced the surface nucleation on the surface of heterogeneous seed particles. They found that the DL-SCMC nuclei (fines) take place

on the surface of growing crystals (L-SCMC: s-carboxymethyl-L-cysteine) in the supersaturated solution of DL-SCMC. Furthermore, they discussed how the nuclei of DL-SCMC affect the surface of L-SCMC crystals under crystallization conditions.

Dorozhkin [DOR97] explained the formation and the crystal growth of $\text{CaSO}_4 \cdot \frac{1}{2}\text{H}_2\text{O}$ on the surface of FAP (fluorapatite) crystals as an aggregation mechanism. The mechanism includes two stages: The first stage is the formation of ultramicrocrystals on the surface of the FAP by aggregation. The second stage is that the crystallization process results in a continuous formation of a multi-layer coating of $\text{CaSO}_4 \cdot \frac{1}{2}\text{H}_2\text{O}$ on the surface of FAP crystals. He has only elucidated the coating mechanism as an agglomeration phenomenon.

However, coating mechanisms in crystallization processes are explained not by the agglomeration mechanisms alone but also by crystal growth mechanisms. Here it can be defined that the formation of coatings in the crystallization processes involves the phenomena that high numbers of nuclei are generated on the surface of the seed particle and than the surface nuclei agglomerate and grow together to form a layer on the surface of the heterogeneous seed particle.

Figure 3-3 shows the general phenomenon of coating of a surface of a seed particle in a crystallization process. At the beginning of the crystallization process the surface nucleation takes place at the same conditions that would lead to nucleation in supersaturated solution. After the surface nucleation crystal growth (layer thickness) would progress on the surface of the seed particles. It is clear that both crystal growth and agglomeration mechanisms effect the formation of the crystalline coating. At the beginning while the nuclei grow for the coating process the agglomeration mechanism is dominant in formation of the coating. Since the nuclei are in the best size range for agglomeration and still smaller than the critical size of crystals needed for coating by crystal growth as mentioned in the *section 3.2.1*. After the crystals have agglomerated to some critical size, the crystal growth mechanism is dominant in formation of the coating. Here the critical crystal size depends on fluid dynamics, the suspension density and the growth rate.

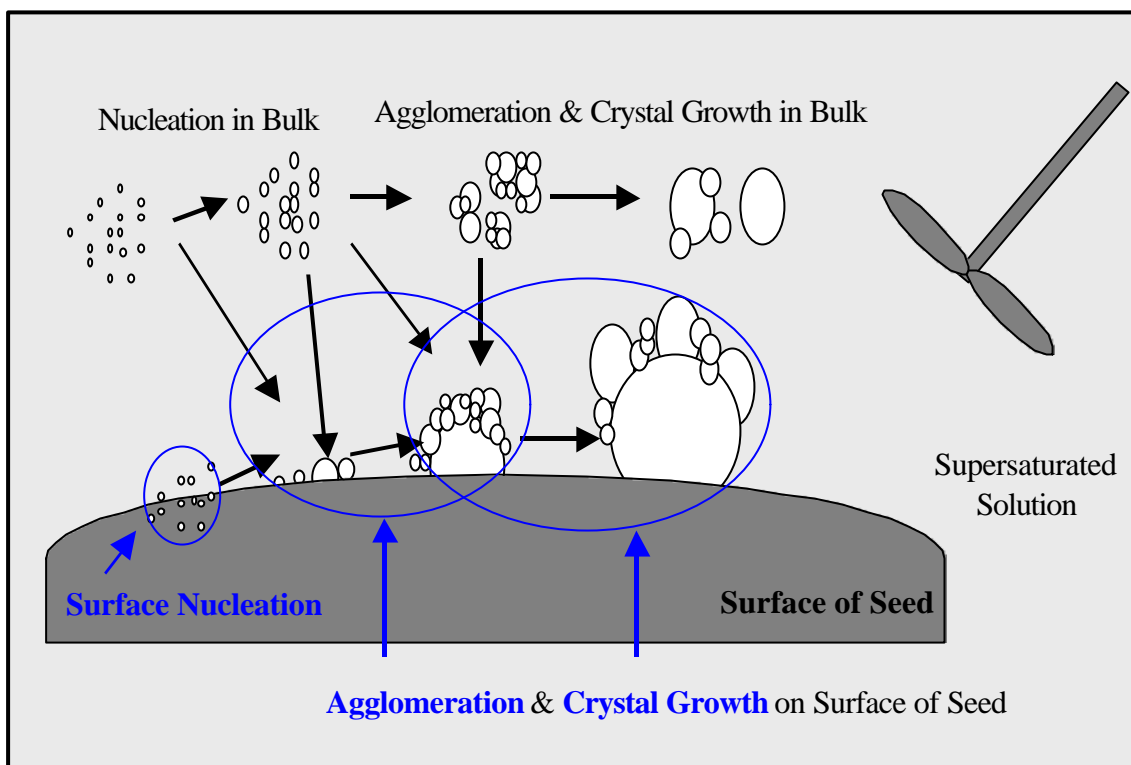


Figure 3-3: Phenomena of coating on a surface of a seed particle.

3.2. Objectives of thesis

Both melt and solution crystallization processes have widely been applied in fine chemical and pharmaceutical industries. Until today, however, little attention has been invested in the prediction of the crystallization time in pastillation and the development of novel crystallization technologies. Therefore, the major aim of present investigations is the investigation of the pastillation process and the development of a novel coating technology. Several sub-aims can be distinguished:

Pastillation process

- Measurement of contact angles with regard to spreading and rebounding phenomena
- Determination of the degree of deformation of drops deposited on a cooled substrate for solidification
- Prediction of deformation and crystallization times of such positioned drops

Investigation of porosity in the pastilles

- Characterization of internal and external structure of the pastilles
- Measurement of total porosity in the pastilles
- Determination of correlation between total porosity and overall growth rate of the pastilles

Crystallization coating process

- Introduction of the crystallization coating technology
- Measurement of the metastable zone width of the coatings materials in its solvent
- Investigation of the surface nucleation and the formation of a crystalline coating
- Investigation of surface morphology and growth rate of the coating

With the successful achievement of those sub-aims a new technology featuring the crystalline coating from solutions of a crystallized drop of a melt of an appropriate substance, e.g. a drug should be established.

4. CONTACT ANGLE AND CRYSTALLIZATION TIME

4.1. Introduction

Melt solidification is an important process to control the transition from the liquid into the solid phase in such a way that the products are obtained in an appropriate form for their transport, storage and subsequent use. This should be done by an economical process, employing the smallest and the simplest equipment possible. The transformation of a melt into a solid with in a certain form and with specific physical properties is an important operation in chemical and process industries. In most cases the solidification is a crystallization without the aim of separation. Crystallization under defined process conditions influences properties of the solidified melt such as shape, size, crystalline structure, hardness and dust content. During the last couple of decades the large variety of different requirements for the final size and shape of a product has led to a considerable number of solidification processes [WIN01].

The pastillation process (e.g., Rotoformer[®] system (Sandvik Process Systems GmbH) ([SAN88], [SAN98]), Kaiser SBS System ([KAI89], [KAI70]) is one of the solidification technologies to bring melts into dispersed solid forms in high-speed almost monosized and dust free. In case of a pastille production, many drops are positioned on a cooled surface. The pastillation of melts refers to the disintegration of the liquid directly into monosized individual volumes, which then solidify. In practice this is done by generating drops of the melt which then are positioned on a cooled substrate. In dependence on the size of the drops, the physical properties of the melt and the temperature differences the drops flatten to a certain extent. The solidified drop therefore has a typical pastille-like flattened spherical shape ([BUE98], [BUE99]).

The form of the pastilles depends on one of the physical properties strongly on the surfaces tension respectively the contact angle. Takahashi [TAK96] investigated a contact angle of metals (Au, Ag, Cu, Sn, Al) on three kinds of α -SiC plate. He explained that the contact angle depends on the interfacial tension. Chandra and

Avedisian [CHA91] visually observed drop impingement on a porous ceramic. They found that the resulting contact angle after an impact is influenced by the impact energy of the drop, the temperature of the surface substrate and the surface properties.

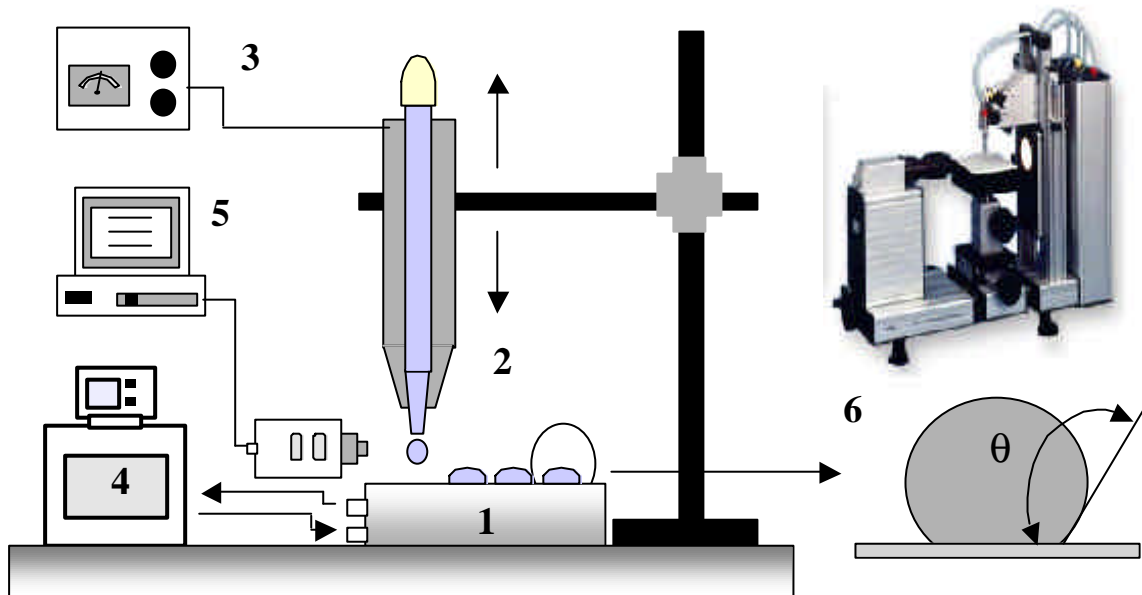
After the contact angle is formed between a drop and a solid surface, the liquid starts spreading and rebounding (Martin [MAR93], [MAR96], Mao et al. [MAO97], Zhang and Basaran [ZHA97]). The kinetic energy of a liquid drop is transformed into viscous energy and/or into interfacial energy and thereby the arresting of the spreading drop is affected.

Many researchers (Bennett and Poulikakos ([BEN93] [BEN94]), Delplanque and Rangel [DEL97], Kang et al. [KAN95], Liu et al. [LIUH94], Lie et al. [LIUW94], Rangel and Bian [RAN97], Prunet-Foch et al. [PRU98], Takahashi and Kuboi [TAK96], Wang et al. [WAN02]) have been studying the deformation and solidification of melt drops, particularly in the field of metal alloys, painting and coating of materials which employ an atomizer. However, little work has been done to investigate the deformation process of fine chemicals and medicines by a pastillation process, when drops impact on the cooled surfaces with consideration of their crystallization time. The outlook of this chapter is as following: An experimental setup and a procedure of pastillation are described in *section 4.2*. Drop size and shape are described by the contract angle in *section 4.3*. The determination of degree of deformation and a numerical study of deformation and crystallization time are investigated in *section 4.4*.

4.2. Experimental setup and procedure

The pastillation experiments were carried out in batch scale. The schematic diagram of the experimental apparatus for the production of pastilles is shown in *Figure 41*. It consists of a crystallizer, pipette with electric heater, controller, thermostatic bath for the control of temperatures, high-speed camera for investigating of the deformation phenomena and the drop shape analysis to measure the contact angle. Pharmaceutical-grade powder of pure Bisacodyl ($C_{22}H_{19}NO_4$) and Urea/Al-sulfate mixtures were used as feed materials. They were completely molten in a 300 ml crystallizer. The melts were employed in a pipette and dropped through an orifice diameter of 0.6 or 1 mm onto a

substrate. The substrate was a cooled stainless steel surface (roughness of surface (R_a : average roughness): 0.15- 0.31 μm) of a crystallizer. The surface roughness is measured by means of Perthometer S2 (Mahr Federal Inc.), which takes the average deviation of the mean height of the entire surface within the sampling length. The space of the upper square and the height of the crystallizer were a 100 cm^2 and 20 mm, respectively. The details of the box-type of crystallizer are described in *Figure 4-2* [ONO97]. The atmospheric temperature was constant at 293 K. The pipette was set in a vertical position to the crystallizer and the orifice was positioned 5,10, 20, 30, 40 and 50 mm above the substrate, respectively.



1. Crystallizer, 2. Pipette with electric heater, 3. Controller, 4. Thermostatic bath, 5. High-speed camera, 6. Drop shape analysis system and contact angle of drop, θ

Figure 4-1: Schematic diagram of experimental apparatus.

A sequence of pictures describing the impact process were taken by a high-speed camera. The focus of the camera was adjusted using the one-dimensional stage. The camera is positioned at an angle 15° below the horizontal in order to obtain clear images of the drop while spreading and rebounding upon impact. The time of each image (ms), measured from the instant of first contact with the surface, is shown. The reflection of each drop in the polished substrate can be seen in the photographs. Using the multiple

exposure features, the drop impact velocities, v_o , the initial diameter, D_o and the phenomena of the drop deformation upon impact could be precisely determined. Then the drops were detached from the substrate. The static contact angle between drop and substrate, θ the diameter of drop, D_t and the vertical height of drop, x were measured by the drop shape analysis system (*DAS 10 MK2 KRUESS*). Experimental and numerical parameters are summarized in *Table 4-1*.

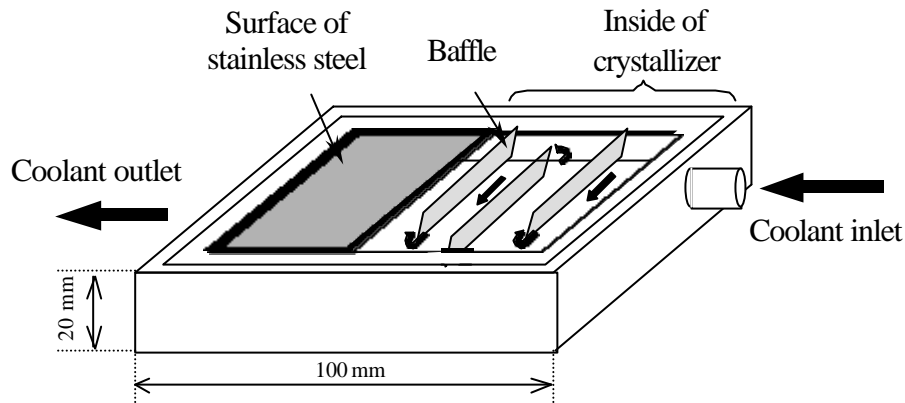


Figure 4-2: Detail of box-type crystallizer [BUE98]

Table 4-1: Experiment conditions and physical properties of pastillation process.

<i>Experimental conditions</i>	
Final impacting velocity	0.17 - 1.85 m/s
Dropping distance between surface and tip of pipette	5 - 50 mm
Degree of subcooling (ΔT)	113 - 143 K
Temperature of molten component	135 - 160 °C
Roughness of crystallizer surface (R_a)	0.15 - 3.1 μm
Temperature of ambient air	25 °C
Thermal conductivity of stainless steel	15.7331 - 16.14536 W/m·K

<i>Physical properties</i>		
	Bisacodyl	Pure Urea ($\text{CH}_4\text{N}_2\text{O}$)
Melting temperature	133 °C	132-135 °C
Density	1.2945 g/ml	1.335 g/ml
Surface tension (between air and melt)	0.020034 N/m	
Viscosity	1.607-2.216 m·Pa·s	
Latent heat	106.5 J/g	

4.3. Measurement of contact angle

4.3.1. Shape and size of pastilles

Figure 4-3 shows productions of Bisacodyl and Urea/Al sulfate mixtures that result after impacting on a surface in the batch scale pastillation process. As result of the optical measurement, they show a narrow particle size distribution and a hemi-spherical form. Average sizes of Bisacodyl Urea/ Al-sulfate pastilles are 4.1 mm (orifice diameter: 1 mm) and 2.3 mm (orifice diameter: 0.6 mm), respectively. However, the shape and size of pastilles strongly depend on chemical and physical properties of the material and the experimental conditions.

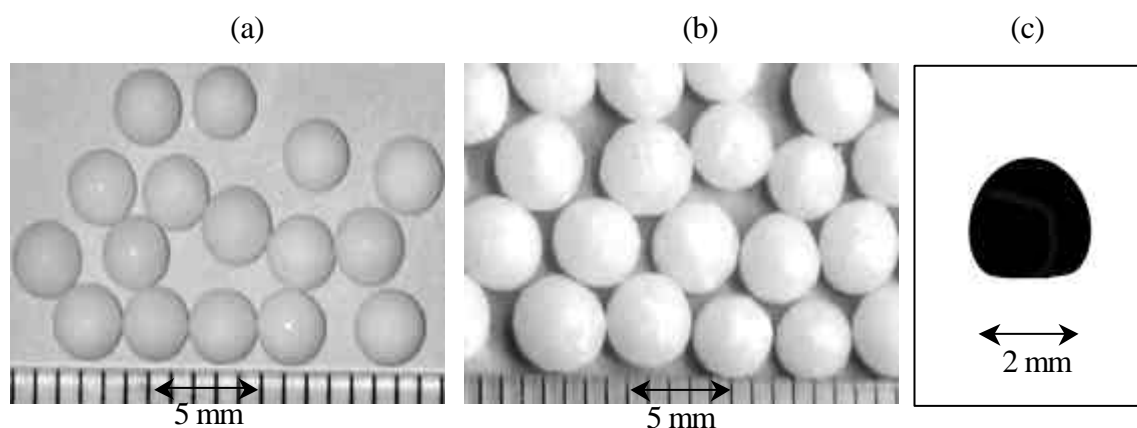


Figure 4-3: Production of Bisacodyl and Urea/Al-sulfate mixtures: (a) Bisacodyl pastilles, (b) Urea/Al-sulfate mixtures pastilles, (c) Side view of a pastille.

4.3.2. Surface and internal structure of pastilles

The porosity of the top part of pastilles is formed because the molten drop crystallizes on a cooled plate. *Figure 4-4* shows a surface morphology of the top part and the internal structure of bisacodyl and urea/Al-sulfate mixture pastilles. Cracks and splits can be observed on the surface of pastilles (*Figures 4-4 (a) and (c)*). Pores are entrapped in bodies of pastilles (*Figure 4-4 (b)*) because of the crystallization kinetics (nucleation and growth rate). Impurity (additive: Al-sulfate) is moved from bottom to top part of pastille (Urea/Al-sulfate mixtures, see *Figure 3-4(d)*) because of the temperature gradient. The entrapped porosity in the pastilles will be discussed in *chapter 5*.

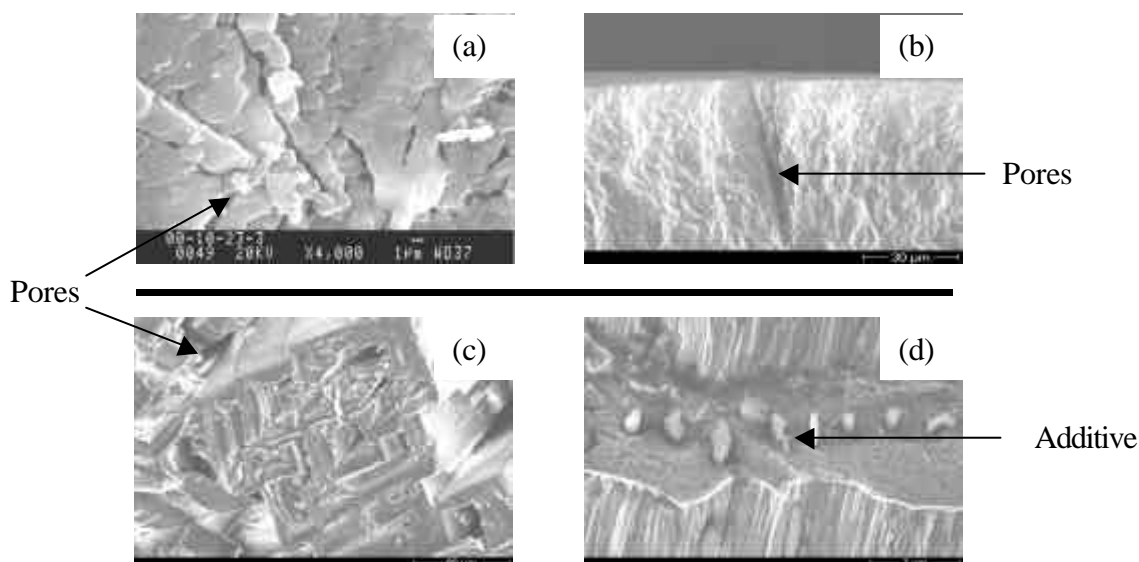


Figure 4-4: Surface and internal structure of pastilles: (a) top part of surface of Bisacodyl pastille, (b) cross section of Bisacodyl pastille, (c) top part of surface of Urea/Al-sulfate mixtures pastille, (d) cross section of Urea/Al-sulfate mixtures pastille.

4.3.3. Spreading and rebounding phenomena

Figure 4-5 shows the general impact sequence of molten Bisacodyl drops on the substrate at the conditions: final impacting velocity of 0.28 m/s, surface temperature of 10 °C and surface roughness of 0.23 μm. The time of each image (ms) is shown measured from the instant of first contact with the surface. At $t = 0$ ms, just before the impact, the drop is clearly spherical in shape. The impacting drop possesses big kinetic

energy relatively to the surface and viscous energy. The drop deforms and spreads rapidly upon impact in the radial direction due to the rapid kinetic energy release at the point of impact. At $t = 6.6$ ms, the drop reaches its maximum spreading and is momentarily at a rest because of the depletion of kinetic energy. The initial impact energy of the drop is dissipated in overcoming viscous flow and in producing new surface area. The drop moves back toward the center and rebounds upwards as a result of the interfacial tension. At $t = 20.5$ ms the drop reaches the maximum contraction. Here the kinetic energy is zero and the surface energy is maximum. At steady state, the drop possesses a minimum energy that is equal to the static surface energy at the same time the drop is rapidly solidified.

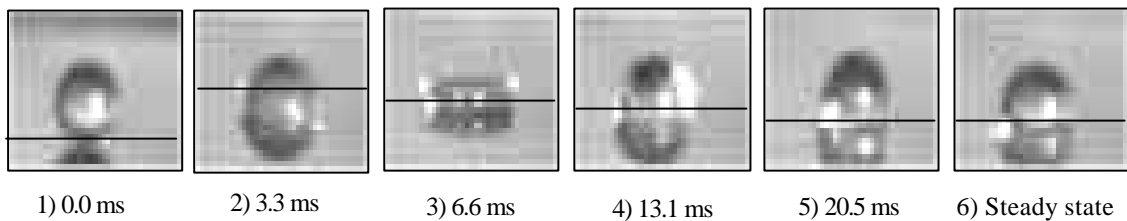


Figure 4-5: Spreading and rebounding phenomena by elapsed time.

4.3.4. Measurement of contact angle

In this section the contact angles between a single drop and the surface (stainless steel) are investigated at experimental conditions which are initial diameter of drop, viscosity, degree of subcooling, final impacting velocity and characteristic of used surface. Initial diameter, density, final impacting velocity and viscosity of the drop can be expressed through the Reynolds number.

4.3.4.1. Influence of viscosity

Figure 4-6 shows the relationship between contact angle and viscosity of molten Bisacodyl for the following set of parameters: 2 pipette orifices (diameter sizes of 0.6 or 1 mm), velocity of 0.17 m/s, degree of subcooling of $\Delta t = 133$ K, and roughness of substrate of 0.23 μm . Moreover, it additionally shows the correlation between the viscosity of molten Bisacodyl and the temperature. The viscosity is decreased with increasing the operating temperature ranging from 135 °C to 160 °C. The viscosity is

calculated by the method of van Velzen et al. [VEL72]. The deformation is represented by the static contact angle. It can be shown that contact angle increases with increasing viscosity of the molten Bisacodyl.

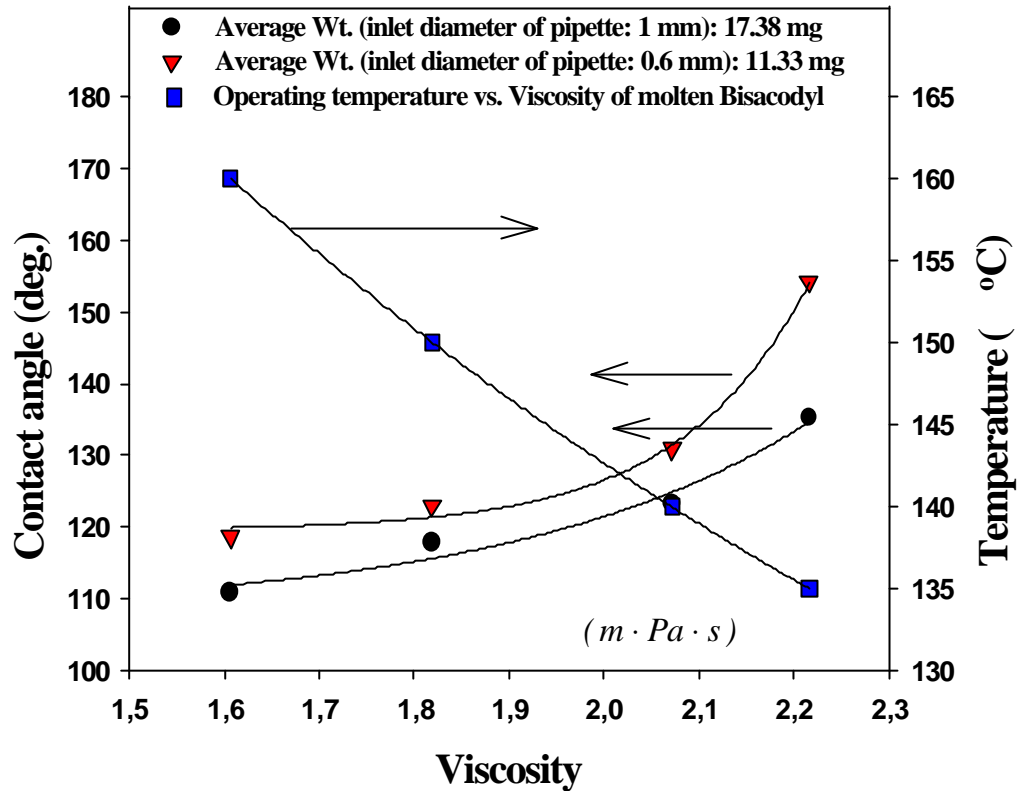


Figure 4-6: Contact angle vs. viscosity of molten bisacodyl and operating temperature versus molten bisacodyl viscosity.

4.3.4.2. Influence of Reynolds number

Figure 4-7 shows that the relationship between the contact angle and the final impacting velocity on various viscosities. The final impact velocities are measured by the high-speed camera. It corresponds to the height of drop-off, which is varied ranging from 5 to 50 mm. The degree of contact angle is exponentially decreased with increasing final impacting velocity. A larger contact angle of the drop at the low impacting velocity is a result of the interfacial tension and viscous energy dominant in the formation of shape of the drop. On the other hand, a higher impacting velocity corresponds to a smaller

contact angle. As expected, the kinetic energy decreases as the viscous energy does with the increase of the free surface area.

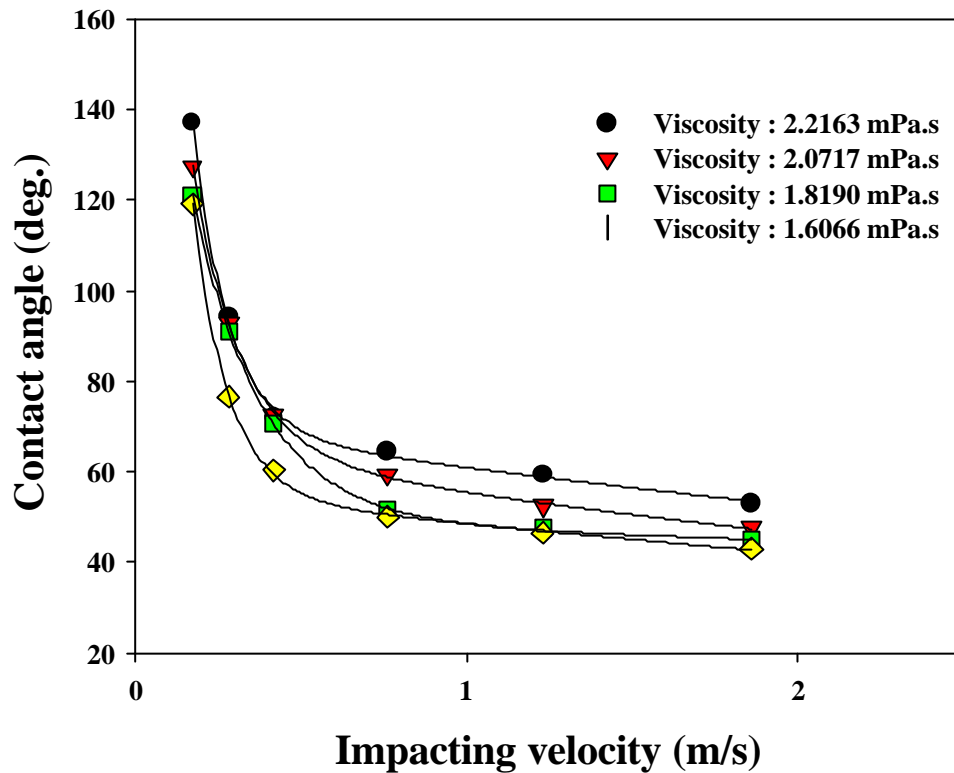


Figure 4-7: Contact angle versus velocity at various viscosities.

The contact angle of the drop is directly a function of the Reynolds number according to Figures 4-6 and 47. The correlation between the contact angle and the Reynolds number is shown in Figure 4-8. Each point is based on measurement of all four parameters in equation 2-2. The Reynolds number has, therefore, a range between 200 and 3000. Figure 4-8 enables a discussion of potential contact angles in formation of a drop. Increasing the Reynolds number results in a smaller contact angle of the drops. This is due to the fact that at high Reynolds numbers, the vertical height for the drop-off of drops is much higher than at low Reynolds numbers. It means that the kinetic energy is dominant in the deformation of drops. At low Reynolds numbers, there is a big contact angle because the viscous dissipation and the interfacial tension are dominant in the formation of the shape of the drops.

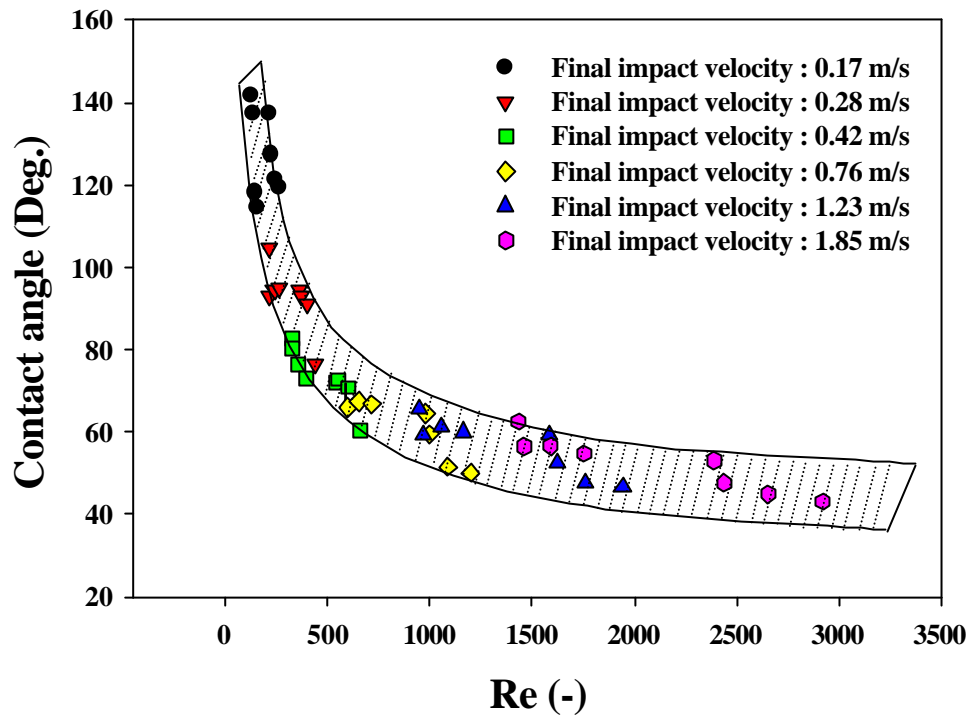


Figure 4-8: Contact angle versus Reynolds number.

4.3.4.3. Influence of surface properties

Figure 4-9 shows the characteristics of the used stainless steel substrates on the impact process at various final drop velocities. A 17.38 mg Bisacodyl drop impacts on the surface with different types of roughnesses ranging from 0.15 to 0.31 μm . Under the same impact conditions the contact angle of the drop on the surface with 0.31 μm roughness is consistently larger than that on the surfaces with the two lower roughnesses. There are different effects affecting spreading and rebounding after the impact of a drop. When a drop impacts the interfacial energy increases with increasing surface roughness. Then the surface area covered by the spreading becomes smaller due to the fact that the motion of drop is restricted. Therefore, the drop on the coarsest surface is rebounding faster than drops on the other two surfaces. In all three cases, the drop reaches equilibrium after its excess energy is completely dissipated. However, it

takes much longer time to reach equilibrium on the roughest surface compared to the other two surfaces because of a much stronger rebounding.

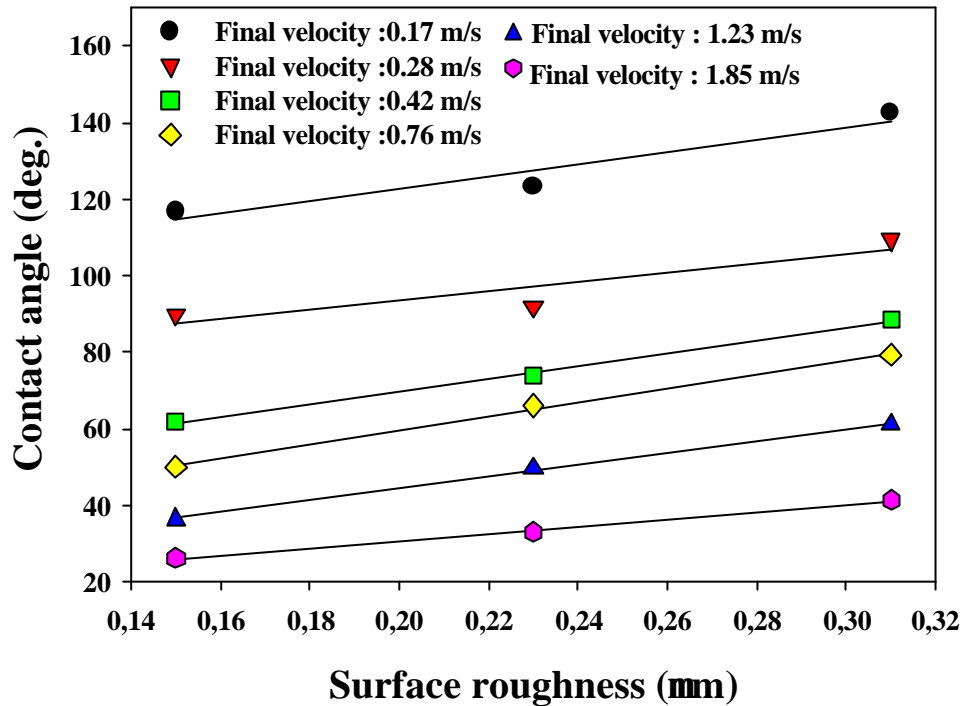


Figure 4-9: Contact angle versus degree of surface roughness at various velocities.

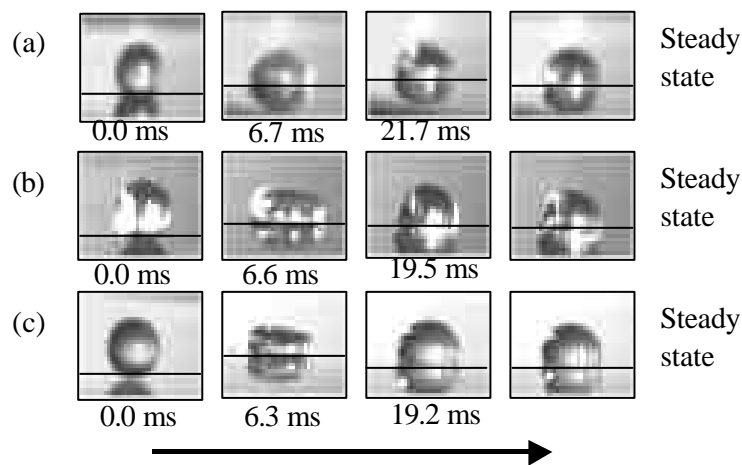


Figure 4-10: Sequences of pictures of side views of drops impacting on surfaces with different roughness ((a) $R_a = 0.15 \mu\text{m}$, (b) $R_a = 0.23 \mu\text{m}$, (c) $R_a = 0.31 \mu\text{m}$).

Figure 4-10 shows a sequence of photos of drops after impacting on three stainless steel surfaces with different roughnesses. The setting of the experimental parameters are final impacting velocity of 0.28 m/s and degree of subcooling of $\Delta T = 133$ K. From these photos it can be visually certified that on the coarsest surface (see Figure 4-10 (c)), it takes much shorter time to reach the maximum rebounding compared to the other two surfaces.

4.3.4.4. Influence of degree of subcooling

Figure 4-11 shows a drop impacting on the stainless steel substrate at 4 different degrees of subcooling. All other parameters are kept constant: final impacting velocity of 0.28

m/s, surface roughness of $0.23 \mu\text{m}$ and viscosity of $2.072 \text{ mPa}\cdot\text{s}$. The degree of subcooling is defined as difference between operating temperature of the cooled substrate and the melting temperature of Bisacodyl. After the drop reaches steady state the contact angles in case of higher degrees of subcooling (143 or 133 K) are smaller than those of the lower degrees of subcooling (113 or 123 K).

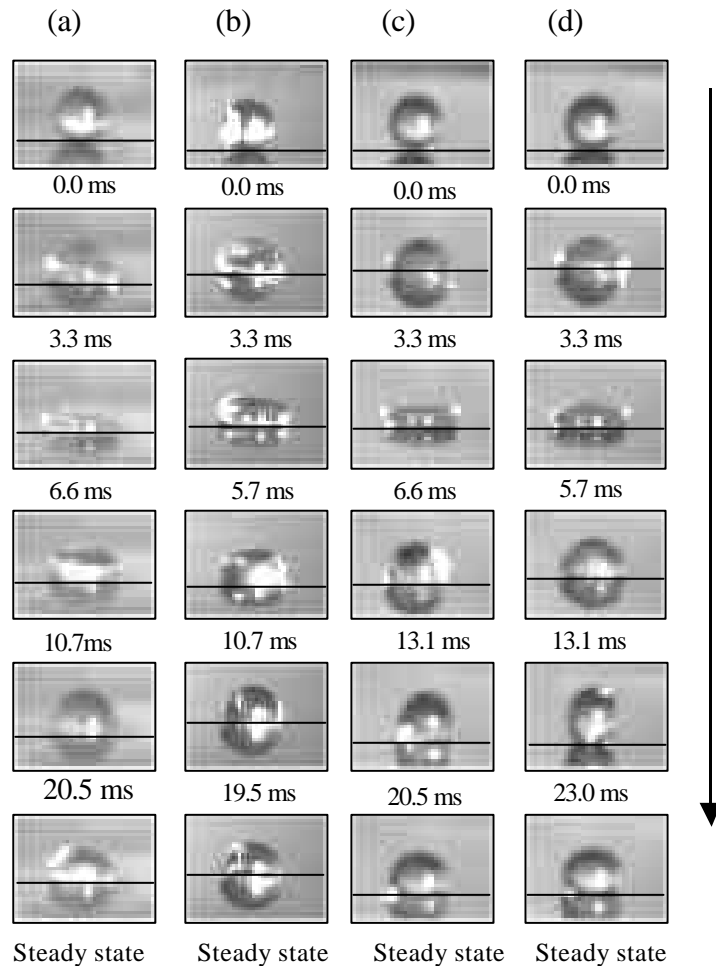


Figure 4-11: Sequences of pictures of side views of drops impacting on a medium roughness, cooled, stainless steel surface at various degrees of subcooling ((a) $\Delta T = 143$ K, (b) $\Delta T = 133$ K, (c) $\Delta T = 123$ K, (d) $\Delta T = 113$ K).

As expected the degree of rebounding at the lower degrees of subcooling is much higher compared to that of a higher degree of subcooling. This is due to a lower value of interfacial tension between the molten drop and the cooled substrate, while the drop is rapidly solidified.

Figure 4-12 shows the relationship between contact angle of the drop and degree of subcooling for 2 different impacting velocities. In case of pure Bisacodyl the maximum contact angle of the drop was 142 degree at the final impacting velocity of 0.17 m/s and the degree of subcooling of 112 K. The contact angle of the drop is decreasing as the degree of subcooling is increasing.

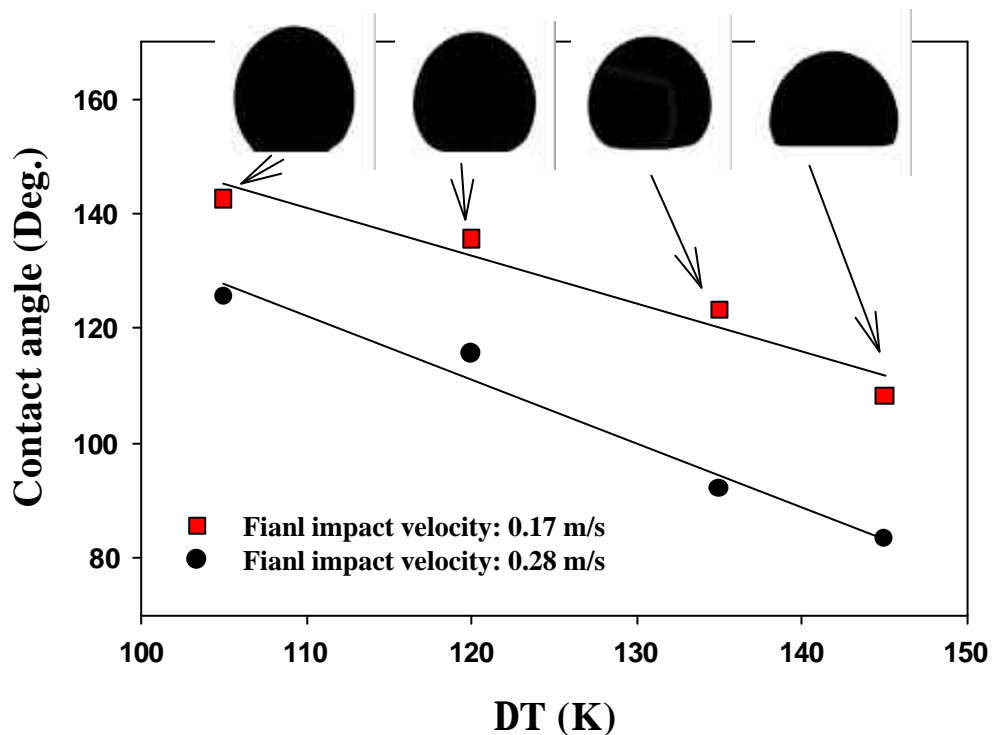


Figure 4-12: Contact angle, θ versus degree of subcooling, DT at 2-difference impact velocities.

As shown by Figures 4-11 and 4-12, the contact angle of a drop is found to be directly proportional to the degree of subcooling. It, however, is found to be inversely proportional to the Reynolds number and increasing degree of surface roughness.

4.4. Determination of normalized deformation and crystallization time

In this section the phenomenon of deformation by a pastillation process is investigated by considering its crystallization time. Degree of deformation, normalized deformation and crystallization times are introduced through Madejski's model [MAD76], simple drop solidification model [HAM89] and experimental data.

4.4.1. Degree of deformation

Madejski has developed a simple model for the motion and solidification of a drop on a surface based on an energy balance. Madejski's equations are solved for one dimensional half-space heat conduction and solidification of superheated liquids. Madejski was able to produce analytical expressions for some special cases. Namely, the solidification is independent of the surface tension. He stated also that solidification does not contribute significantly to the termination of spreading of drops. As mentioned in *chapter 2.1.2*, Madejski produced analytical expressions based on his analysis of some special cases. In the case in which the flattening of the drop is arrested solely by viscous dissipation of energy within the splat, $\mathbf{k} = 0 = We^{-1}$, the model introduces the relationship between the degree of deformation and the Reynolds number as follows:

$$\frac{D_t}{D_o} = 1.29(Re + 0.9517)^{0.2} \quad (4-1)$$

Alternatively, for $Re > 100$, *equation 4-1* can be approximated as following equation.

$$\frac{D_t}{D_o} = 1.29 Re^{0.2} \quad (4-2)$$

The degree of deformation is defined as the ratio of the final diameter of a drop, D_t , to the initial diameter of a drop, D_o . This is only a function of the Reynolds number. Hamarani et al. [HAM89] obtained a similar equation from a numerical calculation with the SMAC (simplified Marker and Cell) algorithm:

$$\frac{D_t}{D_o} = 0.83 Re^{0.2} \quad (4-3)$$

Watanabe et al. [WAT92] also calculated the relationship between degree of the deformation and the Reynolds number as follows:

$$\frac{D_t}{D_o} = 0.82 Re^{0.2} \quad (4-4)$$

As shown in the Madejski model not considering the surface tension. Therefore, the degree of deformation of a drop is only a function of the Reynolds number. The experimental results show the measured degree of the deformation (see *Figure 4-13*). The relationship between the degree of deformation and the Reynolds number can be summarized in the form of the following equation calculated from the results by using a regression method:

$$\frac{D_t}{D_o} = 0.6 Re^{0.2} \quad (4-5)$$

In all equations the degree of deformation is proportional to the 0.2 power of the Reynolds number. A high Reynolds number gives a fast deformation and a large diameter of the drop.

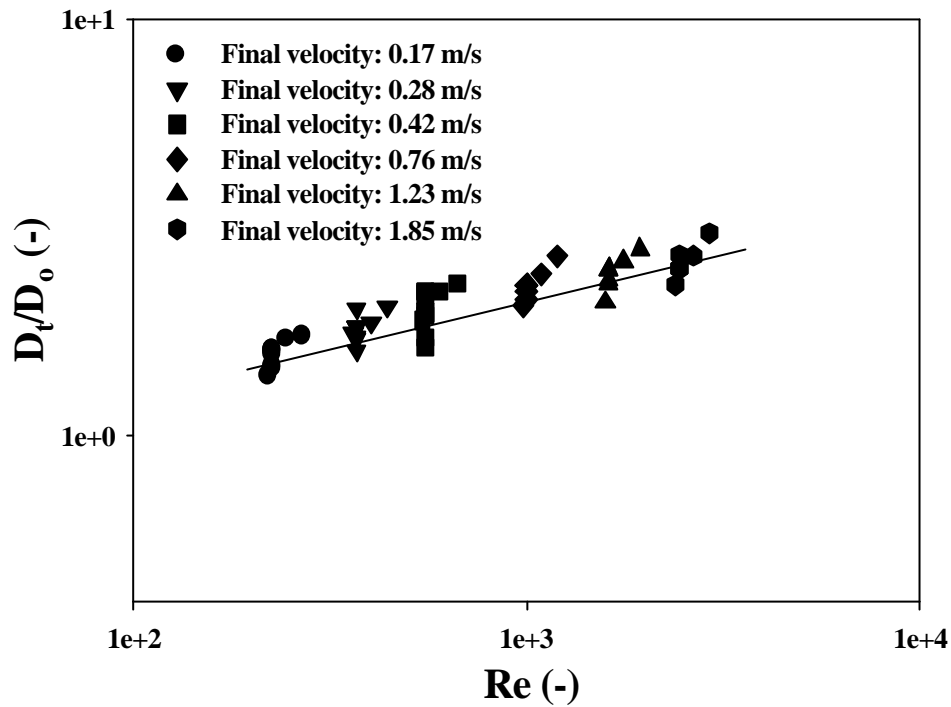


Figure 4-13: Degree of deformation of a drop D_t/D_0 versus Re number at impact.

4.4.2. Crystallization time

From the simple model for drop solidification [WAT92] the normalized crystallization time can be calculated by the degree of the deformation. A cylindrical drop still molten while impacting on a substrate is illustrated in *Figure 3-1*. The latent heat of crystallization at differential layers is conducted to the substrate through the solid layers with the height. Here the height of solid layer, x_s can be derived from *equation 3-1* and expressed as follows:

$$x_s = \frac{E}{r_l(1/4\rho D_t)} \quad (4-6)$$

Combining *equation 4-6* and *equation 3-1* gives:

$$E^2 = k_s L r_l \left(\frac{1}{4} \rho D_t^2 \right)^2 (T_{mp} - T_{sub}) t \quad (4-7)$$

The degree of deformation, $D_t = 0.6 Re^{0.2} D_o$ is substituted in *equation 4-7*:

$$E = 0.283 Re^{0.4} D_o^2 \left[k_s L r_l (T_{mp} - T_{sub}) t \right]^{0.5} \quad (4-8)$$

The crystallization time, t_c can be derived from *equations 3-1, 4-5 and 4-8*. By the boundary conditions and the *equation 3-1*, it can be derived:

$$E^2 = r_l^2 L^2 \left(\frac{1}{4} \rho D_t^3 \right)^2 \quad (4-9)$$

By combining *equation 4-8* and *equation 4-9*, the crystallization time can be expressed as follows:

$$t_c = \left(\frac{0.36 \rho_l L D_o^2}{k_s \rho} \right) Re^{0.4} \quad (4-10)$$

From *equations 3-3* and *3-4*, the normalized deformation and crystallization times are numerically calculated. *Figure 4-14* shows that relationship between normalized deformation and crystallization times and the Reynolds number.

$$\mathbf{t}_d = \frac{t_d \mathbf{n}_o}{D_o} = 0.0372 Re^{1.23} \quad (4-11)$$

$$\mathbf{t}_c = \frac{t_c \mathbf{n}_o}{D_o} = 0.924 Re^{1.23} \quad (4-12)$$

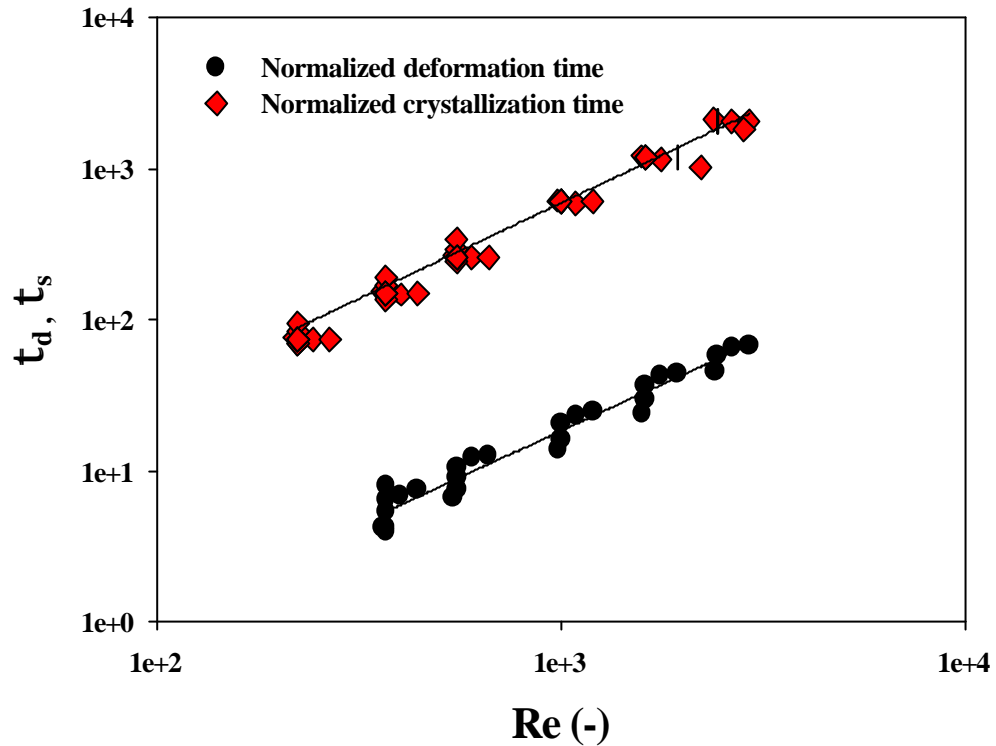


Figure 4-14: The normalized deformation and crystallization time versus Re number.

The normalized deformation and crystallization times are found to be proportional to the Reynolds number of the same power of 1.23. In case of pure Bisacodyl the normalized crystallization time is about 25 times higher than the normalized deformation time. It means that the required crystallization time should be estimated on the basis of that relation because the deformation time can easily be measured experimentally. The required crystallization time is, however, the important parameter for the design of the solidification technology since the crystallization time as kinetic value determines the size of equipment, the size of crystallizer and the speed of cooling belt.

5. INVESTIGATION OF POROSITY IN THE PASTILLES

5.1. Introduction

Many different types of controlled dosage forms have been developed to improve clinical efficiency of drug and patient compliance. In vivo performance of these dosage forms, however, depends greatly on their physical and structural properties, and consequently on their drug release mechanisms and its kinetics. A solid complex (matrix) mostly produced by tableting techniques are commonly used in pharmaceutical industries in order to retard the drug dissolution rate. The solid complex is, however, still not optimal since there are problems such as instability of tablet, selection of binder and excipient (additive). Under compressing pressure drug crystals agglomerate, thereby porosity is entrapped in the solid complex. Some researchers ([HOG02], [PAU03], [WES98]) already investigated the entrapment of porosity in the tablets, because it is an important parameters concerning bioavailability and quality of tablets.

Pharmaceutical materials require careful consideration of their porous structure and in fact their physical properties. Moreover, their application and performance are strongly influenced by their pore volume, size and shape. During the pastillation process, the pores and the cracks are formed in the bodies or on the surface of pastilles. Both pores and micro-cracks are critical surface features. Some researchers ([BUD69], [EME01]) investigated the kinetic equation of pore formation in granules of mineral materials with additives under firing. The obtained equations are recommended for mathematical modelling of the pore formation process. However, investigations of porosity (pores and cracks) in pastilles have not been studied until today. Therefore, the total porosity, the pore structure and the pore size distribution are investigated to determine the internal and external structure of the pastilles. These parameters are essentially influenced by manufacturing conditions of the pastille as the temperature gradient between surface of substrate and the melting point of the materials (degree of subcooling), the surface property of used substrate (surface roughness), the impacting velocity of droplet (Reynolds number) and the composition of the materials. The amount and the size

distribution of porosity should be estimated for the design of the drug delivery system and the selection of the solidification technology. The outlook of *chapter 5* is therefore, as follows: introduction of mercury porosimetry technique is described *in section 5.2*. Pore structure and size distribution are determined in *section 5.3*. The phenomena of pores and cracks formation by experimental conditions is investigated *in section 5.4*. The relationship between the total porosity and the crystallization kinetic is numerically elucidated *in section 5.5*.

5. 2. Preparation of solid drugs and mercury incursion porosimeter

5.2.1. Preparation of pastille and tablet

In order to minimize the porosity of the pastilles, they are manufactured by a solidification technique [KIM03c] as described in *chapter 4*. The monosized hemispherical Bisacodyl pastilles are shown in *Figure 5-1*. A SEM (Scanning Electronic Microscope)^{*1} technique is used to measure the surface morphology and the structure of the pastilles and the tablets. Manufacturing variables of the pastilles are: Reynolds number of impacting drops, degree of subcooling and characteristic of used substrate. To compare the pore structure, the total porosity and the pore size distribution, Bisacodyl tablets are manufactured by a tablet compression technology (HBM GmbH)^{*2}. It consists of a tablet compression machine and the molds, which hold a measured volume of material to be compressed, the upper punches, which exert pressure on the down stroke, and the lower punches, which control the volume of mold fill and thus the



tablet weight. The lower punches moves upward after the compaction to eject the tablet from the molds. It is the most common tableting method. The operating conditions of the tablet manufacturing are summarized in *Table 5-1*.

Figure 5-1: Monosized hemi-spherical Bisacodyl pastilles.

^{*1} The help of M.Sc. J. Choi, Max-Plank Institut in Halle is gratefully acknowledged.

^{*2} The help of Prof. Dr. P. Kleinebudde and his team, faculty of pharmacy of the Martin-Luther-University Halle-Wittenberg are gratefully acknowledged.

Tablet 5-1: Operating conditions of the tablet manufacturing.

<i>Parameter</i>	<i>Value</i>
Pressure (Max pressure: 20 MPa)	10, 13.5, 18 MPa
Type of mold	Flatted cylindrical form
Size of dies (Radius)	6, 9, 12 mm
Thickness of tablet	≈ 3.5 mm

5.2.2. Technique of mercury porosimetry

Physical and chemical gas adsorption (so called BET) as well as mercury intrusion porosimeter are the most widely used techniques to characterize powders and solid materials. These techniques can provide reliable information about the pore size/volume distribution, the particle size distribution, the bulk density and the specific surface area for porous solids regardless of their nature and shape. However, the applicable pore size ranges of each technique are different. *Figure 5-2* shows a limit of application of both techniques and classifies three kinds of pores in the size.

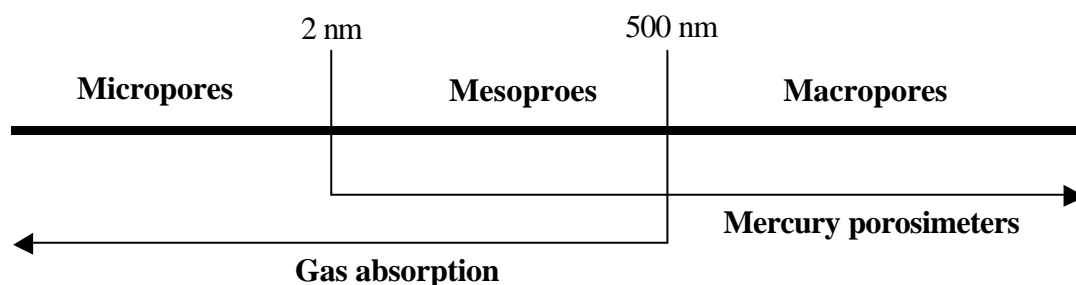


Figure 5-2: Limit of application of gas adsorption (BET) and mercury intrusion porosimetry.

The mercury porosimetry technique (Instruments Pascal 140 and 440, *Thermo Finnigan*) used to measure the total porosity, the pore size distribution and the pore structure of the tablet and the pastille. The rate of the pressure change has been discussed to affect the result of the porosity measurement [MOS81]. The technique is based on the mercury property to behave as non-wetting liquid with a lot of solid materials. As results of this property mercury penetrates through the open pores of a solid sample under an increasing pressure. The pore radius is inversely proportional to

the applied pressure according to a relation proposed by the Washburn equation ($pr = -2\gamma\cos\theta$) [KAM94] in which some assumptions have to be taken into consideration: (1) The surface tension of mercury and contact angle of the solid material are constant during the analysis. (2) The intrusion pressure must be in equilibrium. (3) Solids are not deformed under the effect of pressure. By measuring the quantity of mercury penetration in the pores and the equilibrium pressure at which intrusion occurs, experimental data are obtained to calculate the pore volume distribution as a function of their radius. Here intrusion and extrusion pressure rates are approximately 0.098 and 0.186 MPa/s, respectively. The total pore volume, the total pore surface area, the mean pore diameters and the pore size distributions of tables and pastilles were determined by both a low- and a high-pressure mercury porosimeter. Determination range of pores can be measured starting from 4 nm (pressure = 400 MPa) up to 200 μm (pressure = 0.01 kPa). In addition, a microscopic image analyzing technique is employed to support the results of mercury porosimeter.

5.3. Structure and size distribution of pores in pastilles and tablets

5.3.1. Pores structure of pastilles and tablets

In this section, pore structures and pore size distributions are investigated by the mercury intrusion porosimeter and the scanning electron microscopy techniques. Mercury porosimeter data can enable the calculation of the specific surface area (m^2/g) of the samples. There are 4 models available for the surface area calculation. Here are the cylindrical, conical, plates and spherical models. It can be distinguished by intrusion or extrusion curves between the cumulative volume of mercury and the compression pressure.

Figure 5-3 shows the relationship between cumulative volume of mercury and the compressing pressure. According to the intrusion and the extrusion curve of the pastilles, a conical model can be applied to the pastille. Moreover, these types of pores are commonly found in natural materials, for instance in carbon coke, rocks and soils. The model represents that the pores are located on the surface and in internal of pastilles. The intrusion curve features a quite flat slope, indicating that mercury penetration

increases just according to the pressure. Pores of this type are progressively filled by mercury as the pressure rises. The extrusion curve is generally following the intrusion curve resulting in a very small hysteresis.

The cylindrical model can be applied to tablets. According to shape of *Figure 5-2*, pores are considered to be cylindrical. This type of model should be applied when the sample is a solid and the penetration curve shows a steep slope (sharp pore size distribution) and the extrusion curve follows the penetration with a hysteresis. In this case a small amount of mercury is retained by the sample in the interconnections between pores. According to the cylindrical model the surface area is calculated knowing the incremental specific pore volume and the relevant average pore radius.

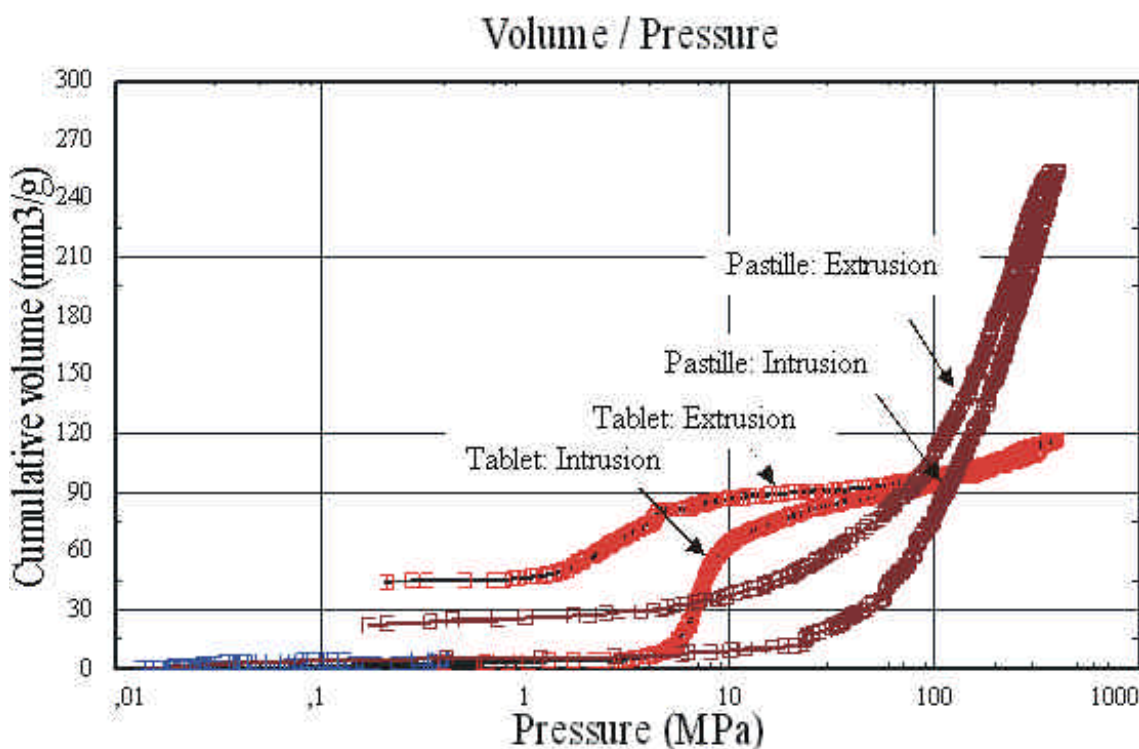


Figure 5-3: Type of pore modes of tablets and pastilles.

5.3.2. Pore size distribution of pastilles and tablets

Pore size distributions of pastilles and tablets are investigated by the mercury porosimeter and the scanning electron microscope images are used to support the result of pore size distribution. The pore size distribution can be displayed in a shape of histograms. The histograms numbers and dimension can be generated automatically by

the software according to the radius limit selection given by operating conditions.

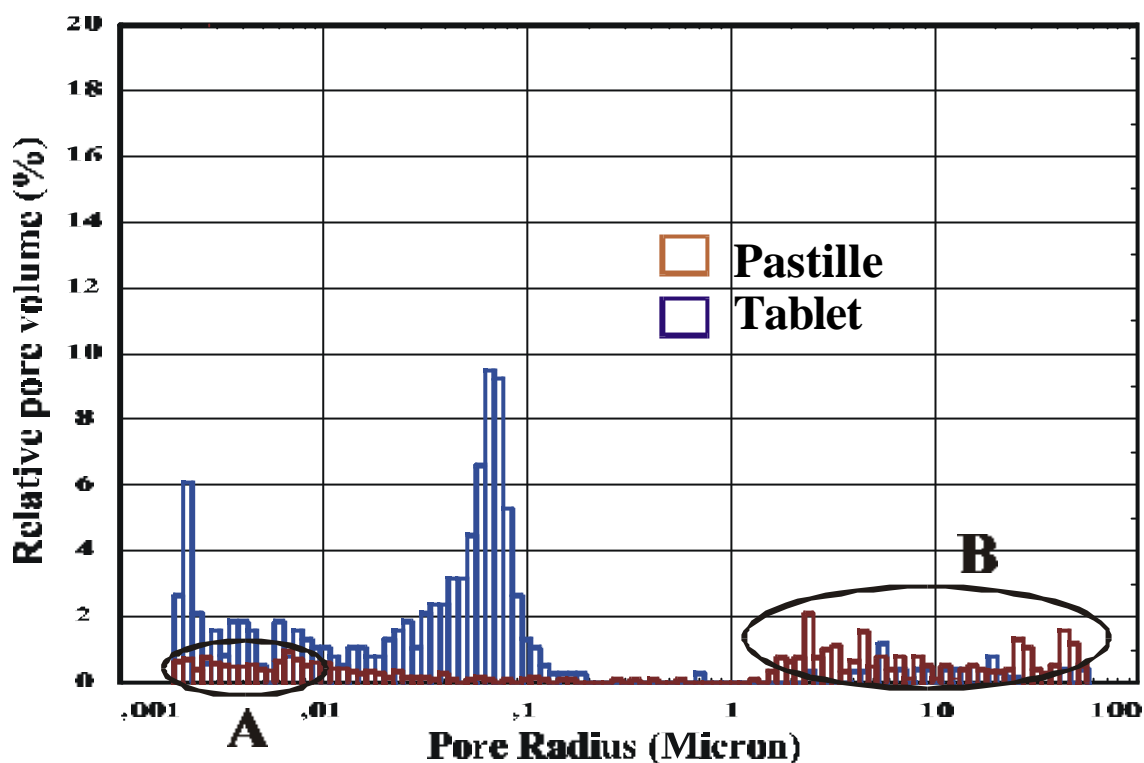


Figure 5-4: Pore size distribution of pastilles and tablets (radius range: 0,001 – 100; histograms number: 100).

Figure 5-4 shows the relationship between the relative pore volume and the pore radius of the pastilles and tablets, respectively. From the histogram the pore size distribution of pastilles and tablets are constituted as bimodal-model. In case of pastilles the first group of histogram (A) is occurrence of porosity due to rapid nucleation on the bottom side of the pastille. Nucleation usually takes place concentrically around the starting point of the cooled surface. However, the dominant pore in the pastilles is placed in a pore diameter range between 1 and 20 μm (B). In case of tablet the dominant pores are placed in a pore diameter range between 0.5 and 1 μm . From the results of analyses the dominant pore size distributions in tablets are smaller than those in pastilles. However, it is analytically found that the total porosity in pastilles is much smaller than the total porosity in tablets. Here the total porosity (%) is defined as the ratio of the sample void volumes (in- and external porosity) to its external volume (inverse of bulk density). It can be observed that cracks are the dominant “pores” that when present on the surface

of pastilles as the molten drop crystallizes. In case of the tablets, it can be seen that the main pore distribution is positioned in the body of tablets when the powder agglomerates.

Figure 5-5 shows SEM photos of the pastilles, surface morphology of the pastilles, grade cross-sections and cross-section of the pastilles. It can be visually confirmed by the SEM photos of Figures 5-5 (b) and (c) that the dominant pore distribution is ranging between 1 and 20 μm and the cracks are formed on the surface of the pastilles. Moreover, pores are constituted the conical form (see Figure 5-5 (d)). Unfortunately, it is impossible to investigate the length and width of porous depth.

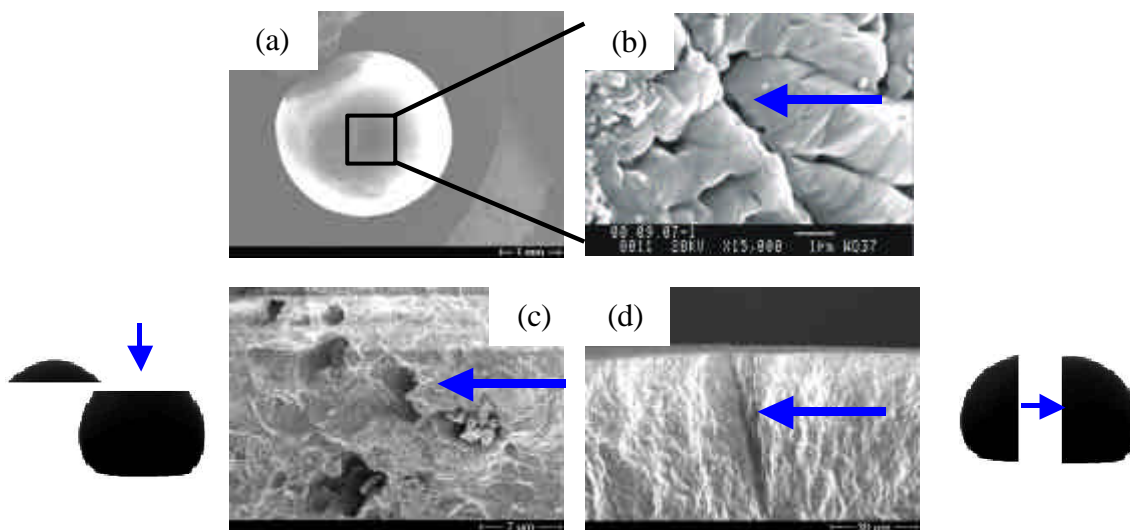


Figure 5-5: SEM photos; (a) pastille, (b) surface morphology (magnification: 15000), (c) grade cross-section and (d) cross-section of pastille (magnification: 4000).

5.4. Total porosity

5.4.1. Total porosity in tablets

Figure 5-6 shows the relationship between the total porosity and the density of the tablet at various compressing pressures which are chosen to 10, 13.5 and 18 MPa. The SEM photos show cross-sections of the tablet. As mentioned before pores are entrapped in the inner body of the tablet. The total porosity is decreased with increasing the compressing pressure. Thereby the density is increased. The founding can be confirmed by SEM

photos, see *Figure 5-6*. At the low compressing pressure, 10 MPa, the structure of tablet was composed as a powder (agglomeration). The total porosity and the density are approximately 15 % and 1.29 g/ml, respectively. However, at the high compressing pressure, 18 MPa, the structure was more compact than the structure of other two compression pressures. The total porosity and the density are approximately 8.5 % and 1.35 g/ml, respectively.

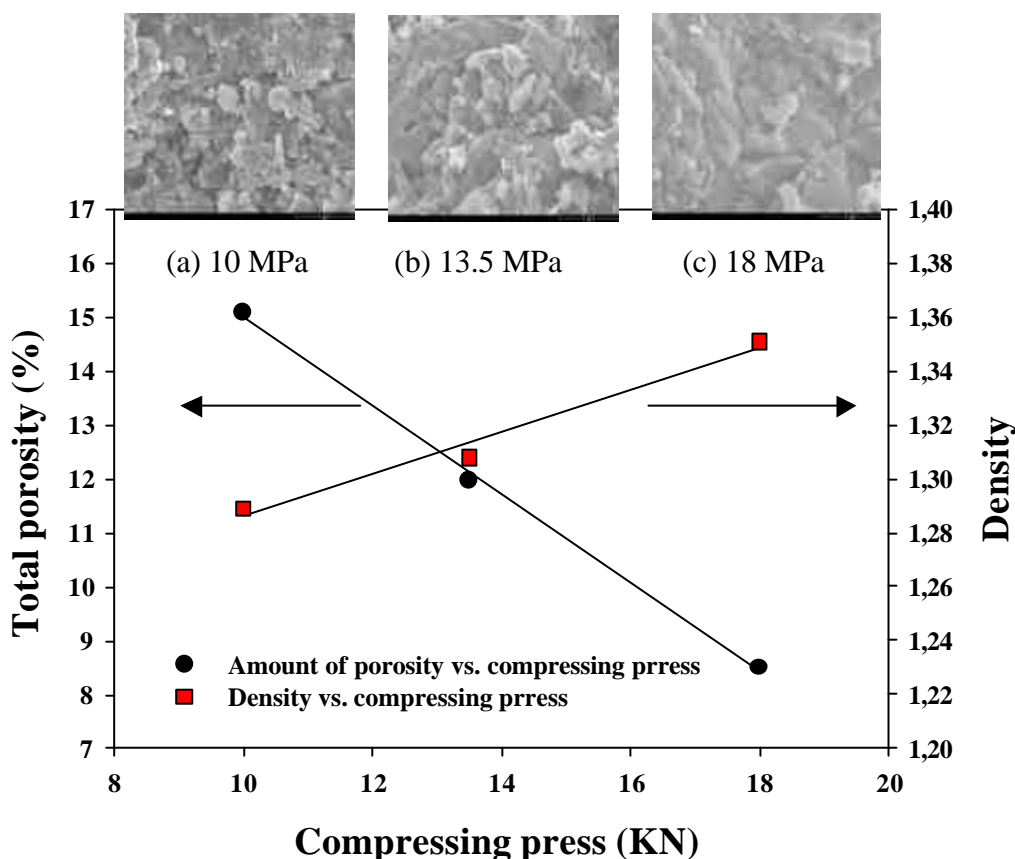


Figure 5-6: Amount of porosity at various compressing pressure (MPa).

5.4.2. Total porosity in the pastille

While the molten drop impacts and crystallizes the cracks and the pores are generated on surface of the pastilles (e.g., *Figure 5-7*). Manufacturing parameters of pastilles should affect an occurrence of micro-pores and crack. The main factors are here: temperature gradient between the melting and the surface temperature of cooled substrate (degree of subcooling), Reynolds number of impacting drop and properties of the substrate. It will be discussed how manufacturing conditions of drops affect the

surface structure of pastilles and the total porosity in a pastille. However, the pore size distribution haven't discussed due to the difficulty of distinguishing. These data will give a basis for a design of the drug delivery system and the improvement of the pastille quality.



Figure 5-7: Surface layer and growth direction of pastilles.

5.4.2.1. Effect of degree of subcooling

To investigate the total porosity, pastilles were produced at different temperatures of the cooled surface. *Figure 5-8* shows SEM photos of surface morphology of the top part of a pastille and the total porosity at different degrees of subcooling. All other solidification parameters are kept constant such as final impacting velocity of 0.28 m/s, surface roughness of 0.23 μm and viscosity of 2.072 mPa·s.

In *Figure 5-8 (a)* are the top part of the pastilles at relatively lower degree of subcooling ($\mathbf{D} = 113$ K) shown where no individual crystals and cracks can be identified. On the other hand in *Figure 5-8 (c)* and *(d)*, the cracking phenomenon with increasing degree of subcooling ($\mathbf{D} = 133$ and 143 K) is shown. This could be caused by relatively high nucleation and growth rates at the initial stage of solidification. According to the relationship between the total porosity and the degree of subcooling, it can be analytically confirmed that the total porosity is increased with increasing the degree of subcooling.

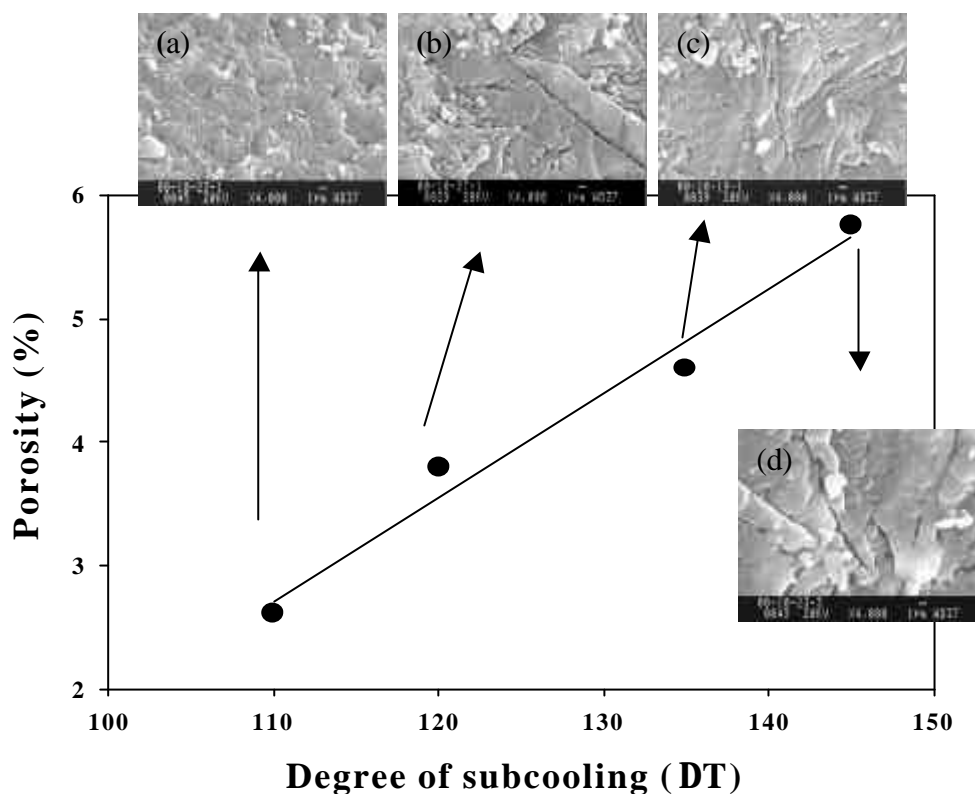


Figure 5-8: Total porosity vs. degrees of the subcooling and surface morphology of the top part of the pastille at different degrees of subcooling ((a) $DT = 113$ K, (b) $DT = 123$ K, (c) $DT = 133$ K, (d) $DT = 143$ K (Magnification: 4000)).

5.4.2.2. Effect of surface properties

Figure 5-9 shows SEM photos of the surface morphology of the top and at the bottom of the pastilles resulting from different roughnesses of the surfaces of the cooling surface. The producing parameters of the pastilles are the final impacting velocity of 0.28 m/s, the viscosity of 2.072 mPa·s and the degree of subcooling of 133 K. The crystals at the bottom part of the pastille have been in contact with the cooled plate. After the impact the molten drops rapidly start to nucleate on the surface of cooled plate and then crystallize in vertical direction because of a high heat transfer. From the SEM photos of Figure 5-9 it is clearly visible that the size of crystal/pore at the bottom of the pastilles is smaller than these of the top part of the pastilles. Therefore, relatively high amounts of porosity are incorporated in the top part of pastille compare to the bottom part of the pastilles. Gum [GUM02] explained that the pores in the top part of surface of the pastille are approximately 10 times large than the pores at the bottom surface of the

pastille. The mentioned effect is, however, influenced by the manufacturing conditions and the physical properties of materials.

The size and the structure of pores on the top and bottom of the pastilles are investigated at different surface roughness, whose surface roughnesses are chosen ranging from 0.15 μm to 0.31 μm . According to *Figures 5-9 (b-1), (c-1) and (d-1)* the size of the pores at the top and bottom of pastilles with the surface roughness of 0.31 μm is larger than that on the surfaces with the two lower roughnesses.

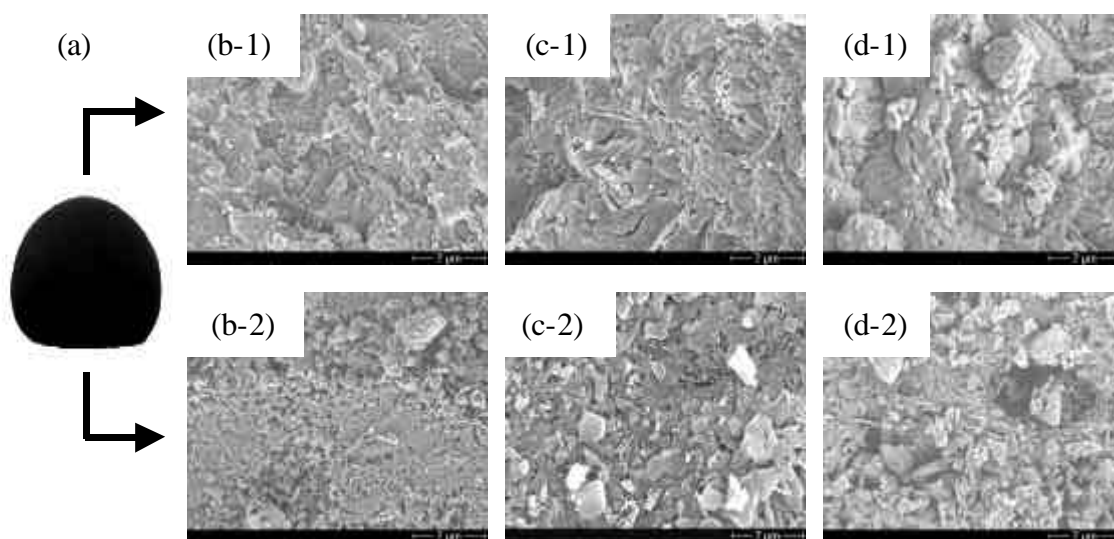


Figure 5-9: Surface morphology of SEM photos of the top and the bottom of pastilles at different cooled plates. (a) side view of pastille, (b-1) and (b-2) surface morphologies of top and bottom of pastille at a smooth plate ($R_a = 0.15$), (c-1) and (c-2) surface morphologies of top and bottom of pastille at a medium plate ($R_a = 0.23$), (d-1) and (d-2) surface morphologies of top and bottom of pastille at a course plate ($R_a = 0.31$).

Figure 5-10 illustrates a porosity measured by a porosimeter on three different surface roughnesses. Each sample of a pastille is analyzed 3 times under the same conditions. From the *Figure 5-10* it can be seen that the total amount of pores is increased with increasing the surface roughness. All was confirmed by SEM photos, *Figure 5-9*.

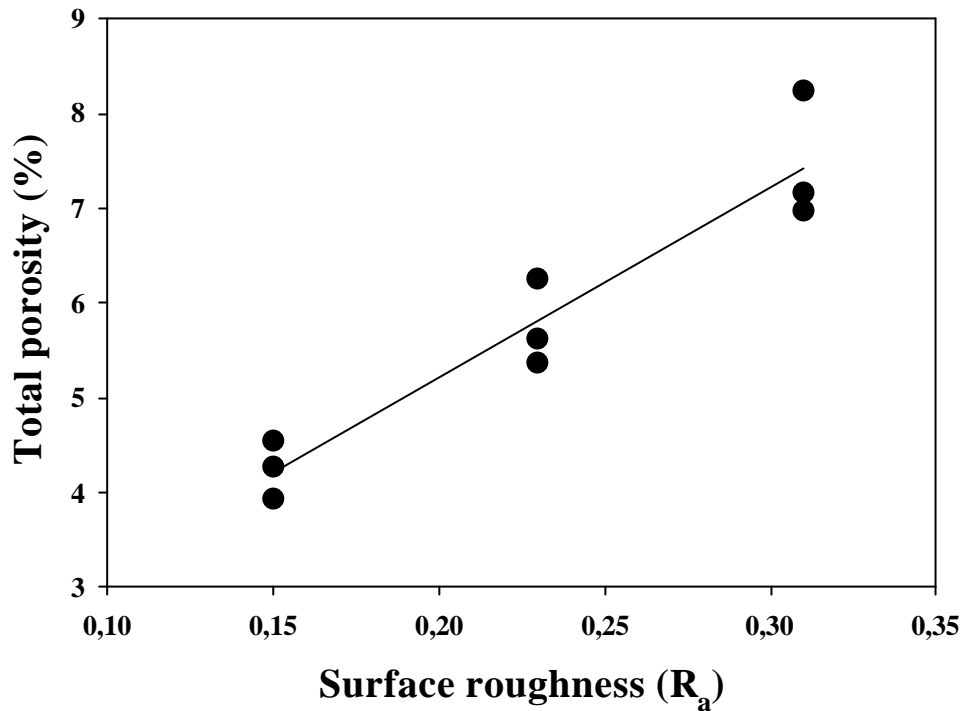


Figure 5-10: Porosity verses surface roughness of 3 different cooled plates.

5.4.2.3. Effect of Reynolds number

Figure 5-11 shows the correlation between the total porosity and the Reynolds number of two-different masses of the drops. The Reynolds number is already defined in chapter 4. The surface roughness of $0.23 \mu\text{m}$, the viscosity of $2.072 \text{ mPa}\cdot\text{s}$ and the degree of subcooling of 133 K are maintained constant. Figure 5-11 shows that the total porosity is logarithmically increasing with increasing Reynolds number. This is due to the effect of the degree of deformation and the effect of high growth rate of pastilles. Here the degree of deformation is defined as the ratio of the final diameter of a drop to initial diameter of a drop. As the impacting velocity is increased the degree of deformation is increased. Thereby, the nucleation and growth rates are increased since the contacted surface area between the drop and the surface of substrate is increased.

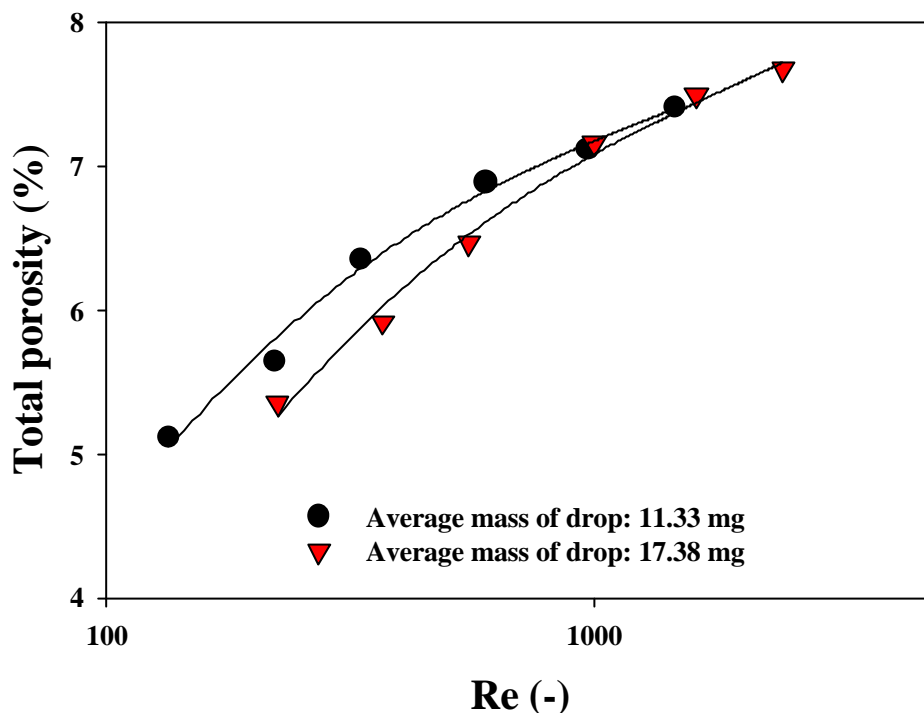


Figure 5-11: Porosity versus *Re* number at two-different masses of drops.

Figure 5-12 illustrates the surface morphology of SEM photos on the top part of the pastilles at various final impacting velocities which are experimentally measured by the high-speed camera. The impacting velocity is corresponding to Reynolds numbers which are varied ranging from 200 to 3000. Increasing the impacting velocities leads to larger surface area of pastilles in contact with cooling plate. Therefore, at high velocities as 1.23 and 1.85 m/s relatively big amounts of porosity are entrapped, because of the high degree of deformation and the high growth rate of pastilles. However, at low velocities as 0.17 and 0.28 m/s relatively small amounts of porosity are entrapped in the pastille, because of the low degree of deformation and the low growth rate of pastilles. Therefore, it can be concluded that the formation of pores is related to the Reynolds number.

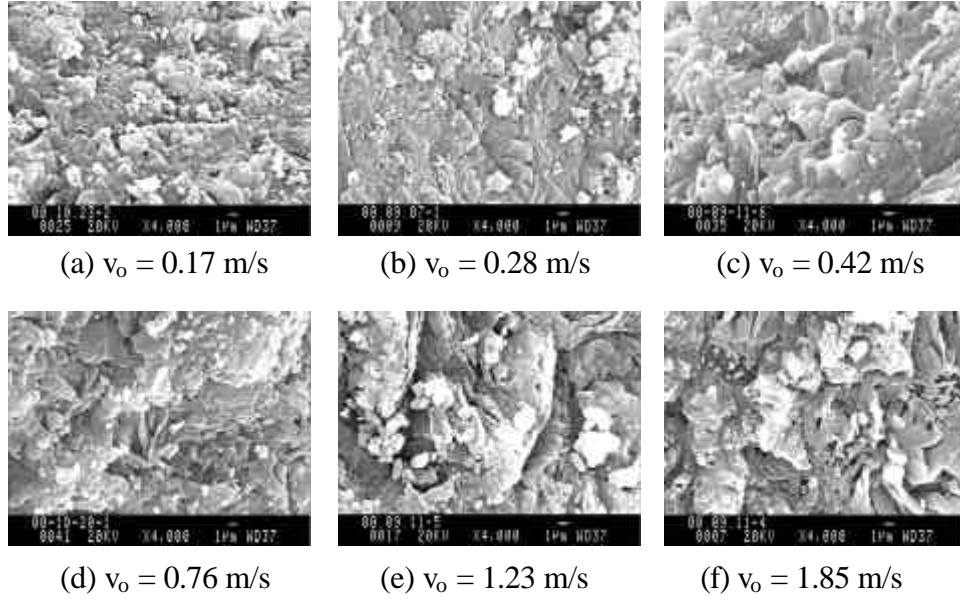


Figure 5-12: Surface morphology shown by SEM photos at the top of pastilles at various impacting velocities ((a) $v_o = 0.17$ m/s, (b) $v_o = 0.28$ m/s, (c) $v_o = 0.42$ m/s, (d) $v_o = 0.76$ m/s, (e) $v_o = 1.23$ m/s, (f) $v_o = 1.85$ m/s (Magnification: 4000)).

5.5. Correlation between total porosity and overall growth rate

During the solidification process the growth rate of liquidus drop is extremely fast due to a high temperature gradient. The high nucleation and growth rate evokes constitutional pores in the surface and the layer of the pastilles. In this section the relationship between the growth rate and total porosity will be investigated. The relationship will be given to determine the processing conditions that are required in order to minimize the porosity in pastilles.

The overall growth rate, G_f is already introduced in *chapters 2 and 3*. As mentioned previously in *equations 2-5 and 4-10*, the layer thickness of pastille, x_s is an input taken from the measured data while the crystallization time, t_c can be numerically found. The overall growth rate, G_f can be derived as:

$$G_f = \frac{x_s}{t_c} = \frac{Df k_s x_s}{0.36 r_l D_o^2} Re^{0.4} \quad (5-1)$$

Here surface roughness ($R_a = 0.23$ mm) is fixed. And assumed that the spreading and rebounding phenomena of drops don't contribute the formation of porosity. *Figure 5-13* shows the relationship between the overall crystal growth rate and the total porosity. It is found that the total porosity has a tendency to increase as the overall crystal growth rate is increasing. This means that the pores and cracks are influenced by the crystallization kinetics (nucleation, growth rate). Especially, pores and cracks are strongly depended the growth rate of the pastilles. The total porosity of the pastilles is increased with the increase of the overall crystallization rate. In case of the pure Bisacodyl the overall crystal growth rate can be explained as a function of total porosity, F by a regression method:

$$G_f = 0.00067 \times 10^{0.0768F} \quad (5-2)$$

By combing *equations 5-1* and *5-2* the total porosity, F can be described as a function of Reynolds number and degree of subcooling.

$$F \cong 13.02 \log \left[\frac{k_s x_s}{r_l L D_o^2} D \Gamma Re^{0.4} \right] + 47.13 \quad (5-3)$$

The entrapped total porosity can be minimized with decreasing the overall growth rate since the degree of subcooling and the Reynolds number is decreased. The relationship between the total porosity and the overall growth rate of pastilles will contribute to the design of the drug delivery system and the selection of manufacturing parameters of pastillation process.

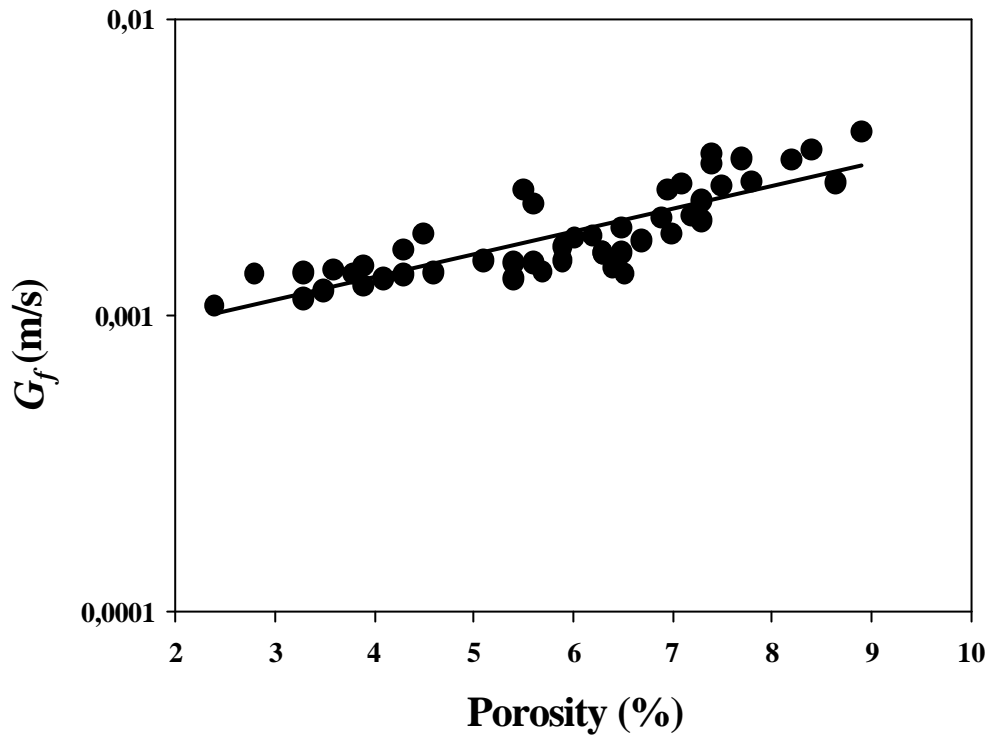


Figure 5-13: Total porosity versus overall crystal growth rate.

6. COATING OF PASTILLES BY A CRYSTALLIZATION PROCESS

6.1. Introduction

Some of the original reasons for coating solid dosage forms, such as pills, granules and tablets, are *e.g.* the unpleasant taste or smell of a drug, the corrosive action of the active ingredients on the mucous membranes of the gastrointestinal tract, the too low stability of the active component in the solid dosage form [GRA95], [KLE95], [PAU02], [SHU98]).

Until now, quite often a spray-drying coating process with an atomizer has been employed to produce coatings in pharmaceutical industries ([GUO02], [JON02], [KAG96], [KAG98], [KAG99], [KAG01], [LIN02], [LIU93], [PAN01], [ROG02], [RUO02], [WAN92], [WNU89], [WU01]). The process is, however, still not optimal since there are problems such as cracking and splitting on the surface of the coating and non-uniformities in thickness of the coatings, because the final coatings are formed in non-crystalline forms.

In pharmaceutical industry the controlled release tablets and pastilles are very important. An agglomerated and non-crystalline formed coating is, however, not so favourable to be used, for a controlled release medicine compared to a medicine with a crystalline-formed coating. For those reasons, pharmaceutical industries needs processes to make crystalline coatings and uniform coatings to control the drug release.

The batch crystallization technology is wildly used for the production of high-value bulk pharmaceutical chemicals (BPC), especially in size and shape control of particles and in separation and purification processes. Unfortunately, only few researchers have applied this process to achieve coatings ([DOR97], [KIM03a], [KIM03b], [SEO01], [TOY94]). In this study, therefore, a crystallization process is applied in order to produce crystalline coatings and to improve the quality of such coatings. The coating

process by crystallization compared to an atomization technique, has several advantages for the production of effective coatings, such as compact equipment, no necessity to use binders and/or additives and the ability to control the coating thickness.

It is found that important parameters to achieve homogeneous crystalline-formed coatings in the crystallization process are the metastable zone width of the solution, the surface nucleation and the crystal growth on the surface of heterogeneous seed particles ([KIM02a], [KIM02b], [KIM02c]).

When the coating materials are chosen, it has to be considered that they should be non-soluble, non-poisonous, non-reactant against the core materials and have good cohesion at the surface of the core materials. The core materials are used as heterogeneous seed materials ([FUN01], [HEF99], [KUB01], [TOY99]). Core materials are generally added at a supersaturation of the solution of the coating material at which a crystal free solution does not nucleate unintended. Nucleation on the surface of the seed particles is occurring at the same conditions as nucleation would occur in a supersaturated solution. After nucleation the crystal growth would progress on the surface of the seed particles. The crystal growth on the surface of the core materials and the surface morphology of the coating are controlled by operating conditions.

This chapter is to examine how a crystalline coating can be formed by solution crystallization and how a operating conditions affect to the surface morphology and the crystal growth rate of the coating. The outlook of this chapter is as follows: An experimental set-up of a crystallization coating process is described in *section 6.2*. The metastable zone width of the solutions will be experimentally investigated in *section 6.3*. Surface nucleation and formation of a coating are visually explained in *section 6.4*. The effect of experimental conditions on surface morphology and growth rate is microscopically elucidated in *section 6.5*.

6.2. Material and experiment setup

6.2.1. Metastable zone width of coating materials

Here a pharmaceutical-grade Isomaltulose ($C_{12}H_{22}O_{11}$) and L-ascorbic acid (Vitamin C, $C_6H_8O_6$) are chosen as coating materials. Distilled water is selected as solvent. The solubility of Isomaltulose and L-ascorbic acid in water and the nucleation behaviour were measured at various temperatures. The solubility is measured at temperatures ranging from 273.15 K to 353.15 K. The equilibrium data were determined by the polythermal method [NYV68]. As equilibrium cell, a cylindrical glass vessel, was used with a thermostatic bath with a PID controller (JULABO F32). The content in the equilibrium cell was stirred. The cell was sealed tightly to protect the system from dust and moisture exchange. Binary mixtures were cooled and heated very slowly at less than 0.05 K/min, especially, near the equilibrium and the nucleation point. The crystal disappearance and occurrence temperatures were precisely measured with a calibrated thermocouple connected to temperature recorder. Each experiment was repeated at least two times. Summarized experimental conditions of measurement of solubility and metastable zone width are shown in *Table 6-1*.

Table 6-1: Experimental conditions of measurement of solubility and metastable zone width.

<i>Experimental conditions</i>	
Solvent	Distilled water
Coating materials	Isomaltulose, L-ascorbic acid
Seeding materials	Bisacodyl pastilles (≈ 2.3 mm)
Percent of loaded seed (core) (%)	0.1 and 0.3
Temperature range (K)	275.15 – 353.15
Agitation speed (rpm)	250
Cooling/heating rate (K/min)	0.05

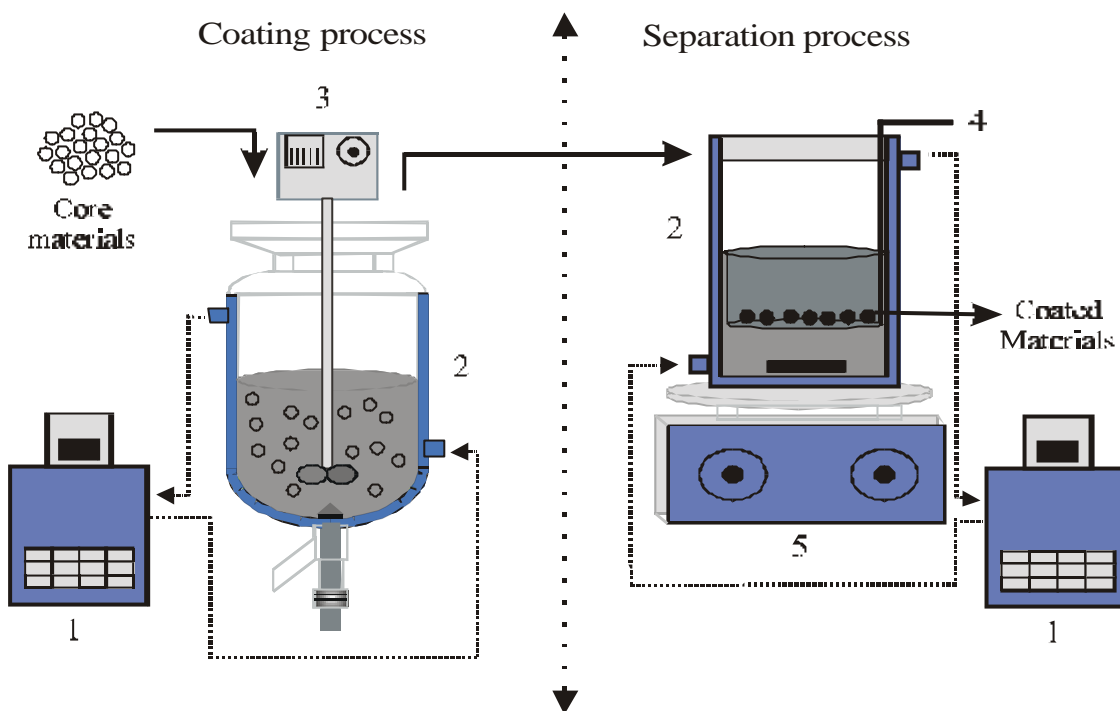
6.2.2. Core materials and procedure of the crystallization coating process

Hemi-spherical pastilles from Bisacodyl powder (bis (p-acetoxyphenyl)-2-pyridylmethane, $C_{22}H_{19}NO_4$) were formed. The pastilles, produced by a melt solidification process as described in *Chapter 4* are used as heterogeneous seeds. The average size of the seeds has a diameter of 2.3 mm [KIM03a]. In order to determine the surface characteristics of Bisacodyl pastilles, spherical type Glass beads and Aluminium oxide (Al_2O_3) beads are also used as heterogeneous seed particles.

The interfacial tension as a function of the surface characteristic of the seed particles and the concentration of solution was measured using the pendant drop method with an optical contact angle measuring system (DAS10, KRUESS GmbH). The solution density plays a fundamental part when determining the interfacial tension. The density measurements (DMA 4500, Anton Paar) are performed by an oscillation method ([WU98], [WU99]).

The batch crystallization apparatus is used for the production of effective coatings and is described in *Figure 6-1*. It consists of 300 ml-double jacketed crystalliser, programmed thermostatic bath, agitator with turbine-type stirrer and separation apparatus with a sieve. The seed particles (heterogeneous core materials) were prepared and loaded into the supersaturated solution after it has been prepared in the crystallizer. In all experimental works the amount of seed particles was about 0.1 wt.%, which is corresponding to total mixtures in weight percent.

The coating process was carried out at different experimental conditions. Parameters varied are such as the concentration of the solutions (Isomaltulose and Vitamin C) and the surface characteristics of the used seed particles, the agitation speed, the degree of subcooling and the retention time. Details of the experimental conditions are summarized in *Table 6-2*. At the end of the coating process the coated seed particles are separated by means of a sieve from the mother liquid and are dried at room temperature. An image analysis system with a CCD camera and the SEM (Scanning Electronic Microscope) technique are used to measure growth rates of the layer thickness of the crystals representing the coating and to investigate the surface morphology and the structure of core materials and coatings, respectively.



1. Thermostatic bath, 2. Batch crystallizer, 3. Agitator, 4. Sieve, 5. Stirrer.

Figure 6-1: Crystallization coating process.

Table 6-2: Experimental conditions of the crystallization coating process (in case of the Isomaltulose as coating material).

<i>Experimental conditions</i>	
Core materials	Hemi-spherical pastilles, spherical type Glass beads and Aluminium oxide
Degree of subcooling (ΔT)	15 - 45
Agitation speed (rpm)	100 - 400
Concentration (wt.%)	50 – 65
Retention time (min)	10 – 180

6. 3. Measurement of metastable zone width

The metastable zone width of the binary systems of Isomaltulose-water and L-ascorbic acid-water were measured. The parameters for the coating process are decided by the metastable zone width revealed macroscopically under the superimposed effects of

operating conditions, such as cooling rate, agitation intensity, fluid dynamic situation, feed concentration, specific properties of the crystallizer and the presents of seeds. A big width of the metastable zone is an essential element for a good coating by crystallization, because nucleation behaviour and growth rates can then more easily be controlled.

Figure 6-2 shows the experimentally determined solubility line and the upper limit of the metastable zone of the Isomaltulose-water and L-ascorbic acid-water systems with seeds and without seeds. Solubility and nucleation lines are directly proportional to the increasing temperature. In Isomaltulose-water system the chosen parameters lead to an area of the supersaturation ranging from 0.249 to 0.314 (g/g) at a range of weight percents of Isomaltulose of 50 wt.% to 80 wt.%. The solution, which has more than 80 wt.% of Isomaltulose, becomes so highly viscous that it prevents from crystallization and would settle to a glass-like state. In the case of less than 50 wt.% of Isomaltulose, however, not Isomaltulose but ice crystallizes. In L-ascorbic acid-water system the selected parameters are as follows: supersaturation is ranging from 0.02 to 0.11 (g/g) and the range of weight percents of L-ascorbic acid is 25 wt.% to 55 wt.%. Above or below the selected weight range, the phenomena of glass-like state and ice crystallization takes place in the L-ascorbic acid-water system, too. Moreover, it can be predicted that the binary mixtures of isomaltulose-water and L-ascorbic acid-water represent eutectic systems.

These results underline that the width of the metastable zone increases with decreasing temperature and with decreasing concentration of the Isomaltulose and L-ascorbic acid. After homogeneous or heterogeneous seed particles were added, nucleation occurred. As shown in *Figure 6-2*, nucleation is generated in the bulk by 0.1 and 0.3 wt. % of heterogeneous seed particles, which are added in such a supersaturated solution. It is found that the metastable zone width became more narrow as the amount of heterogeneous seed particles was increased. The heterogeneous seeds lead to initial bredding which is considered a type of secondary nucleation. The experimental results show that the Isomaltulose-water and L-ascorbic acid-water system have a big metastable zone width, respectively.

In case of a narrow width of the metastable zone (e.g. over 40 wt.% of L-ascorbic acid), easily a too high supersaturation can be created which leads to sudden nucleation which will generate too many crystals. In such an operation it can be difficult and tricky to induce surface nucleation and crystal growth on the surface of the seed particles. As a result, the possibility of nucleation on surface of seed particles (surface nucleation) is very low compared to that of the nucleation in the bulk, which is discussed in *section 6.5*. The nucleation rate is, therefore, an important kinetic parameter for the coating process. It can determine whether there is surface nucleation or not.

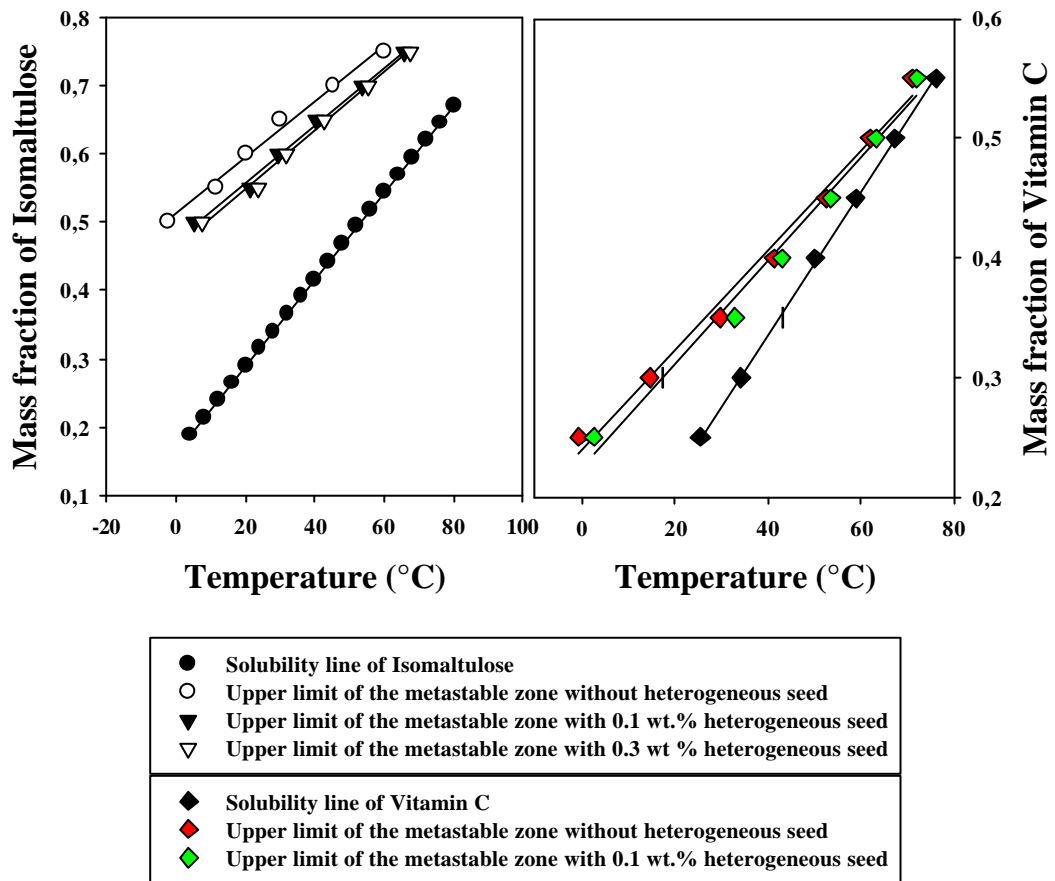


Figure 6-2: Solubility and upper limit of the metastable zone lines with and without seeds of the Isomaltulose-water and Vitamin C-water system. Experimental conditions: agitation speed of 250 rpm and cooling and heating rates of 0.05 K/min.

6. 4. Surface nucleation and formation of a coating

6.4.1. Surface nucleation

Figure 6-3 shows the surface nucleation of the Isomaltulose (Figure 6-3 (a)) and Vitamin C (Figure 6-3 (b)) on the surface of the Bisacodyl. As shown in Figure 6-3 a high number of nuclei occur and the nuclei agglomerate and grow on the surface of the Bisacodyl. As mentioned *chapter 2.3.1.3*, the surface nuclei are formed when the supersaturation is exceeded after nuclei take place in the supersaturated bulk. Therefore, the probability of surface nucleation rises due to increasing number of nuclei in the bulk. However, too high supersaturation (driving force) generates a high number of spontaneous nuclei that automatically restrict the growth rate of the coating layer. There are suitable zone of surface nucleation which is changeable depend on the chemical properties of materials and operating conditions (i.e., cooling rate, agitation speed). It will be visually explained in *section 6.5* in detail. The surface properties of used the seed particles (i.e., interfacial tension) and the specific power input (i.e., agitation speed) are also effect for the formation of the surface nucleation. It also will be explained in *section 6.5*.

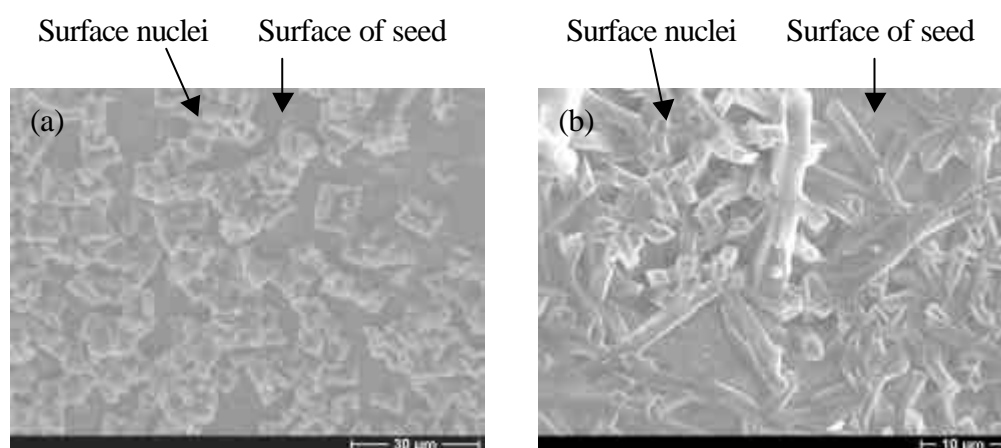


Figure 6-3: Surface nucleation of Isomaltulose (a) and Vitamin C (b).

6.4.2. Formation of a coating

A homogeneous crystalline-formed coating is obtained by solution crystallization

process. *Figure 6-4* shows the SEM photos of seed material (*Figure 6-4 (a)*), coating with Isomaltulose and Vitamin C (*Figures 6-4 (b-1)* and (*c-1*)) and morphology of surface of the coating (*Figures 6-4 (b-2)* and (*c-2*)). In *Figures 6-4 (b-1)* and (*b-2*) it is shown that Bisacodyl seeds are coated by Isomaltulose and Vitamin C. The coatings were very uniform and the surfaces were consistent crystallines. The data of X-ray diffraction (BRUKER axs, D4 ENDEAVOR) proved that these coatings are crystallines. The crystal surfaces of the coatings are found to be composed of evenly systematic pyramid morphology (*Figure 6-4 (b-2)*) and orthorhombic morphology (*Figure 6-4 (c-2)*), respectively.

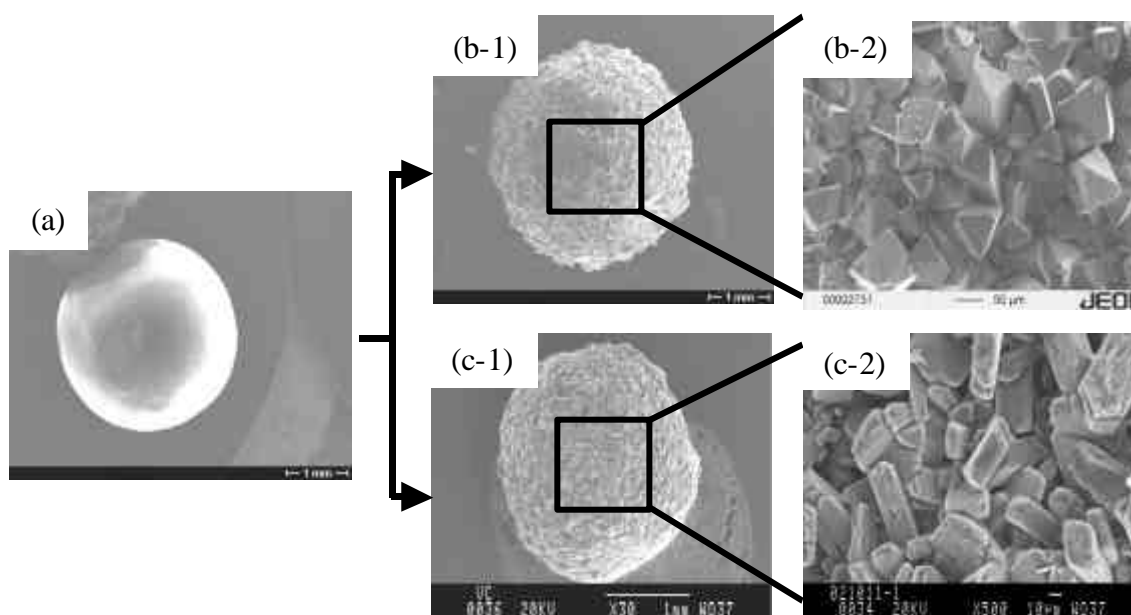


Figure 6-4: Crystalline coating and surface morphology of coating with Isomaltulose and Vitamin C: coating with Isomaltulose (b-1); surface morphology of coating with Isomaltulose (b-2; coating with Vitamin C (c-1); surface morphology of coating with Vitamin C (c-2).

Also Paraffin wax and Urea are used to coat the Bisacodyl pastilles. Ethanol is selected as solvent. *Figure 6-5* shows the coatings and the surface morphologies of coatings with Paraffin wax and Urea. In supersaturated Paraffin wax-ethanol and Urea-ethanol systems, poor quality of coatings were obtained, because these surfaces consisted of non-crystalline material (amorphous). Cracks occur on the surface of the coatings. It can be concluded that the formation of the coating in these systems is happening only by agglomeration mechanism, not by a growth mechanism. There is no surface nucleation

phenomenon on the surface of the seeds. All explanations are confirmed by SEM photos see *Figures 6-5 (b-2) and (c-2)*.

From *Figures 6-4 and 6-5* it is found that the surface nucleation is a crucial parameter for the formation of a crystalline coating.

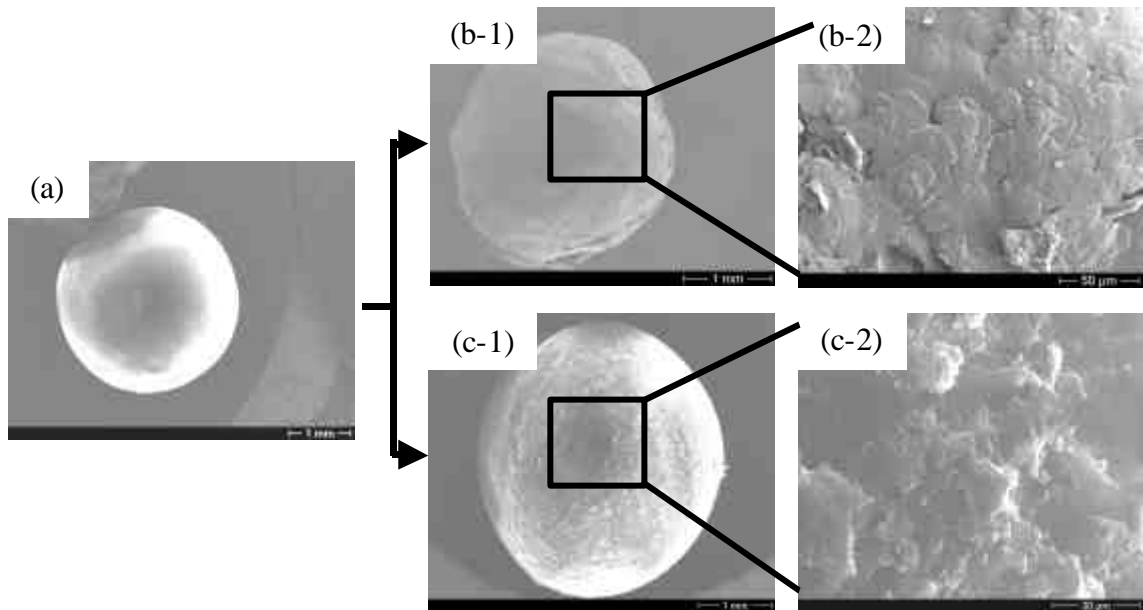


Figure6-5: Coating and surface morphology with Paraffin wax and Urea: coating with Paraffin wax (b-1); surface morphology of coating with Paraffin wax (b-2); coating with Urea (c-1); surface morphology of coating with Urea (c-2).

Isomaltulose is, hereafter, selected as coating materials for further investigation. This is due to the metastable zone width of Isomaltulose-water system which is much bigger than the one of Vitamin C-water system. In order to investigate how the surface nucleation takes place and how the crystals of Isomaltulose grow on the surface of the seed particles a sequence of SEM photos is taken and shown in *Figure 6-6*. A photo per time (min.) detected after nucleation in bulk is shown. The surface nucleation occurs first, and then the fine crystals grow on the surface of the seed. At a short retention time of 10 minutes, it can be seen that the crystals of Isomaltulose start to nucleate directly onto the surface of the Bisacodyl seeds as shown in *Figure 6-6 (a)*. It can be concluded that the interfacial tension between the surface of the seed particles and the solution of Isomaltulose reflecting the degree of subcooling is the main driving force of the surface nucleation on the seeds.

After surface nucleation both mechanisms crystal growth and agglomeration affect the formation of the crystalline coating. The thickness of crystalline coat is rapidly increasing on the surface of the Bisacodyl pastilles as time is progressing. The morphology of crystalline coating on the surface of the seed particles is, however, not uniform until 60 minutes (*Figure 6-6 (d)*), because the agglomeration mechanism is at the beginning dominant in formation of the coating.

At long retention times of 120 or 180 minutes (*Figure 6-6 (e)* and (*f*)), when the size of nuclei pass the critical size, the morphology of the coatings is formed complete uniform, crystalline and it is sequentially grown on the surface as a crystalline layer, because the crystal growth mechanism is dominant in formation of the coating. After 180 minutes the crystal morphology on the surface of the seed particles does not change any more but the thickness of crystalline layer is slowly increased. The influencing parameters on crystal growth and the morphology of crystals on the surface of the seed particles are operating conditions such as degree of subcooling, retention time, agitation speed, concentration of the solution.

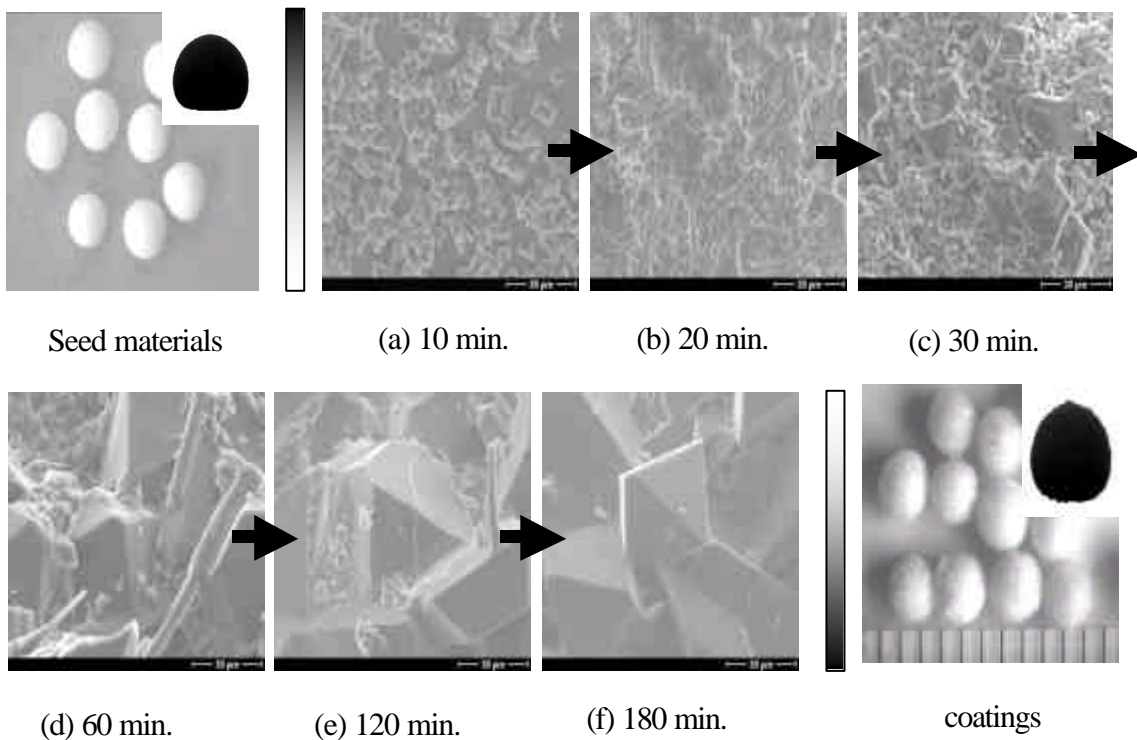


Figure 6-6: Microphotographs of coating surface by elapsed times.

6.4.3. Structure of coating

Figure 6-7 shows the thickness of the coating on the surface of the seed particles (Figures 6-7 (a) and (b)) and a cross section of a coated particle (Figure 6-6 (c)). The structure of the crystalline coating was formed very compact and the crystalline layer is grown in one direction without splitting and cracking. As shown in Figure 6-7 (b) the thickness of the coating reached approximately 110 μm at parameters: agitation rate of 250 rpm, Isomaltulose concentration of 55 wt.%, degree of subcooling of 35 K and retention time of 180 minutes. However, the thickness of the coating is influenced by the experimental parameters. Here the parameters are chosen that high numbers of nuclei are generated on the surface of the seed particle and than the surface nuclei agglomerated and grew together to form a crystalline layer on the surface of the heterogeneous seed particles.

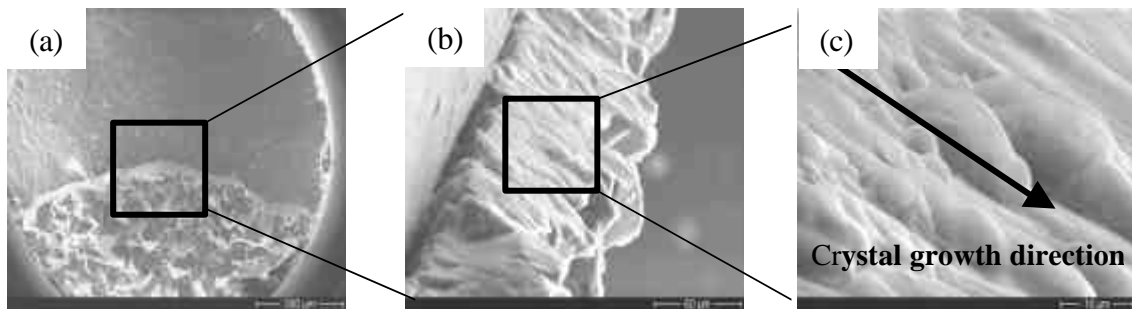


Figure 6-7: SEM photos of the cross section and the surface of the cross section ((a) and (b)); thickness of coating on surface of seed particles, (c); cross section of coated particle).

6.5. Surface morphology and thickness of coating

The quality of a coating is normally estimated by the thickness, by the surface morphology and by the structure. As already noted in section 6.4.3, the structure of the coating layer was formed very compact without cracking (in case of the Isomaltulose-water and Vitamin C-Water systems). Therefore, the thickness and the surface morphology of the coating are discussed here with respect to the experimental

conditions such as interfacial tension, retention time, degree of subcooling and agitation speed. The interfacial tension is induced by the concentration of solution and the surface characteristics of the used seed particles.

6.5.1. Interfacial tension

6.5.1.1. Effect of surface properties

The surface characteristic related to a surface roughness has an effect on the surface nucleation and the crystal growth rate as well as on the crystal morphology of the coating. Especially, the surface nucleation is strongly influenced by the condition of the surface of the seed particles. To investigate the effect of the interfacial tension on the surface nucleation, three different surface characteristics of the seed particles (Bisacodyl pastilles, spherical type Glass beads and Aluminium Oxide beads) are used as heterogeneous seed surfaces (particles). In the first place the interfacial tensions of three different seed materials are measured by the pendant drop method (by contact angle), which is the most practical way to obtain the surface energy (vapor-liquid, solid-vapor and solid-liquid surface tensions) ([WU98], [WU99]). It is well established that contact angle measurements can be used to calculate surface tensions of solids. Generally the interfacial tension is increasing with increased surface roughness.

Figures 6-8 (a-2), (b-2) and (c-2) show SEM photos of the surface morphologies of the coated particles at retention times of 10 minutes. Changes in surface properties play an important role in a coating process. On the surface of Glass seed particles, the nucleation does not occur under the chosen conditions. However, a high number of nuclei are already formed on the surface of the Bisacodyl and Aluminium particles. The degree of surface nucleation is influenced by conditions of the surface properties of the seed particles. The surface nucleation could be improved by a rougher surface of the seed particles.

Figure 6-8 shows how the interfacial tension affects the morphology of crystals on the surface. *Figure 6-8 (a-3)* shows the surface morphology of the coating obtained on very smooth Glass seed particles (interfacial tension: 7.547 mN/m). This uneven surface constitution is easily destroyed, because it is formed out of a number of small

fragments. In *Figure 6-8 (b-3)* the crystal morphology obtained on the Bisacodyl particles with medium surface roughness (interfacial tension: 12.396 mN/m) is presented. A systematic evenly pyramid formed surface of crystals can be seen. These layers grow perpendicular to the surface. In *Figure 6-8(c-3)*, the morphology of the crystalline layers obtained on a surface of Aluminium oxide bead with a coarse roughness (interfacial tension: 18.633 mN/m) can be seen. It can easily be recognized that the surface morphology and the crystal growth on the seed with a high interfacial tension is much coarser and faster than that of the other two surfaces.

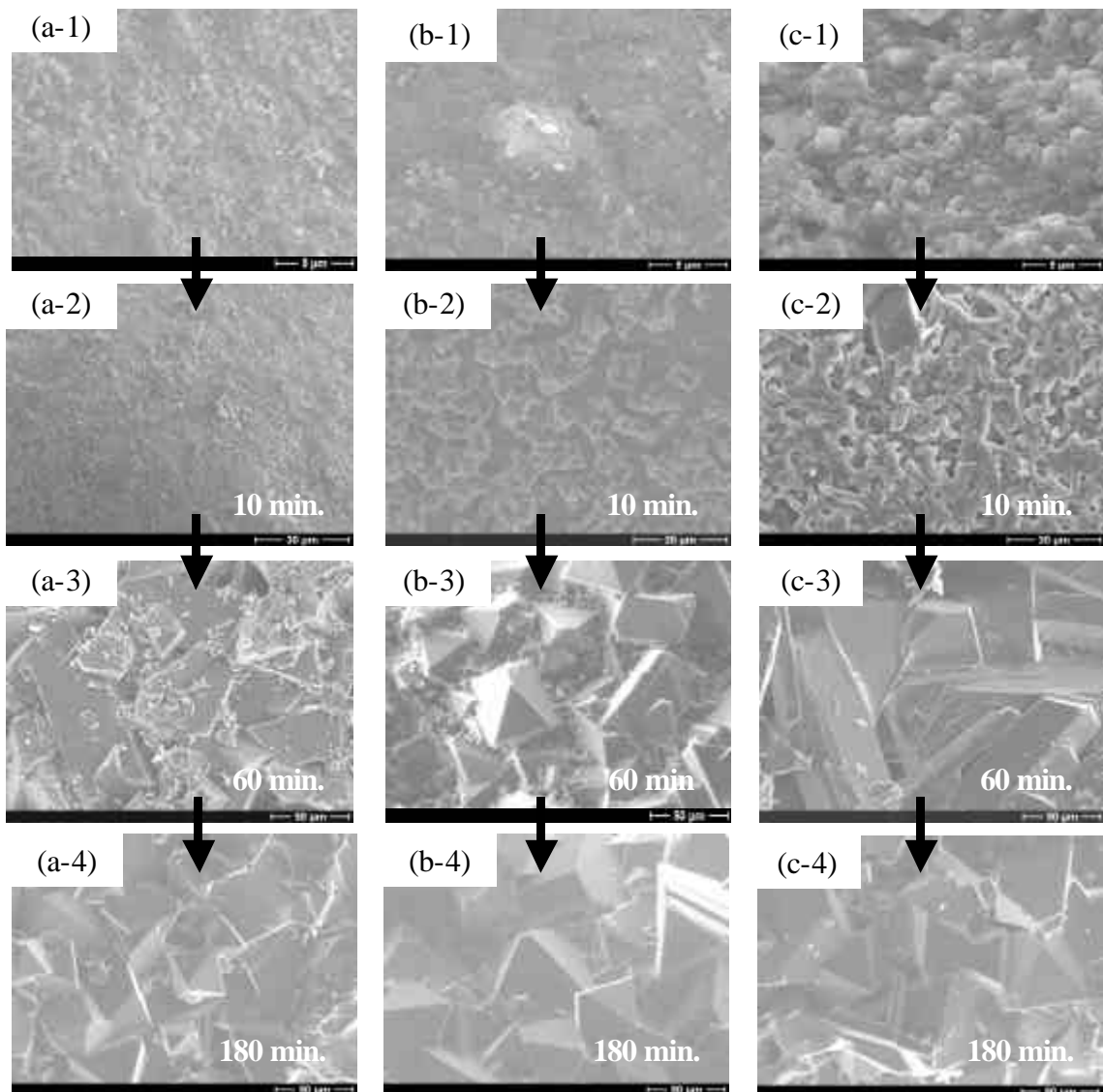


Figure 6-8: Surface morphology of seed particles and coated seed particles ((a); Glass bead, (b); Bisacodyl pastille, (c); Aluminium oxide bead). Experimental conditions: agitation speed of 250 rpm, Isomaltulose of 55 wt.%, degree of subcooling of 35 K and retention time of 10, 60 and 300 minutes.

Figures 6-8 (a-4), (b-4) and (c-4) show the surface morphology of three-different type of seed particles after a retention time of 180 minutes. These photos show that the coatings eventually have the same surface morphology. Since the crystal habit is affected by solvent/crystal interactions it is significantly dominating the formation of the surface morphology. It is clear that the surface properties to a certain extent influence the formation of the surface morphology while the crystal growth proceeds.

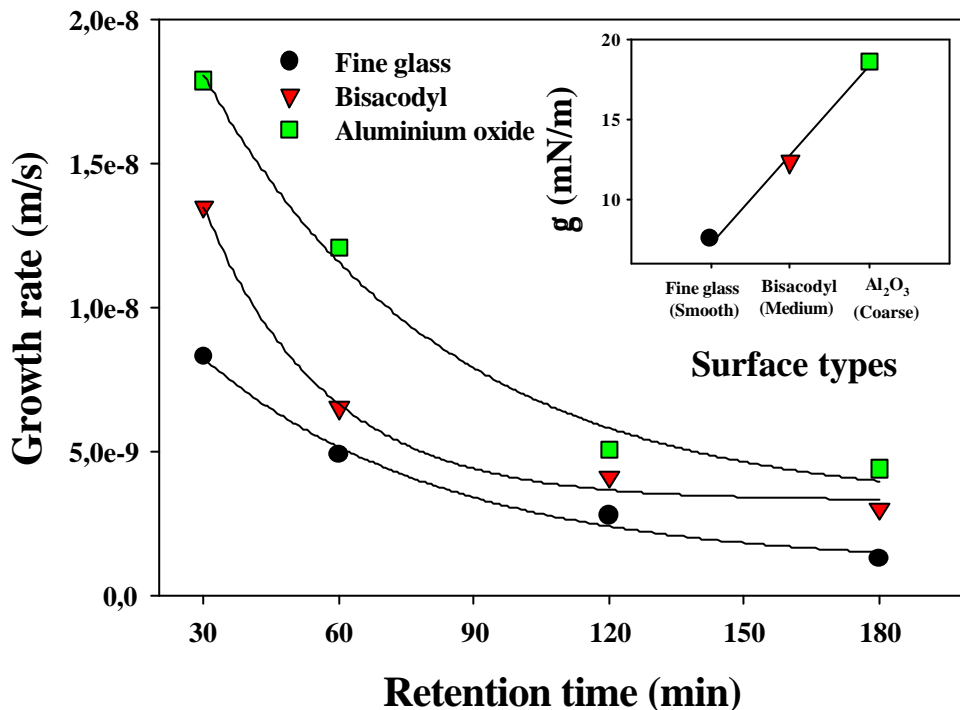


Figure 6-9: Interfacial tension versus surface types and crystal growth rate versus retention time at three different seed materials.

Figure 6-9 shows the relationship between the crystal growth rate on the surface of the seed, G and the retention time at three different interfacial tensions reflecting each seed material. The interfacial tension was measured at constant temperature (283.15 K or degree of subcooling of 35 K) by an optical contact angle measuring system. The interfacial tension increases as the surface of the seed particles gets rougher. A crystal growth rate obtained on the surfaces of the seed particles with a high interfacial tension

is relatively larger than the one of the other two surfaces with lower interfacial tensions. Here, the increasing thickness, D is measured by an image analysis system. The growth rate is defined by the ratio of increasing thickness and retention time, \mathbf{D} as it is mentioned in *equation 2-20*.

6.5.1.2. Effect of concentration of solution

Variable concentrations of the solution are used to investigate the crystal growth rate and the surface morphology of the coating. *Figure 6-10* shows the value of the interfacial tension of each concentration. The measuring temperature of the interfacial tension was always 283.15 K. The interfacial tension is getting higher with increased concentration of Isomaltulose. It seems that the viscosity may play the decisive role at the constant temperature.

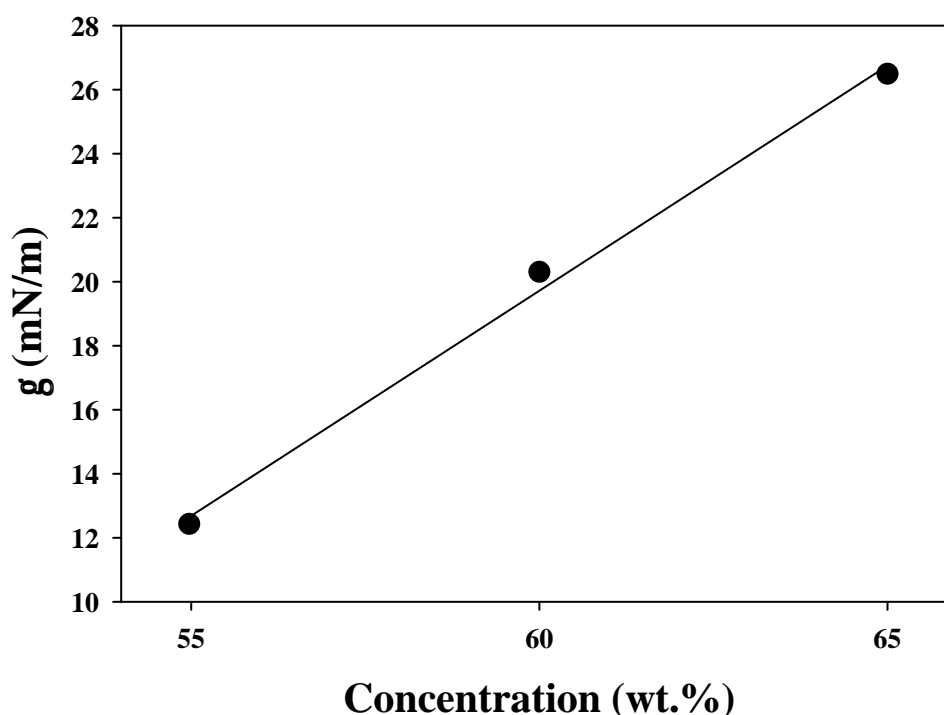


Figure 6-10: Interfacial tension versus concentration at the temperature of 283.15 K.

Figure 6-11 shows the relationship between the growth rate and the concentrations of Isomaltulose at various operating times. In principle the probability of surface nucleation rises with increasing supersaturation, because the number of surface nuclei increases rapidly. The growth rate of the Isomaltulose on the surface of the Bisacodyl pastille is, however, only increased until 55 wt.% of Isomaltulose and then the growth rate begins to decrease. This phenomenon can be seen at each retention time. The reason for the mentioned behaviour is that a high number of nuclei are suddenly occurring not only on the surface of seed particles but also in the bulk, while the supersaturation decreases and the viscosity of solution increases. At such a high supersaturation and viscosity the crystal growth (by agglomeration and the growth mechanism) should be restricted. Therefore, at a relatively high concentration of e.g. 65 wt.% of Isomaltulose the possibility of surface nucleation on the surface of the seed particle is lower than at a lower concentration as 55 wt.% as Isomaltulose.

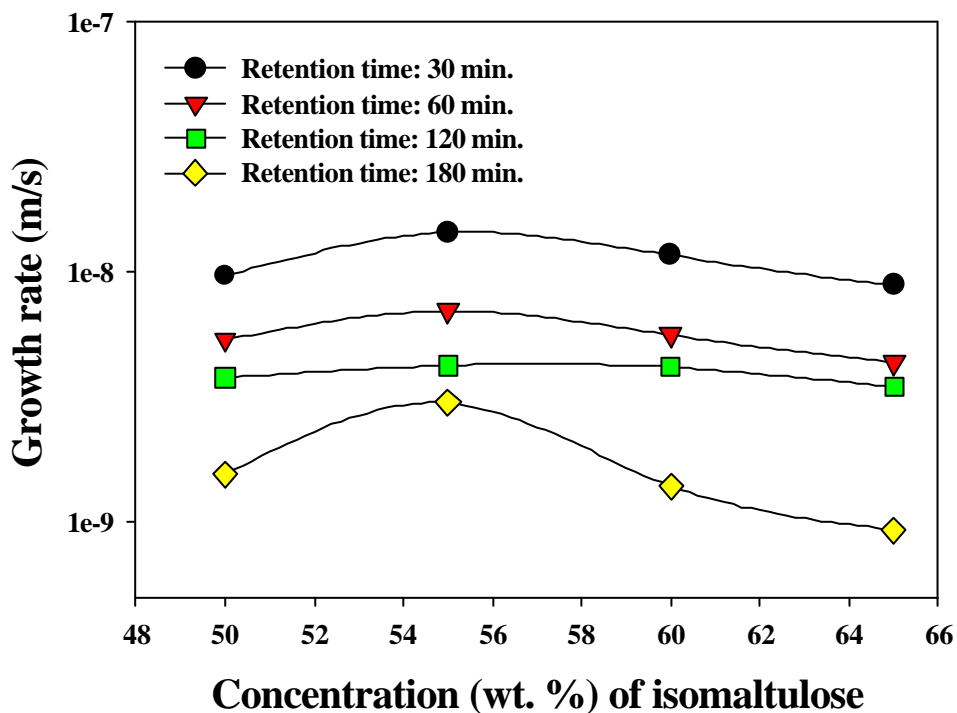


Figure 6-11: Crystal growth rate versus concentration with retention time as parameter.

From the experimental results it is found that the interfacial tension is related to surface properties and solution concentrations. Both parameters have an effect on the surface nucleation and the crystal growth rate as well as on the crystal morphology of the coating.

6.5.2. Effect of degree of subcooling

6.5.2.1. Degree of subcooling

The thickness and the uniformity of coating are investigated to improve the quality of the coating (taste, surface morphology, durability etc.) as function of the degree of subcooling. Normally the crystal growth rate is increased with increasing the degree of subcooling until the maximum value is reached. This maximum is then maintained within certain limits and before the growth rate begins to decrease. The reason for the behaviour lays in the increased viscosity of the solutions, which leads to a reduction in heat and mass transport rates (i.e. nucleation and growth rate). The crystal growth phenomenon can be observed in *Figure 6-12*. The crystal growth rate is increased with increasing degree of subcooling. However, if the degree of subcooling exceeds 35K suddenly the growth rate decreases. Too high degrees of subcooling (driving force) will generate a high number of spontaneous nuclei that automatically reduce the driving force, hence, the growth rate.

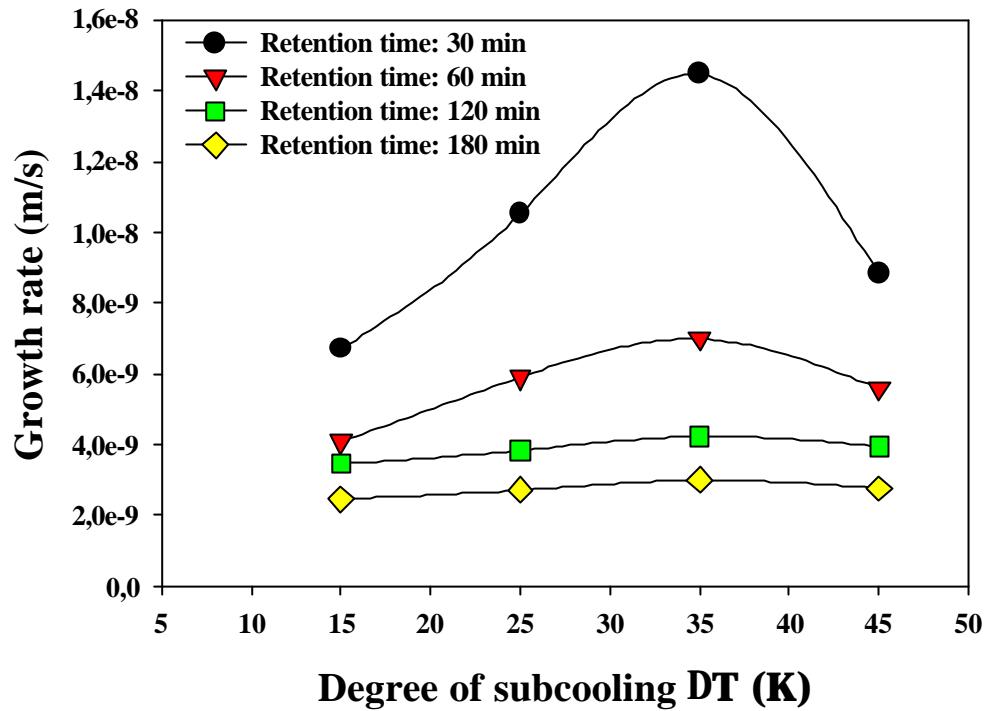


Figure 6-12: Growth rate versus degree of subcooling.

Figure 6-13 shows crystal morphologies at various degrees of subcooling and elapsed retention times. As shown in Figure 6-13 (b) and (c) (at degree of subcooling of 25 K and 35 K), the morphology of the crystals on the surface of the seed particles is still formed non-uniformly at short operation time, 30 minutes. The morphology of the crystals is formed completely uniform and it is sequentially grown on the surface as a crystalline layer at a longer operation time as e.g. 180 minutes.

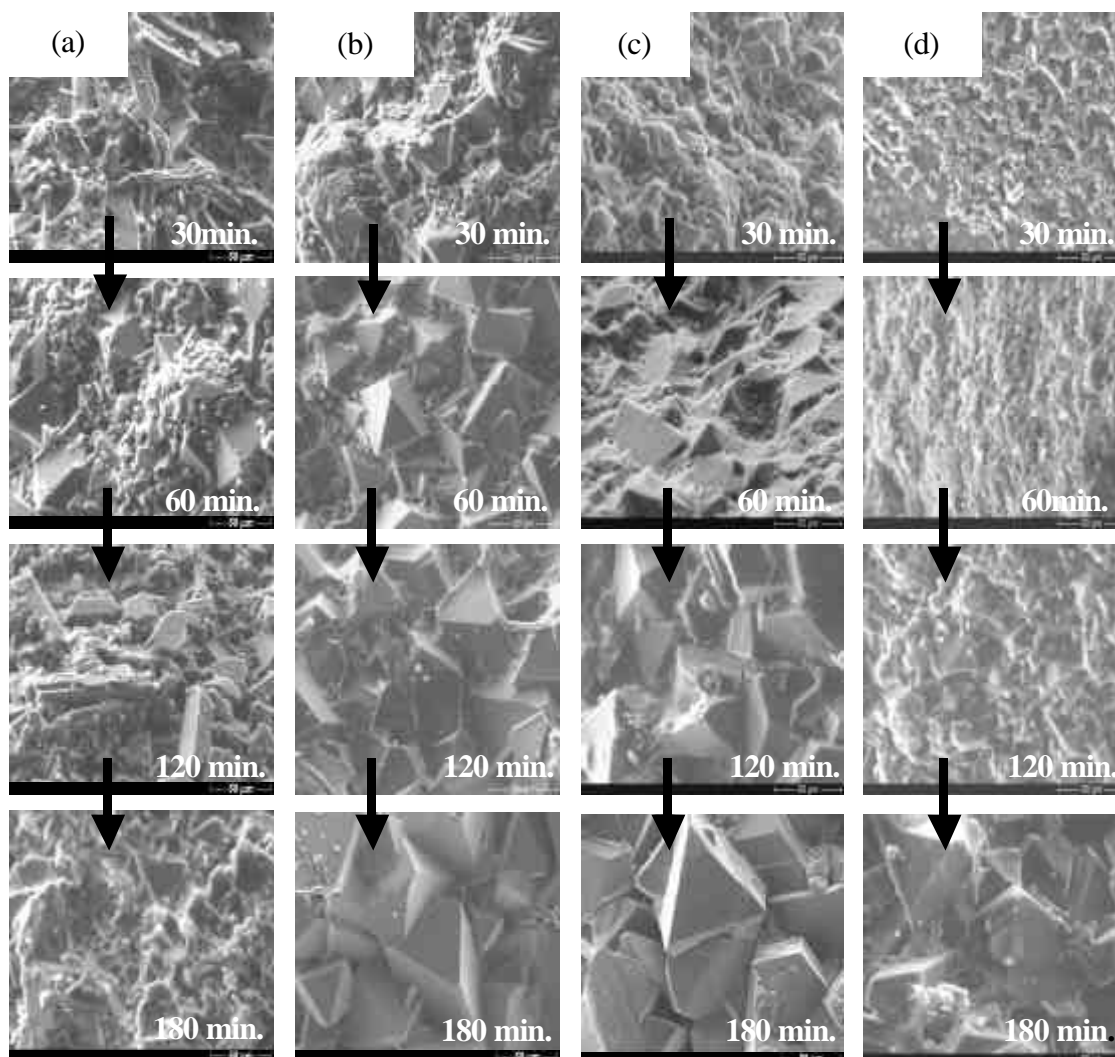


Figure 6-13: Crystal morphologies at a medium surface roughness at various degrees of subcooling and operating temperatures ((a); $DT=45$ K, (b); $DT=35$ K, (c); $DT=25$ K, (d); $DT=15$ K)). Experimental conditions: agitation rate: 250 rpm; Isomaltulose: 55 wt.%.

The crystalline uniformity is further more related to the degree of subcooling. It can be seen that the crystalline uniformity is fast formed with increasing degree of subcooling up to a degree of subcooling of 35 K due to an increasing driving force. However, the crystalline uniformity is quickly decreased again when the degree of subcooling exceeds $DT = 35$ K because of the too high number of spontaneous nuclei. Therefore, the degree of supersaturation of 35 K is the optimum condition to coat the Bisacodyl pastilles in case of the Isomaltulose-water system. The phenomenon of the crystal growth rate on a surface of a seed particle can be confirmed as described in Figure 6-12.

6.5.2.2. Growth rate versus supersaturation in a coating process

In the previous *section 6.5.2.1* the crystal growth rate is investigated by the degree of subcooling on the basis of the experimental data. In solution crystallization normally the growth rate, G is expressed by the power of the supersaturation. *Figure 6-14* shows the relationship between the overall growth rate of the crystals on the surface of the seeds and the supersaturation. The log-log plot of the growth rate and the supersaturation was found to give a straight line. The growth rate is expressed by:

$$G = k_g \mathbf{DC}^g = -3.09 \mathbf{DC}^{5.7} \quad (6-1)$$

Here \mathbf{DC} and g are the supersaturation and the coefficient of crystal growth rate, respectively. The growth rate of Isomaltulose on a surface of the seed system is proportional to the supersaturation to the power of 5.7. The growth rate, G was expressed by the power of the supersaturation, which is related to the growth mechanism (agglomeration and crystal growth). The thickness of the coating, therefore, is controlled by a combination of the two mechanisms agglomeration and crystal growth in the crystallization coating process. At the beginning of crystallization coating process the agglomeration mechanism is dominant in formation of the coating. After the crystals agglomerated, the crystal growth mechanism is dominant in formation of the coating. Moreover, it can be predicted that the experimental result of the mass (thickness) increase of the crystals on the surface of seed particles is smaller than the result of the crystal growth in solution of the Isomaltulose-water system, because the crystals on the surface of seed particles grow only in one direction.

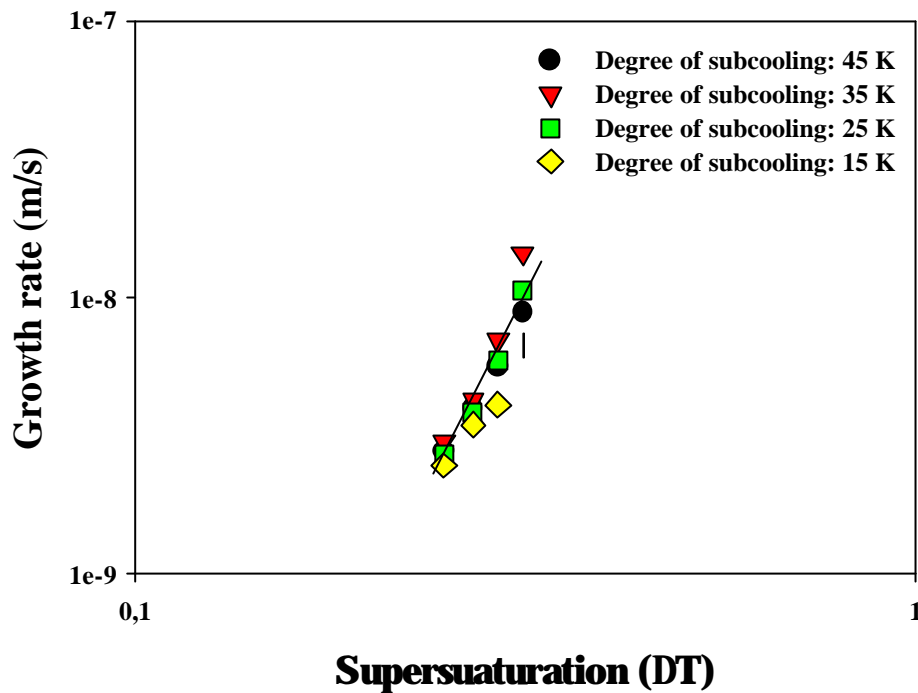


Figure 6-14: Overall growth rate versus supersaturation.

6.5.3. Effect of agitation speed

Here the surface morphology and the growth rate of the coating are investigated as function of the agitation speed. The agitation speed was chosen ranging from 100 to 400 rpm. If the agitation rate is less than 100 rpm, the solid Bisacodyl particles are still just laying on the bottom of the crystallizer and are not suspended. If, however, the agitation rate is higher than 400 rpm a fragmentation process of the crystals takes place. From the microscopic photos the size and shape of crystals on the surface of seed particles were determined experimentally as shown in *Figure 6-15*. It can be visually seen that the crystal sizes on the surface of the seed particles is decreased with increasing agitation rate.

Most of the nuclei are generated by contact with the crystallizer walls and the stirrer. With increasing agitation rate the size of nuclei should become smaller. This phenomenon also takes place on the surface of the seed particles. As shown the *Figure*

6-15 at a high agitation rate of 300 or 400 rpm, relatively small crystals are poisoned on the surface of the seeds compared to a slow agitation rate of 100 or 150 rpm. *Figure 6-16* shows the relationship between the growth rate and the retention time at various agitation rates. Decreasing the agitation rate leads to an increased thickness of coating. It can be proved as described in *Figure 6-16*.

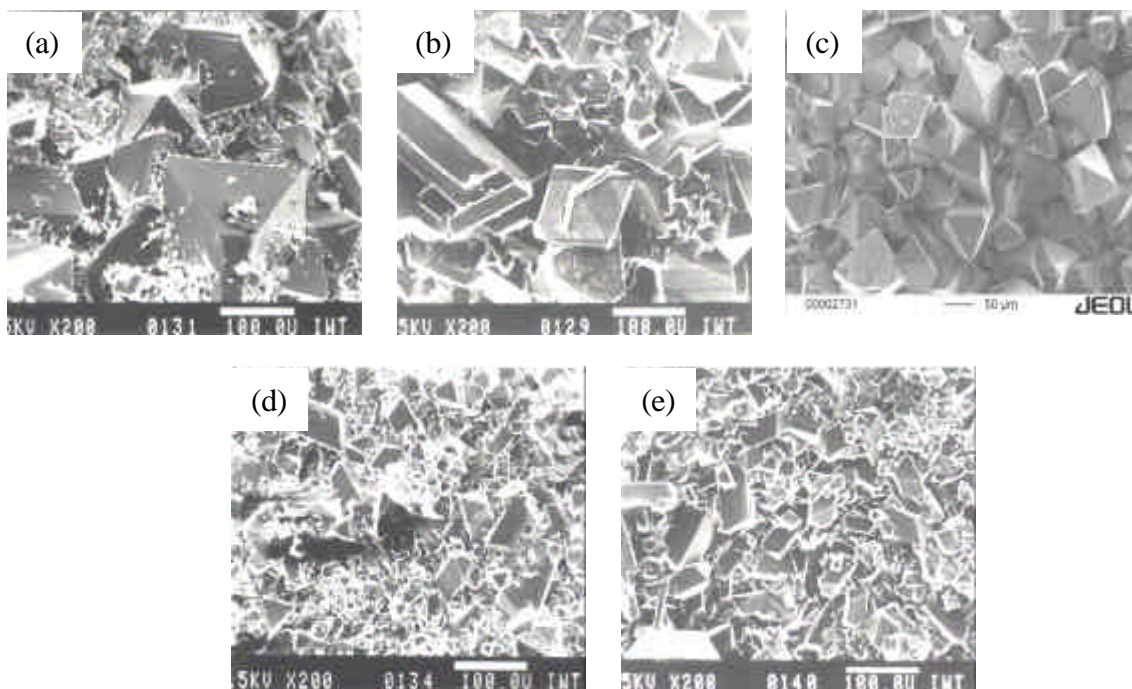


Figure 6-15: Crystal morphologies of seed particle coatings at various agitation rates ((a); 100 rpm, (b); 150 rpm, (c); 250 rpm, (d); 300 rpm, (e); 400 rpm). Experimental conditions: degree of subcooling: 35 K, concentration of Isomaltulose: 55 wt. % and operating time: 180 minutes.

The optimized conditions for an excellent crystalline coating by solution crystallization in the case of the Isomaltulose-water system can be summarized: agitation speed of 250 rpm, concentration of solution of 55 wt.%, degree of subcooling of 35 K and retention time of 180 minutes.

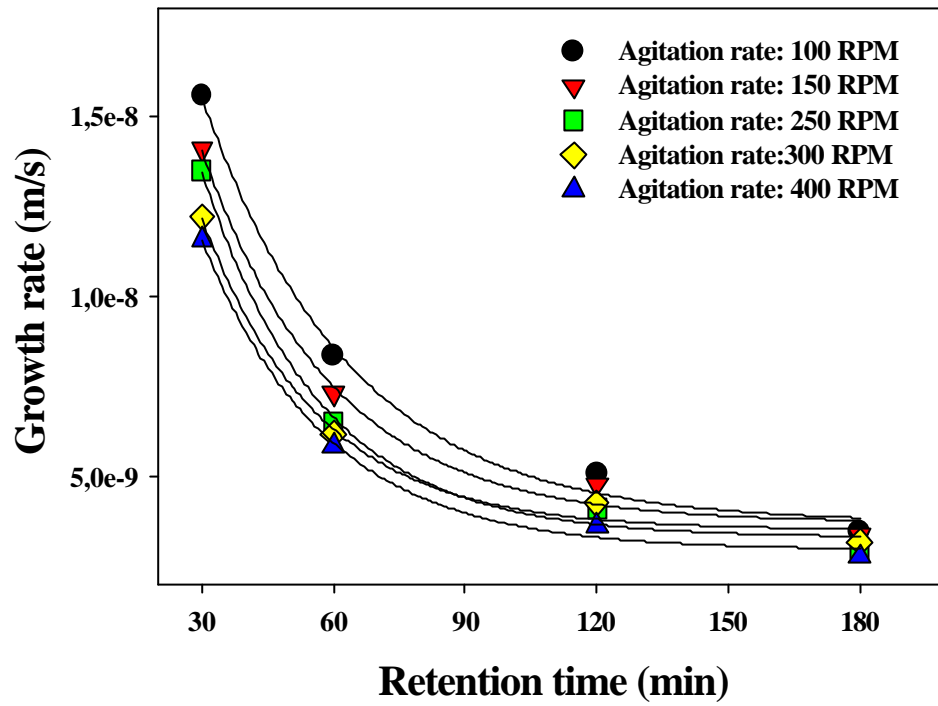


Figure 6-16: Growth rate versus retention time at various agitation rates.

7. SUMMARY

It was shown from literature that drugs needed to be in crystalline form and need crystalline coatings for a controlled release rate. Existing technologies are still not good enough to fulfill wishes of the market. Therefore, the aim of this work is to design a melt solidification (crystallization) technology and to develop a new coating technology by solution crystallization. A pastillation process is employed to achieve the desired size and shape of pastilles and to determine the deformation and crystallization times. The total porosity, the pore structure, the pore size distribution and the behaviour of pore formation are investigated by mercury porosimetry technique. A solution crystallization process is applied to obtain an uniform and crystalline coating.

7.1. Pastillation process

The crystallization and deformation (by pastillation technology) of drops on a cooled substrate is examined to achieve the desired size and shape of the product and to predict the required crystallization time. As example a Bisacodyl melt is chosen. The crystallization occurs immediately after the deformation. The rule of the contact angle of the drop on a substrate is investigated by different experimental variables. The static contact angle is increased with increasing degree of surface roughness. It is, however, decreased with increasing Reynolds number and degree of subcooling. The phenomenon of spreading and rebounding of drops is observed and used to discuss the deformation process. Madejski's model predicts the degree of deformation. It is increased with increasing Reynolds number and found to be proportional to the 0.2 power of the Reynolds number. Using a simple drop solidification model allows to numerically study the degree of deformation based on the achieved experimental data. To estimate the normalized deformation and crystallization times, which are found to be proportional to the Reynolds number to the power of 1.23 the numerical study can also be used. On basis of the crystallization time the solidification equipment (size of equipment, size of crystallizer and speed of cooling belt) can be designed.

7.2. Investigation of porosity in the pastilles

In order to determine the total porosity, the pore structure, the pore size distribution and the behaviour of pore formation, the surface and internal characteristics of pastille and tablets are investigated by the mercury intrusion porosimetry and the scanning electron microscopy (SEM) techniques. To compare the pore structure, the total porosity and the pore size distribution, Bisacodyl tablets are used. It is found that the pore size distribution of pastilles and tablets are constituted in a bimodal-model. The total porosity in pastilles is much smaller than the total porosity in tablets. The micro-pores and cracks are the dominant pores in the pastilles. It is experimentally found that the manufacturing parameters of the pastilles influenced the occurrence of micro-pores and cracks in the pastilles while the molten drop impacts and crystallizes. The total porosity is increased with increasing degree of subcooling, Reynolds number and surface roughness. It is explained via the crystallization kinetics (nucleation, growth rate). It is found that manufacturing parameters of pastilles should affect an occurrence of pores and crack. The main factors are here degree of subcooling, Reynolds number of impacting drop and properties of the substrate. In order to minimize the porosity in the pastilles the relationship between overall growth rate of the pastilles and total amount of porosity is numerically investigated. The total porosity is increased with increasing the overall growth rate. The data of the porosity are estimated because they are necessary for the design of the drug delivery system and the selection of manufacturing parameters.

7.3. Crystallization coating process

A new coating process is developed using solution crystallization. It is experimentally found how the crystalline coating can be formed by solution crystallization and how the operating conditions affect the surface morphology and the crystal growth rate of the coating. The metastable zone width of the binary system of Isomaltulose/water and Vitamin C/water are measured. It is found that a big width of metastable zone is essential for a good coating by crystallization. The mechanism of coating of a seed particle by a crystallization process is defined by a few steps: 1. the generation of a high

number of nuclei on a surface of a seed particle (surface nucleation), 2. a surface nuclei agglomeration, 3. an agglomeration and crystal growth of nuclei and 4. crystal growth to form a layer on the surface of the heterogeneous seeds. Effective crystalline-formed coatings are achieved by this technology. Here the crystal layer is found very compact and without porosity and cracking in the structure of the coating. The crystal growth is influenced by the interfacial tension related to the surface characteristic of the used seed particles and the concentration of the solution. The growth rate of the crystalline coating is increased with an increasing value of interfacial tension of the used seed particles. It is, however, only increased to a certain extent of concentration and then it begins to decrease because of a high number of nuclei. The growth rate of the coating on the surface of seed particles is increased with the increasing degree of subcooling to a certain extent, with increasing retention time and with decreasing agitation speed. The overall growth rate on the surface of the Bisacodyl seed particles in the Isomaltulose/water system is proportional to the supersaturation to the power of 5.7. The surface morphology of coating is investigated by operating conditions. Experimental conditions also have an effect on the crystalline uniformity. The optimized conditions in the case of Isomaltulose-water system have been found experimentally.

In summary the design of a solidification technique of pastilles can be taken from the contact angle, an estimation of the crystallization time and an assessment of the determination of the pores in the pastilles. An effective estimation of size and shape of crystalline dosage form is possible on that grounds, too. It has been proven that a crystallization coating technology can successfully be applied to produce crystalline coatings. This technology will enlarge the field of applications of crystallization technologies.

8. ZUSAMMENFASSUNG

In der Literatur zeigt sich, dass pharmazeutische Wirkstoffe in kristalliner Form vorliegen und kristallin beschichtet sein müssen, um eine kontrollierte Freigabe der Substanzen sicher zu stellen. Vorhandene Technologien sind noch nicht ausgereift genug, um die Wünsche des Marktes zu erfüllen. Folglich ist es das Ziel dieser Arbeit eine Verfestigungstechnologie auf Basis der Schmelzkristallisation zu entwerfen und eine neue Beschichtungstechnologie durch Lösungskristallisation zu entwickeln. Ein Schmelzeerstarrungsprozess wird eingesetzt, um die gewünschte Größe und die Form der Pastillen zu erzielen und um die Deformations- und Kristallisationszeiten festzulegen. Die Gesamtporosität, die Porenstruktur, die Porenkorngößenverteilung und das Verhalten der Porenanordnung wird durch ein Quecksilber-Porosimeter vermessen. Um eine gleichmäßige kristalline Schicht zu erzeugen, wird ein Lösungskristallisationsprozess eingesetzt.

8.1. Pastillationsverfahren

Die Kristallisation und Deformation von Tropfen auf einem gekühlten Träger wurde untersucht, um eine gewünschte Partikelgröße und Form vom Produkt zu erzeugen und die nötige Kristallisationszeit zu bestimmen. Als Beispiel wurde Bisacodyl ausgewählt. Die Kristallisation geschieht sofort nach der Deformation des Tropens nach dem Aufprallen. Die Rolle des Kontaktwinkels vom Tropfen auf einem gekühlten Träger wurde untersucht. Der statische Kontaktwinkel erhöht sich mit steigendem Rauheitsgrad. Er nimmt aber ab mit steigender Reynolds-Zahl und steigendem Unterkühlungsgrad. Das Phänomen von "Spreading" und "Rebounding" von Tropfen wurde beobachtet und für die weiteren Diskussionen über die Deformation benutzt. Nach von Madejski's Model steigt der Deformationsgrad mit steigender Reynolds-Zahl und wurde zur 0.2 Potenz von der Reynolds-Zahl ermittelt. Zur Abschätzung der normalisierten Kristallisations- und Deformationzeit, die proportional zur 1.23 Potenz der

Reynolds-Zahl ermittelt wurden, kann man auch numerische Methoden anwenden. Anhand von der Kristallisationszeit kann die Erstarrungsanlage ausgelegt werden.

8.2. Untersuchung der Porosität in den Pastillen

Für die Ermittlung, der Porenstruktur, der Verteilung der Porengröße und des Verhaltens der Porendeformation, der oberflächlichen und internen Charakterisierungseigenschaften von Tabletten und Pastillen, wurde die Quecksilber Porosimetry und das Ruster-Elektronen-Mikroskopie verwendet. Es wurde gesehen, dass die Porengrößenverteilung von Tabletten und Pastillen durch ein bimodales-Model dargestellt werden kann. Die Porosität in Pastillen ist viel kleiner als die Porosität in Tabletten. Risse sind die dominanten Poren in den Pastillen. Es wurde experimentell herausgearbeitet, dass die Herstellungsparameter von Pastillen das Auftreten von Poren und Rissen beeinflussen, während zeitgleich der geschmolzene Tropfen kristallisiert. Die gesamte Porosität stieg mit steigendem Unterkühlungsgrad, Reynolds-Zahl und Rauheit der Oberfläche. Das wurde über die Kristallisationskinetik (Keimbildung, Wachstumsrate) begründet. Es wurde ermittelt, dass die Herstellungsparameter der Pastillen das Auftreten von Poren und Brüchen beeinflussen. Die Haupteinflußgrößen sind hier der Grad der Unterkühlung, die Reynolds-Zahl der auftreffenden Tropfen und die Eigenschaften des Substrates. Um die Porosität in den Pastillen zu minimieren, wurde die Beziehung zwischen der Wachstumsgeschwindigkeit und der Porosität numerisch untersucht. Die Porosität steigt mit steigender Wachstumsgeschwindigkeit. Die Porositätsdaten wurden intensiv diskutiert, weil sie die, unbedingte Voraussetzung für die Entwicklung von den Arzneimittelherstellungssystemen und für die Wahl der Herstellungsparameter darstellen.

8.3. Kristallisation Beschichtungsverfahren

Ein neues Verfahren wurde unter Verwendung der Lösungskristallisation entwickelt. Es wurde experimentell ermittelt, wie eine kristalline Beschichtung mittels Lösungskristallisation stattfindet und wie die Betriebsbedingungen, die Oberflächenmorphologie und die Kristallwachstumsrate eine Beschichtung beeinflussen

kann. Die metastabilen Bereiche von den binären Systemen von Isomaltulose/Wasser und Vitamin C/Wasser wurden vermessen. Es wurde gezeigt, dass ein breiterer metastabiler Bereich für eine gute Beschichtung günstiger ist. Das Phänomen der Beschichtung eines heterogenen Kristallisationskeimes wurde in einige Schritte zerlegt: 1. Die Bildung einer großen Anzahl von Keimen auf der Oberfläche der Partikeln (surface nucleation). 2. die Oberflächenagglomeration und 3. ein Wachstum gekoppelt mit den agglomerierten Keimen um eine Schicht auf der Oberfläche des heterogenen Keimes zu erzeugen. Es wurde eine effektive kristalline, sehr kompakte Beschichtung mit dieser Technologie erreicht. Das Kristallwachstum wird von der Grenzflächenspannung beeinflusst, welche von den Oberflächeneigenschaften der verwendeten Saatkeime und der Konzentration der Lösung abhängig ist. Das Kristallwachstum der kristallinen Schicht steigt mit steigender Grenzflächenspannung der Partikeln. Es steigt aber nur bis zu einer bestimmten Konzentration und dann beginnt es wegen der hohen Anzahl der Keime wieder zu sinken. Das Kristallwachstum der Beschichtung auf der Oberfläche steigt mit steigendem Unterkühlungsgrad bis zu einer bestimmten Höhe bei steigender Verweilzeit und sinkender Rührerdrehzahl. Das gesamte Wachstum auf der Bisacodyl-Oberfläche im Isomaltulose/Wasser System ist proportional zur 5.7 Potenz der Übersättigung. Die Oberflächenmorphologie der Beschichtung wurde untersucht. Die experimentellen Bedingungen beeinflussen auch die Einheitlichkeit und Gleichmäßigkeit der Kristallinität. Zum Schluss werden die optimalen Bedingungen für das Isomaltulose/Wasser System experimentell ermittelt.

Zusammengefasst: Es wurde eine Strategie entwickelt, für ein Erstarrungsverfahren, welches auf dem Kontaktwinkel, der Kristallisationszeit und der Porenstruktur basiert. Eine effektive Abschätzung der Größe und der Struktur von kristallinen Dosierungsformen ist somit möglich. Eine neue Kristallisationsbeschichtungs-Technologie ist entwickelt worden und kann erfolgreich angewendet werden. Diese Technologie wird die Einsatzmöglichkeiten der industriellen Kristallisationsverfahren erweitern.

9. NOMENCLATURES

A	Constant	(-)
A_{agg}	Attachment factor of agglomeration	(-)
\dot{a}	Coefficient of Reynolds number	(-)
B	Nucleation rate	($\text{m}^{-3}\text{s}^{-1}$)
B_S	Surface nucleation rate	($\text{m}^{-3}\text{s}^{-1}$)
\mathbf{DC}	Supersaturation ($=C-C^*$)	(kmol/m^3)
$\mathbf{DC}_{met, S}$	Metastable supersaturation	(kmol/m^3)
C_i	Molar concentration of component	(kmol/m^3)
C, c	Concentration of solution	(-)
C^*, c^*	Solution concentration at equilibrium	(-)
c_p	Heat capacity	($\text{J}/\text{kg}\cdot\text{K}$)
D	Drop diameter	(m)
D_{AB}	Diffusion coefficient	(m^2/s)
D_o	Initial drop diameter	(m)
D_t	Terminal drop diameter	(m)
d_m	Molecular diameter	(m)
E	Energy	(J)
E_G	Activation energy	(J/mol)
G	Growth rates	(m/s)
G_f	Overall growth rate of pastille	(m/s)
$\mathbf{DG}_{max, S}$	Maximum difference on the free energy	(J/mol)
g	Coefficient of crystal growth rate	(-)
h	Heat transfer coefficient	($\text{W}/\text{m}^2\cdot\text{K}$)
K	Equilibrium (distribution) coefficient, factor	(-)
K_d	Mass transfer coefficient	(m/s)
K_g, k_g	Constants	(-)

NOMENCLATURES

K_r	Growth integration rate constant ($\text{kmol}^{1-r} \text{m}^{3r-2} \text{s}^{-1}$)	(-)
k	Thermal conductivity	(W/m·K)
k_N, k'_N, k''_N	Constants	(-)
L	Latent heat due to solidification	(J/g)
m_T	Suspension density	(kg/m^3)
N	Number of particles per unit suspension volume	(m^{-3})
N_0	Starting number of crystals per unit volume	(m^{-3})
R	Gas constant (8.314J/mol·K)	(-)
R_a	Roughness of crystallizer surface	(μm)
r^*_S	Critical radius	(m)
S	Supersaturation ratio ($S = c/c^* = \sigma + 1$)	(-)
ΔT	Degree of subcooling	(K)
T_{mp}	Temperature of melting point	(K)
T_{sub}	Temperature of the cooled substrate	(K)
t_c	Crystallization time (overall solidification time)	(s)
t_d	Deformation time	(s)
V_p	Pore volume of a pastille	(m^3)
V_b	Bulk volume of a pastille	(m^3)
W	Agitation rate	(-)
x_s	Thickness of drop (crystalline layer thickness)	(m)
Z	Degree of agglomeration	(-)

Greek symbols

\mathbf{a}	Volume shape factor, fraction	(-)
\mathbf{F}	Porosity	(%)
\mathbf{F}_{eff}	Effective porosity	(%)
\mathbf{g}	Surface energy (surface tension)	(J/m^2)
$\mathbf{g}_L, \mathbf{g}_C$	Interfacial tension	(J/m^2)

NOMENCLATURES

\dot{g}	Shear rate	(s ⁻¹)
g	Edge energy	(J/m)
g^{AB}	Surface energy of Lewis acid-base component	(J/m ²)
g^{LW}	Surface energy of Lifshitz-van der Waals component	(J/m ²)
g_i^+	Election-acceptor parameter of the acid-base surface free energy component/Lewis acid parameter of surface free energy	(J/m ²)
g_i^-	Election-donor parameter of the acid-base surface free energy component / Lewis base parameter of surface free energy	(J/m ²)
h, m	Viscosity	(m·Pa·s)
j	Volumetric crystal holdup	(m ³ /m ³)
n	Impacting velocity	(m/s)
r	Density	(kg/m ³)
s	Relative supersaturation (= c/c^*)	(-)
q	Contact angle	(deg.)
t_d	Normalized deformation time (= $t_d n_o / D_o$)	(-)
t_c	Normalized crystallization time (= $t_c n_o / D_o$)	(-)
u_{PN}	Polynuclear growth rate	(m/s)

Subscripts

agg	Agglomeration
$B+S$	Birth and spread
BCF	Burton-Cabrera-Frank
b	Bulk
CL, SL	Crystal-liquid, Solid-liquid
d	Deformation
eff	Effective
i	Inclusion
L	Liquid

<i>PN</i>	Polynuclear
<i>p</i>	Pore
<i>S</i>	Surface, Solid
<i>s</i>	Solidification
<i>t</i>	Total

Superscripts

<i>AB</i>	Acid-base
<i>d</i>	Disperse
<i>g</i>	Kinetic order of growth
<i>LW</i>	Lifshitz-van der Waals
<i>p</i>	Polar
<i>r</i>	Order of the integration process
*	Equilibrium state, saturation

Dimensionless groups

<i>Re</i>	Reynolds number ($= \mathbf{m}_o D_o / \mathbf{m}$) (-)
<i>We</i>	Weber number ($= \mathbf{m}_o^2 D_o / \mathbf{m}$) (-)
<i>Pe</i>	Péclet number ($= D \mathbf{n}_o \mathbf{r} C_p / k$) (-)
<i>k</i>	Dimensionless parameter of Madejski's equation

10. REFERENCES

[ALD92] B. Al-Dhuri, G. Makay:

“Pore diffusion: Dependence of effective diffusivity on the initial sorbate concentration on single and multi-solute batch adsorption systems” J. Chem. Tech. Biotechnol, 55 (1992) 245-252

[BEC35] R. Becker, W. Doering:

“Kinetische Behandlung der Keimbildung in übersättigten Dämpfen” Annalen der Physik, 24 (1935) 5, 719-752

[BEN93] T. Bennett, D. Poulikakos:

“Splat-quench solidification: estimation the maximum spreading of a droplet impacting a solid surface” J. Materials Science, 28 (1993) 963-970

[BEN94] T. Bennett, D. Poulikakos:

“Heat transfer aspects of splat-quench solidification: modelling and experiment” J. Materials Science, 29 (1994) 2025-2039

[BER97] M. Berg, J. Ulrich:

“Experimental-based detection of the splash limits for the normal and oblique impact of molten metal particles on different surfaces” Journal of Materials Synthesis and Processing, 5 (1997) 45-49

[BRO97] L. Bronfenbrener, E. Korin:

“Kinetic model for crystallization in porous medium” Int. J. Heat and Mass Transfer, 40 (1997) 5, 1053-1059

[BUD69] P. P. Budnikov, F. Y. Kharitonov:

“Certain regularities of the formation of pores structure in ceramic materials in swelling” Stroit. Material, (1969) 5-12

[BUE97] H.C. Bülau, J. Ulrich:

“Parameters influencing the properties of drop formed pastilles” In: Proceedings of Crystal Growth of Organic Materials, University of Bremen, Ed: J. Ulrich, Shaker Verlag, 1997, 123-130

[BUE98] H. C. Büla, J. Ulrich:

“Purification potential of drop formed pastilles in dependence on their crystalline structure” In: Proceedings of World Congress on Particle Technology 3, Brighton (UK), 1998, CD-ROM, session 2, Theme E

[BUE99] H. C. Büla:

“Zum Aufreinigungspotential Pastillierter Schmelzen” Ph. D Thesis, University of Bremen, Shaker Verlag, Aachen, 1999

[CAR59] H. S. Carslaw, J. C. Jaeger:

“Conduction of heat in solids” Oxford University Press, 2nd Ed., Oxford, 1959

[CHA91] S. Chandra, C. T. Avedisian:

“On the collision of a droplet with a solid surface” In: Proceedings of Proceedings of the Royal Society of London, Series A, The Royal Society, 1991, 13-41

[COL90] E. W. Collings, A. J. Markwirth, J. K. McCoy, J. H. Saunders:

“Splat-quench solidification of freely falling liquid-metal drops by impact on a planar substrate” J. Materials Science, 25 (1990) 3677-3682

[DEL97] J. P. Delplanque, R. H. Rangel:

“An improved model for droplet solidification on a flat surface” J. Materials Science, 32 (1997) 1519-1530

[DIR91] J. A. Dirksen, R. A. Ring:

“Fundamentals of crystallization kinetic effects on particle size distribution and morphology” Chem. Eng. Sci., 46 (1991) 2389-2427

[DON02a] D. Donchev, J. Ulrich:

“The controlled growth of ice crystals in ceramic slurries” In: Proceedings of 15th International Symposium on Industrial Crystallization, Sorrento, Ed. A. Chianese, Chemical Engineering Transactions, AIDIC, Milano, 2002, 1071-076

[DON02b] D. Donchev, D. Koch, L. Andersen, J. Ulrich:

“Freeze casting-controlled ice crystallization for pore design in green ceramic bodies” In: Proceeding of 9th BIWIC, ed. J. Ulrich, Martin-Luther-Universität Halle-Wittenberg, Halle (Saale), 2002, 237-244

[DOR97] S. V. Dorozhkin:

“Fundamentals of the wet-process phosphoric acid production. 2. Kinetics and mechanism of $\text{CaSO}_4 \cdot 0.5\text{H}_2\text{O}$ surface crystallization and coating formation” *Ind. Eng. Chem. Res.*, 36 (1997) 467-473

[DUL92] F. Dullien:

Porous media-fluid transport and pore structure
San Diego, Academic Press, 1992

[EME01] A. N. Emelyanov:

“Formation of pores in granulated mineral materials under firing” *Glass and Ceramics*, 58 (2001) 1, 34-35

[FOW87] F. M. Fowkes:

“Role of acid-base interfacial bonding in adhesion” *J. Adhes. Sci. Technol.*, 1 (1987) 7-27

[FUK99] S. Fukusako, M. Yamada:

“Recent advances in research on water-freezing and ice-melting problems” *Experimental Thermal and Fluid Science*, 6 (1999) 90-105

[FUK01a] T. Fukasawa, Z. -Y. Deng, M. Ando, T. Ohji, and Y. Goto:

“Pore structure of porous ceramics synthesized from water-based slurry by freeze-dry process” *J. Material Sci.*, 36, (2001) 10, 2523-2527

[FUK01b] T. Fukasawa, M. Ando, T. Ohji, Sh. Kanzaki:

“Synthesis of porous ceramics with complex pore structure by freeze-dry processing” *J. Am. Ceram. Soc.*, 84, (2001) 1, 230-232

[FUN01] K. Funio, H. Takiyama, M. Matsuoka:

“Influences of seed crystals on agglomeration phenomena and product purity of m-chloronitrobenzene crystals in batch crystallization” *Chemical Engineering J.*, 81 (2001) 307-312

[GRA95] C. C. Graham:

“Pharmaceutical Coating Technology” Taylor and Francis Ltd, London, 1995

[GUM02] M. A. van der Gum:

“Production and purification of crystalline particles in a melt – Development of novel melt crystallization process” PhD thesis, University of Delft, Bruno production B.V., Delft, 2002

[GUO02] H. X. Guo, J. Heinämäki, J. Yliruusi:

“Diffusion of a freely water-soluble drug in aqueous enteric-coated pellets” AAPS PharmSciTech., 3 (2002) 2, article 16

[HAM89] H. Hamarani, T. Okada, T. Yoshida:

“Radio frequency and hybrid plasma spraying of ceramics” In: Proceeding of 9th Int. Symp. Plasma Chemistry ISPC, Pugnochiuso (Italy), 1989, 1527-1532

[HAR86] R. W. Hartel, B. E. Gottung, A. D. Raddolph, G. W. Drach:

“Mechanisms and kinetic modeling of calcium oxalate crystal aggregation in a urinlike liquor – Part I: Mechanisms” AICHE J., 32 (1986) 7, 1176-1185

[HEF99] S. K. Heffels, M. Kind:

“Seeding technology: An underestimated critical success factor for crystallization” In: Proceedings of 14th International Symposium on Industrial Crystallization, Cambridge, Ed: J. Garside, 1999

[HIL95] R. Hilfer:

“Transport and relaxation phenomena in porous media” PhD thesis, University of Mainz, 1995

[HOG02] S. Hoge Kamp, M. Pohl, H. Schubert:

“Porosity measurement of fragile agglomerates” In: Proceedings of Symposium Produktgestaltung in der Partikeltechnologie, Pfinztal, Ed. U. Teipel, DWS Verlag GmbH, Karlsruhe, 2002, 453-456

[HOS91] J Hostomsky, A G Jones:

“Calcium carbonate crystallization, agglomeration and form during continuous precipitation from solution” J. Phys. D: Appl. Phys. 24 (1991) 165-170

[JON71] H. Jones:

“Cooling freezing and substrate impact of droplets formed by rotary atomization” J. Phys. D, Appl. Phys., 4 (1971) 1657-1660

[JON02] K. Jono, H. Ichikawa, M. Miyomoto, Y. Fukumori:

- “Review of particulate design for pharmaceutical powders and their production by spouted bed coating” *Powder Technology*, 113 (2000) 269-277
- [KAG96] H. Kage, T. Takahashi, R. Yoshida, H. Ogura, Y. Matsuno:
“Coating efficiency of seed particles in a fluidized bed by atomization of a powder suspension” *Powder Technology*, 86 (1996) 243-250
- [KAG98] H. Kage, T. Takahashi, R. Yoshida, H. Ogura, Y. Matsuno:
“The coating surface and agglomeration of seed particles in a fluidized bed coater” *Advanced Powder Technology*, 9 (1998) 245-259
- [KAG99] H. Kage, M. Dohzaki, H. Ogura, Y. Marsuno:
“Powder efficiency of small particles and their agglomeration in circulating fluidized bed” *Korean J. Chemical Engineering*, 16 (1999) 630-634
- [KAG01] H. Kage, K. Nishihara, H. Ishimatsu, H. Ogura, Y. Matsuno:
“Effect of drying on powder coating efficiency and agglomeration in vitro-fluidized bed” *Drying Technology*, 19 (2001) 359-373
- [KAI70] G. Kaiser, H. Kaiser:
“Pastillieren” *Verfahrenstechnik*, 4 (1970) 390-394
- [KAI89] H. Kaiser:
“Vorrichtung zur Erzeugung von Granalien oder Pastillen aus fließfähigem Material” *Deutsches Patent*, Nr. DE 39 02 957 C2, Patentanmeldung: 1.2.89
- [KAM94] Y. K. Kamath, S. B. Hornby, H. -D. Weigmann, M. F. Wilde:
“Wicking of spin finishes and related liquids into continuous filament yarns” *Textile Res. J.*, 64 (1994) 1, 33-40
- [KAN95] B. Kang, J. Waldvogel, D. Poulikakos:
“Remelting phenomena in the process of splat solidification” *J. Materials Science*, 39 (1995) 4912-4925
- [KIM02a] J. W. Kim, J. Ulrich:
“Coating of pastilles by crystallization process” In: *Proceedings of Symposium Produktgestaltung in der Partikeltechnologie*, Pfinztal, Ed. U. Teipel, DWS Verlag GmbH, Karlsruhe, 2002, 215-233

[KIM02b] J. W. Kim, J. Ulrich:

“Development of a new coating process in pharmaceutical industry by crystallization” In: Proceedings of 15th International Symposium on Industrial Crystallization, Sorrento, Ed. A. Chianese, Chemical Engineering Transactions, AIDIC, Milano, 2002, 825–830

[KIM02c] J. W. Kim, J. Ulrich:

“Formation of a coating by a crystallization process and the effect of interfacial tension on morphology and growth rate” In: Proceeding of 9th BIWIC, Ed. J. Ulrich, Martin-Luther-Universität Halle-Wittenberg, Halle (Saale), 179-186

[KIM03a] J. W. Kim, J. Ulrich:

“New coating process in pharmaceutical industry by crystallization” Eng. Life Sci., 3 (2003) 121-126

[KIM03b] J. W. Kim, J. Ulrich:

“Coating of pastilles by crystallization” Chemie Ingenieur Technik, 75 (2003) 6, 719-724

[KIM03c] J. W. Kim, J. Ulrich:

“Prediction of degree of deformation and crystallization times of molten droplets in pastillation processes” International Journal of Pharmaceutics, 257 (2003) 205-215

[KLE95] E. Kleinbach, T. Riede:

“Coating of solids” Chemical Engineering and Processing, 34 (1995) 329-337

[KUB01] N. Kubota, N. Doki, M. Yokota, A. Sato:

“Seeding policy in batch cooling crystallization” Powder Technology, 121 (2001) 31-38

[KWO99] D. Y. Kwok, A. W. Neumann:

“Contact angle measurements and contact angle interpretation” Adv. Colloid Interface Sci. 81 (1999) 3, 167-249

[LIN02] Y. L. Lin, T. J. Wang, Y. Jin:

“Surface characteristics of hydrous silica-coated TiO₂ particles” Powder Technology, 123 (2002) 194-198

-
- [LIU93] L. X. Liu, J. D. Litster:
“Spouted bed seed coating: the effect of process variables on maximum coating rate and elutriation” *Powder Technology*, 74 (1993) 215-230
- [LIUH94] H. Liu, E. J. Lavernia, R. H. Rangel:
“Numerical simulation of substrate impact and freezing of droplets in plasma spray processes” *Atomization and Sprays*, 4 (1994) 369-384
- [LIUW94] W. Liu, G. X. Wang, E. F. Matthys:
“Thermal analysis and measurements for a molten metal drop impacting on a substrate: cooling, solidification and heat transfer coefficient” *Int. J. Heat Transfer*, 38 (1995) 1387-1395
- [MAD76] J. Madejski:
“Solidification of droplet on a cold surface” *Int. J. Heat Transfer*, 19 (1976) 1009-1013
- [MAO97] T. Mao, D. C. S. Kuhn, H. Tran:
“Spread and rebound of liquid droplets upon impact on flat surfaces” *AIChE Journal*, 43 (1997) 2169-2179
- [MAR93] R. Martin:
“Phenomena of liquid drop impact on solid and liquid surfaces” *Fluid Dynamics Research*, 12 (1993) 61-93
- [MAR96] R. Martin:
“The transitional regime between coalescing and splashing drops” *J. Fluid Mech.*, 306 (1996) 145-165
- [MAS91] K. Masters:
“Spray Drying Handbook” 5th Ed., John Wiley & Sons, New York, 1991
- [MER89] A. Mersmann:
“Design of crystallizers” In: *Proceeding of 10th International Symposium in Industrial Crystallization*, Eds: J. Nyvlt, S. Zacek, Elsevier Sci. Pub. Comp., Amsterdam, 1989
- [MER95] A. Mersmann:

- “General prediction of statistically mean growth rates of a crystal collective” J. Crystal Growth, 147 (1995) 181-193
- [MER01] A. Mersmann, C. Heyer, A. Eble:
“Activated nucleation” In: Crystallization Technology Handbook 2nd Ed., Marcel Decker, Inc., New York, 2001
- [MOR76] S. Mortensen, S. Hovmand:
“Production of non-dusty granular products by fluid bed spray granulation” In: Proceeding of 18th Chemical Engineering Exhibition Congresses, 1976
- [UHL90] H. Uhlemann:
“Kontinuierliche Wirbelschicht-Sprühgranulation” Chem. Ing. Techn., 62 (1990) 822-826
- [MOS81] L. Moscou, S. Lub:
“Practical use of mercury porosimetry in the study of porous solids” Powder Technology, 29 (1981) 1, 45-52
- [MUL93] J. W. Mullin:
“Crystallization” 3rd Ed., Butterworth-Heinemann, Oxford, 1993
- [MYE01] A. S. Myersen:
“Crystals, crystal growth and nucleation” In: The Handbook of Industrial Crystallization, 2nd Ed., Butterworth-Heinemann, Stoneham, 2001
- [NEU74] A. W. Neumann, R. J. Good, C. J. Hope, M. Sejpal:
“An equation-of-state approach to determine surface tensions of low-energy solids from contact angles” J. Colloid Interface Sci., 49 (1974) 291-304
- [NEU94] M. Neumann, J. Ulrich:
“Purification by diffusion washing – a model” In: Proceeding of BIWIC 1994, University of Bremen, Ed: J. Ulrich, Verlag Mainz GmbH, Aachen, 1994, 19-26
- [NIE81] A. E. Nielsen:
“Theory of electrolyte crystal growth: The parabolic rate law” Pure & Appl. Chem., 53 (1981) 2025-2039
- [NIE84a] A. E. Nielsen, J. M. Toft:

- “Electrolyte crystal growth kinetics” J. Crystal Growth, 67 (1984) 278-288
- [NIE84b] A. E. Nielsen:
“Electrolyte crystal growth mechanism” J. Crystal Growth, 67 (1984) 289-310
- [NYV68] J. Nyvlt:
“Kinetics of nucleation in solutions” J. Crystal Growth, 3 (1968) 4, 377-383
- [NYV85] J. Nyvlt, O. Sohnel, M. Matuchova, M. Broul:
“The kinetics of industrial crystallization” Elsevier, Amsterdam, 1985
- [OHA73] M. Ohara, R. C. Reid:
“Modelling crystal growth rates from solution” Prentice-Hall, Englewood Cliffs, 1973
- [ONO97] K. Onoe, T. Shibano, S. Uji, K. Toyokura:
“Secondary crystallization of paraffin solidified on a cooled plane surface” In: Symposium series, American Chemical Society, 1997, 210-219
- [OOS90] H. Ooshima, G. Sazaki, Y. Harano:
“Effects of lysozyme and some amino acids on precipitation of thermolysin” In: Proceeding of 11th International Symposium in Industrial Crystallization, Garmisch-Partenkirchen, Ed: A. Mersmann, 1990
- [OSS94] C. J. van Oss:
“Interfacial forces in aqueous media” Marcel Dekker, New York, 1994
- [PAN01] R. C. Panda, J. Zank, H. Martin:
“Modelling the droplet deposition behaviour on a single particle in fluidized bed spray granulation process” Powder technology, 115 (2001) 51-57
- [PAU03] Z. Paul:
“Pharmaceutical Dosage Forms” In: Ullman`s Encyclopedia of Industrial Chemistry, VCH-Verlag, 6th Ed, 2003
- [PRE70] M. Preger:
“Anwendung und Bauformen der Kuehlwalze” Aufbereitungstechnik, 11 (1970) 551-557

- [PRU98] B. Prunet-Foch, F. Legay, M. Vignes-Adler, C. Delmotte:
“Impacting emulsion drop on a steel plate: Influence of the solid substrate” J. Colloid and Interface Science, 199 (1998) 151-168
- [RAN97] R. H. Rangel, X. Bian:
“Metal-droplet deposition model including liquid deformation and substrate remelting” Int. J. Heat Transfer, 40 (1997) 2549-2564
- [ROG02] T. L. Rogers, A. C. Nelsen, J. Hu, J. N. Brown, M. Sarkari, T. J. Young, K. P. Johnston, R. O. Williams P²:
“A novel particle engineering technology to enhance dissolution of poorly water-soluble drugs: spray-freezing into liquid” European Journal of Pharmaceutics and Biopharmaceutics, 54, (2002) 3, 271-280
- [RUO02] M. Ruotsalainen, J. Heinämäki, J. Rantanen, J. Yliruusi:
“Development of an automation system for a tablet coater” AAPS PharmSciTech., 3 (2002) 2, article 14
- [SAN88] Sandvik Process Systems:
“Rotoform-Verfahren zur Herstellung von Pastillen” Die Chemische Produktion, 3 (1988) 50-52
- [SAN98] Sandvik Process Systems:
“Sandvik: Ihr Partner in der chemischen” Verfahrenstechnik, Firmernschrift, 4, 1998
- [SCH81] H. Schubert:
“Principles of agglomeration” Int. Chem. Eng., 21 (1981) 363-377
- [SEO01] H. H. Seo, K. J. Kim, H. S. Kim, B. S. Park, J. S. Rho:
“A study for surface coating of octogen by crystallization” In: Proceeding of KIChE, Theories and Applications of Chemical Engineering, 7 (2001) 2, 3419-3422
- [SHU98] A. J. Shukla, R. K. Chang, K. E. Avis:
“Pharmaceutical unit operating: Coating - Drug manufacturing technology” Interpharm Press, Buffalo Grove III, 1998
- [SMO17] M. von Smoluchowski:

“Versuch einer mathematischen Theorie der Koagulationskinetik Kolloider Lösungen” Zeitschr. Phys. Chem., 92 (1917) 129-135

[SPE96] J. K. Spelt, D. Li:

“The equation of state approach to interfacial tension” Marcel Dekker Inc., New York, 1996

[STE84] M. L. Steemson, E. T. White, R. J. Marshall:

“Mathematical model of the precipitation of a bayer plant” Light Metals, (1984) 237-245

[STR68] R. F. Strickland-Constable:

“Kinetic and mechanisms of crystallization” Academic Press, London, 1968

[TAK96] S. Takahashi:

“Study on contact angle of Au, Ag, Cu Al and Al alloys to SiC” J. Materials Sci., 31 (1996) 1797-1802

[TAM22] G. Tamman:

“Aggregatzustände. Die Zustandsänderung der Materie in Abhängigkeit von Druck und Temperature” Leopold Voss., Leipzig 1922

[TOY94] K. Toyokura, I. Hirasawa:

“Surface nucleation, secondary nucleation and their effects on crystal on crystal growth rate and crystal purity” In: Proceeding of BIWIC, University of Bremen, Ed: J. Ulrich, Bremen, 1994, 64-70

[TOY99] K. Toyokura, M. Nishiura, I. Tanaka, Y. Kitaoka:

“Induction time of surface nucleation of D-SCMC on L-SCMC seed crystal and the growth rate of L-SCMC seed crystal in DL-SCMC supersaturated solution” In: Proceeding of 14th International Symposium on Industrial Crystallization, Ed: J. Garside, Cambridge, 1999

[ULR97] J. Ulrich, H. Mohameed, S. -B. Zhang, J. J. Yuan:

“Influence of the pH-value on the growth and dissolution rate of potassium chloride” Bull. Soc. Sea Water Sci. Jpn., 51 (1997) 2, 73-77

[ULR02] J. Ulrich:

“Solid layer crystallization” In: Melt Crystallization: Fundamentals, Equipment and Applications. Aachen, Shaker Verlag, 2003

[VEL72] D. van Velzen, R. Lopes Cardozo, H. Langenkamp:

“Liquid viscosity and chemical constitution of organic compounds-A new correlation and a compilation of literature data” Commission of the European Communities, Luxembourg, 1972

[WAN92] G. -X. Wang, E. F. Matthys:

“Numerical modelling of phase change and heat transfer during rapid solidification processes: use of control volume integrals with element subdivision” Int. J. Mass Transfer, 35 (1992) 1, 141-153

[WAN02] X. Y. Wang, H. Zhang, L. L. Zheng, S. Sampath:

“An integrated model for interaction between melt flow and non-equilibrium solidification in thermal spraying” Int. J. Heat and Mass Transfer, 45 (2002) 2289-2301

[WAT92] T. Watanabe, I. Kuribayashi, R. Honda, A. Kanzawa:

“Deformation and solidification of a droplet on a cold substrate” Chem. Engineering Science, 47 (1992) 12, 3059-3065

[WES98] S. Westermarck, A. M. Juppo, K. Koironen, J. Yliruusi:

“Mercury porosimetry of pharmaceutical powder and granules” J. Porous Materials, 5 (1998) 77-86

[WHI91] J. L. White:

“Twin screw extrusion: Technology and principles” Hanser Publishers, New York, 1991

[WIL71] W. R. Wilcox:

“Preparation and properties of solid-state materials” Lefever, New York, 1971

[WIN01] K. Wintermantel, G. Wellinghoff:

“Layer crystallization and melt solidification” In: Crystallization Technology Handbook 2nd Ed., Marcel Decker, Inc., New York, 2001

[WNU89] P. Wnukowski, F. Setterwall:

“The coating of particles in a fluidized bed (Residence time distribution in a system of two coupled perfect mixers)” *Chemical Engineering Science*, 44 (1989) 493-505

[WU98] W. Wu, G. H. Nancollas:

“Kinetics of heterogeneous nucleation of calcium phosphates on anatase and rutile surfaces” *J. Colloid and Interface Sci.*, 199 (1998) 206-211

[WU99] W. Wu, G. H. Nancollas:

“Determination of interfacial tension from crystallization and dissolution data: a comparison with other methods” *Adv. Colloid Interface Sci.*, 79 (1999) 229-279

[WU01] C. Wu, James W. McGinity:

“Influence of ibuprofen as a solid-state plasticizer in eudragit® RS 30D on the physicochemical properties of coated Beads” *AAPS PharmSciTech.*, 2 (2001) 4, article 24

[YOU05] T. Young:

“Young's works” *Philos. Trans., R. Soc. XCII* 12, 1 (1802) 140-170

[ZHA97] X. Zhang, O.A. Basaran:

“Dynamic surface tension effect in impact of a drop with a solid surface” *J. Colloid and Interface Science*, 187 (1997) 166-178

PUBLICATIONS

Jung-Woo Kim, Danail Donchev, Joachim Ulrich, Investigation of the entrapped porosity in pastilles by a mercury porosimeter technique, *International Journal of Pharmaceutics*, (2003, submitted)

Jung-Woo Kim, Joachim Ulrich, Manufacturing and coating of pastilles by a novel crystallization processes, *Journal of Technology & Health Care*, (2003, to be published)

Jung-Woo Kim, Joachim Ulrich, Coating of pastilles by crystallization, *Chemie Ingenieur Technik*, 75 (2003) 6, 719-724

Jung-Woo Kim, Joachim Ulrich, Prediction of degree of deformation and crystallization times of molten droplets in pastillation processes, *International Journal of Pharmaceutics*, 257 (2003) 205-215

Jung-Woo Kim, Joachim Ulrich, New coating process in pharmaceutical industry by crystallization, *Engineering Life Science in Chemical Engineering and Technology*, 3 (2003) 3, 121-126

Kwang-Joo Kim, **Jung-Woo Kim**, Joo-Seung Chae, Seung-Kon Ryu, Purification of naphthalene from coal tar distillate by solution and melt crystallization, *Separation Science and Technology*, 38 (2003) 11, 2407-2427

Jung-Woo Kim, Joachim Ulrich, Manufacturing and coating of pastilles by a novel crystallization processes, 7th European Society for Engineering and Medicine, Halle, Ed: N. D. Black, 2003

Jung-Woo Kim, Joachim Ulrich, Coating of Pastilles by Crystallization Process, *Symposium Produktgestaltung in der Partikeltechnologie*, Pfinztal, Ed: U. Teipel, DWS Verlag GmbH, Karlsruhe, 2002, 215-233

Jung-Woo Kim, Joachim Ulrich, Development of a new coating process in pharmaceutical industry by crystallization, 15th International Symposium on Industrial Crystallization, Sorrento, Ed: A. Chianese, Chemical Engineering Transactions, AIDIC, Milano, 2002, 825–830

Jung-Woo Kim, Joachim Ulrich, Formation of A coating by a crystallization process and the effect of interfacial tension on morphology and growth rate, 9th BIWIC, Ed: J. Ulrich, Martin-Luther-Universität Halle-Wittenberg, Halle (Saale), 179-186

CURRICULUM VITAE

Jung-Woo Kim

Martin-Luther-Universität Halle-Wittenberg
FB Ingenieurwissenschaften
Institut für Verfahrenstechnik/Thermische Verfahrenstechnik
Hoher Weg 7
D-06120 Halle (Saale)
Tel. +49 (345) 55-28403 (O), +49 (345) 678-2826 (H)
E-mail : jungwoo-kim@lycos.com
Date of Birth : August. 20. 1972
Birthplace : KyoungNam / Korea
Marital Status : Married, One daughter



EDUCATION

Doctor of Engineering (06/2000–12/2003), Department of Chemical Engineering, University of Halle, Germany

Thesis title: Manufacture and characteristic of pastilles and their coating by crystallization process

Thesis supervisor: Prof. Dr.-Ing. habil. Joachim Ulrich

Master of Engineering (03/1998–02/2000), Chemical engineering, ChungNam National University, Korea

Thesis title: Separation and purification of naphthalene from coal tar distillate by crystallization

Thesis supervisor: Prof. Soo-Jin Park

Bachelor of Engineering (03/1991–02/1998, including a 27 month military service) Chemical engineering, GyeongSang National University, Korea

EXPERIENCE

Research Assistant (06/2000–12/2003) Department of Chemical Engineering, University of Halle, Germany

Supervisor: Prof. Dr.-Ing. habil. Joachim Ulrich

Research Assistant (01/1998–05/2000) Chemical Process & Engineering Center, Korea Research Institute of Chemical Technology (KRICT), Korea

Supervisor: Drs. Kwang-Joo Kim and Jung-Min Lee

AREA OF EXPERTISE

Research area in crystallization (Separation, purification, control of crystal size and morphology), coating (pastille, tablet), chemical process and process design

ERKLÄRUNG

Ich erkläre, dass ich die Dissertation selbständig und ohne fremde Hilfe verfaßt habe. Andere als die von mir angegebenen Quellen und Hilfsmittel wurden von mir nicht benutzt und die, den benutzten Werken, wörtlich oder inhaltlich entnommenen Stellen wurden von mir als solche kenntlich gemacht.

Diese Dissertation wurde bisher an keiner Universität oder Hochschule vorgelegt.

Frühere Bewerbungen um den akademischen Grad eines Dr. -Ing. wurden von mir nicht vorgenommen.

ACKNOWLEDGMENT

I express my deepest gratitude to Professor Ulrich for giving me the opportunity to work in his research group as a Ph.D. student and for his careful supervision of this work. Also deep thanks are to examining committee Professor Mäder and Doctor Teipel. My deep thanks are extended to the Martin-Luther-Universität Halle-Wittenberg for their support of this project which led to this work.

I would like to thank all the collaborators (Dr. Mohring, Dr. Wanko, Dr. Jones, Cornelia, Bernd, Torsten, Tero, Christine, Junjun, Uta, Mirko, Peter, Danail, Aiman, Mandy, Andrea, Kerrem, Kai, Anke, Ping, Johanna, Joerg, Eric and Mr Weissbarth) of the Institut für Verfahrenstechnik des Fachbereiches Ingenieurwissenschaften for their help during my studying. Special many thanks to Mr. Donchev, Mr. Tähti, Mr. Bay and Dr. Lu for their friendship, helps and great time that we had together in Merseburg and Halle.

Finally I would like to say thank to my wife, Hye-Kyoung for never ending devoted support. Without her help it would have been impossible to accomplish this work. Also I would like to thank my parent, brothers and sisters in Korea.

Halle (Saale), December 2003

Jung-Woo Kim